UCGE Reports

Number 20357

Department of Geomatics Engineering

Improved Navigation Solution Utilizing Antenna Diversity Systems in Multipath Fading Environments

by

Seyed Nima Sadrieh

October 2012

UNIVERSITY OF CALGARY

Improved Navigation Solution Utilizing Antenna Diversity Systems in Multipath Fading Environments

by

SEYED NIMA SADRIEH

A THESIS

SUBMITTED TO THE FACULTY OF GRADUATE STUDIES

IN PARTIAL FULFILMENT OF THE REQUIREMENTS FOR THE

DEGREE OF DOCTOR OF PHILOSOPHY

DEPARTMENT OF GEOMATICS ENGINEERING

CALGARY, ALBERTA

OCTOBER 2012

Abstract

There is an intense effort on increasing the signal detection and tracking capabilities of Global Navigation Satellite System (GNSS) receivers in shaded areas where receivers suffer significant degradation due to attenuation and multipath. In order to overcome signal attenuation and multipath fading, more processing gain is required. Increasing the coherent integration time is traditionally known as the main source of processing gain. However, the mobile user is typically in motion while using the receiver, which limits the coherent integration gain. Diversity schemes constitute another source of processing gain that can be utilized to enhance signal detection and parameter estimation performance by providing additional processing gain.

Given the coherent integration time limit and spatial/temporal characters of indoor GNSS channels, a diversity system composed of spatially separated antennas is developed and tested in this thesis. The performance of this diversity system is assessed at three different levels namely signal detection, parameter estimation and navigation solution.

The performance of different combining methods at different levels is assessed theoretically and practically using real GPS L1 data collected in different indoor environments.

An analysis of different metrics such as deflection coefficients, ROC curves and satellite availability, shows that the detection performance is considerably enhanced when utilizing the above diversity scheme.

Proposing an analytical model based on sphere of scatterers model and considering the antenna gain pattern, Doppler measurements error sources in multipath environment are

characterized. It is shown that Doppler measurements are of limited value for positioning purpose in harsh multipath environments.

Combining pseudoranges of diversity branches based on their instantaneous qualities, represented by their epoch-by-epoch SNR, the pseudorange precision is enhanced significantly. Finally, improved satellite availability, along with enhanced pseudorange, makes a remarkable improvement in positioning accuracy.

Preface

This thesis includes some materials (e.g. figures, tables and texts) previously published in four conference papers and one journal paper as follows:

1. **Sadrieh, N**., A. Broumandan and G. Lachapelle (2012) "Doppler Measurement Characterization in Multipath Fading Channels for GNSS Applications," *Journal of Navigation*, vol 65, no 3, June, Cambridge University Press, pp. 477-494
2. **Sadrieh, N**., A. Broumandan and G. Lachapelle (2012) **"**Investigating Indoor GPS Doppler and Pseudorange Characteristics," *Proceedings of GNSS12,* 18-21 September, Nashville TN, The Institute of Navigation, 10 pages
3. **Sadrieh, N**., A. Broumandan and G. Lachapelle (2012) "A Weighted Combining Method for GNSS Antenna Diversity," *Proceedings of IEEE/ION PLANS 2012*, 24-26 April, Myrtle Beach SC, 8 pages
4. **Sadrieh, N**. (2011) "Spatial Antenna Diversity Performance for Indoor GNSS Applications," *Proceedings of GNSS 2011,* 20-23 September, Portland OR, The Institute of Navigation, 9 pages. (ION GNSS11 Student Sponsorship Award)
5. **Sadrieh. N**., A. Broumandan, G. Lachapelle, (2010)"Spatial/Temporal Characterization of the GNSS Multipath Fading Channels," *Proceedings of GNSS 2010,* 21-24 September, Portland OR, The Institute of Navigation, 10 pages.

The above papers were produced by the author during the research phase of this thesis. The co-authors' valuable feedback on the above materials is acknowledged. Use of the above material in this thesis is allowed by the co-authors and the journal/proceedings publishers.

Acknowledgements

I would like to express sincere gratitude to my supervisor, Professor Gérard Lachapelle for his continues encouragement, guidance and patience. I will always remember his positive attitude and understanding, which helped me to shape my professional career.

Thanks to my co-supervisor, Dr. Ali Broumandan for his friendship, great ideas, patience and generous support throughout my work. This research would have been much more challenging without his support. I would like to thank Professor Mark Petovello, Dr. Cillian O'Driscoll, Dr. Daniele Borio, and Dr. Vahid Dehghanian for their valuable advice during my studies.

Special thanks to Faranak, my beloved wife, for her support and constant love during my education. I am greatly thankful to my parents, without whose support and encouragement I would never have gotten this far. In addition, I would like to thank my sisters for their encouragement throughout my education.

My thanks go to all of my colleagues and friends in the PLAN Group who helped me to acquire this professional experience. Specifically, I would like to thank Behnam Aminian, Mohammadreza Zaheri, Hatef Keshvadi, Billy Chan, Dr. Pejman Kazemi and Dr. Shashank Satyanarayana for their invaluable assistance.

This work was sponsored by a Research In Motion grant, matched by a Natural Sciences and Engineering Research Council of Canada Collaborative Research and Development grant, and an Industry Sponsored Collaborative grant from Alberta Advanced Education and Technology.

Dedication

To my beloved wife, Faranak, my parents Nahid and Masoud and my daughter Golsa.

Table of Contents

List of Tables

List of Figures and Illustrations

List of Symbols and Abbreviations

Symbol	Definition
A	Signal amplitude
$\mathbf{C}$	Covariance matrix
c	Speed of light
$c(\bullet)$	PRN code
$D(\bullet)$	Navigation data bit
f_d	Frequency offset
$G(\bullet)$	Antenna gain pattern
$\mathbf{H}$	Design matrix
h	Height
H_0	Hypothesis that the desired signal is present
H_1	Hypothesis that the desired signal is present
L	Likelihood function
$\mathbf{p}$	Position vector of moving antenna
$p(\bullet)$	Probability density function
P_{fa}	Probability of false alarm
P_d	Probability of detection
r	Pre-correlation signal
t	Time
T	Coherent integration time
T_s	Sampling period
w	Weight
$x[\bullet]$	Correlator output
α	Azimuth
β	Elevation

$\Delta\hat{f}$	Estimated Doppler
$\Delta\rho$	Differential Pseudorange
$\delta(\bullet)$	Impulse response
ϕ	Latitude
$\Phi(\bullet)$	CDF of a normal Gaussian distribution
η	Noise
λ	Longitude
$\boldsymbol{\theta}$	Vector of unknowns
ρ	Pseudorange
ρ_e	Envelope correlation coefficient
ρ_c	Complex correlation coefficient
τ	Code phase
$\hat{\tau}$	Estimated Code Phase
Ω_s	Signal power density
ψ	Initial carrier phase

Abbreviations	**Definition**
A-GPS	Assisted GPS
CAF	Cross Ambiguity Function
CDF	Cumulative Distribution Function
CDMA	Code Division Multiple Access
DC	Deflection Coefficient
DLL	Delay Lock Loop
DS-SS	Direct Sequence Spread Spectrum
EGC	Equal Gain Combiner

FLL	Frequency Lock Loop
GNSS	Global Navigation Satellite System
GPS	Global Positioning System
HSGPS	High-Sensitivity GPS
ICT	Information and Communication Technology building
INS	Inertial Navigation System
IMU	Inertial Measurement Unit
LOS	Line of Sigh
LS	Least Squares
NLOS	None-Line of Sight
NWLS	None Weighted Least Squares
PDF	Probability Density function
PLL	Phase Lock Loop
PRN	Pseudo-Random Noise
SC	Selection Combining
SNR	Signal to Noise Ratio
SNRWLS	Signal to Noise Ratio based Weighted Least Squares
U of C	University of Calgary
UWB	Ultra-Wide Band
WC.	Weighted Combining
WLS	weighted Least Squares

Chapter One: INTRODUCTION

Hundreds of millions GPS receivers are operating worldwide. Most of them are chipsets in cell phones utilized to satisfy location-based services requirements. Although GPS performs well in open sky situations, in harsh multipath environments such as indoors, it suffers degraded performance or completely fails to provide accurate, reliable and continuous position (Kaplan & Hegarty 2006). This degradation is due to two physical phenomena, namely signal attenuation and multipath (Lachapelle 2009). Numerous approaches to alleviate these difficulties have been investigated to have more accurate and reliable GPS in harsh multipath environments.

This dissertation proposes and assesses a novel technique to enhance GNSS signal detection, parameter estimation and navigation solution based on utilizing an antenna diversity system for handheld receivers.

1.1 Background

From a technical standpoint, getting more processing gain is necessary to alleviate the indoor GNSS difficulties. So far, there are two main technologies utilized in literature and practice to enhance the processing gain for GNSS application namely (i) increasing the coherent integration time and (ii) utilizing diversity schemes. The following sections delineate these two technologies in more details.

1.1.1 Increasing the coherent integration time

Increasing the coherent integration time is traditionally known as the main source of processing gain (Watson 2005) where the achieved gain is a direct function of coherent integration time. However, practically some limits restrict the coherent integration time and its corresponding gain. The primary limitation of increasing the coherent integration time is the 20 ms period of navigation message (Watson 2005). The BPSK-modulated navigation message induces a 180° phase shift across bit transitions.

Although a bit transition does not happen every 20 ms, it statistically negates the constructive effect of increasing the coherent integration time if it remains uncompensated (Van Diggelen 2009). Thus, coherent integrations longer than 20 ms can be realized only when the navigation data is aided to or estimated by the receiver. Another limit is loss of coherency during the coherent integration time (Van Diggelen 2009). This loss is caused by the clock instability (Watson et al 2006a) in static cases, and motion in fading environments for dynamic cases (Broumandan 2009). The clock instability can cause a frequency mismatch (Watson et al 2006a). Accumulation of the frequency mismatch over time can result in phase shift and the same distractive effect as bit transitions. Hence, quality of the receiver's oscillator results is a bound for coherent integration time. The bound ranges from less than one second for low cost oscillators to tens of seconds for precise oscillator such as the rubidium atomic clocks (O'Driscoll & Borio 2009).

The motion in a multipath fading environment can also de-correlate the received signal over time and limit the coherent integration time and its gain. In Sadrieh et al (2010) it is shown that in a Rayleigh faded environment modeled by a ring of scatterers,

half a wavelength antenna motion results in signal de-correlation. In Broumandan et al (2011) it is shown that for a moving receiver in harsh multipath environments, increasing the coherent integration time over a certain limit, does not improve the processing gain. This limit is a function of the scatterers' model and the antenna velocity. Reported limits in Broumandan et al (2011) for a receiver moving with a speed of 50 cm/s in different indoor environments vary from fraction of a second to one second.

1.1.2 Diversity scheme

In order to overcome the received signal insertion loss and fading problems, one of the approaches that can be used is the diversity scheme (Broumandan 2009). In a diversity system, the received signals from different sources are combined to enhance the signal detection, parameter estimation and navigation solution performance (Blaunstein & Andersen 2002, Sadrieh 2011). The main idea behind the diversity scheme is to combine independent receptions of a unique transmitted signal. Independent diversity branches can be realized using different methods. Different types of diversity systems can be launched including time, frequency and antenna diversity. In the antenna diversity system, several antennas are utilized to capture independent copies of a signal. The antenna diversity system more specifically can be implemented by utilizing antennas with different polarizations (Zaheri et al 2009), patterns (Dietrich et al 2001) or spatial distances (Sadrieh 2011). The performance of diversity systems highly depends on the level of independence between signals at diversity branches (Turkmani et al 1995).

After receiving independent signals from diversity branches, the problem of interest is to combine these signals to alleviate multipath fading. From numerous diversity

combining methods, the three most commonly used are the Equal Gain Combining (EGC), the Selection Combiner (SC) and the weighted combining (Broumandan 2009).

The selection diversity scheme chooses “the best” branch in each processing epoch. Generally, the branch with the highest SNR is considered “the best”. For implementation of the selection combining, an epoch-by-epoch Signal-to-Noise Ratio SNR or equivalently Carrier-to-Noise ratio C/N_0 estimator is required. In the EGC, the corresponding signals of diversity branches are added to each other with equal weights to enhance performance. In weighted combining, the signal of each branch is multiplied by a weighting function that depends on the signal quality in each branch. Therefore, branches with higher signal quality are more effective on the combined signal. The weights can be generated using different metrics. Nevertheless, the Signal-to-Noise Ratio (SNR) is the most sophisticated metric commonly utilized. Subsequently, in all combining methods, the combined signal is treated as a single signal and the detector and test statistic function are applied on it (Zaheri 2010).

In addition to the aforementioned techniques, several other approaches have been used to assist the GPS receiver in maintaining its position. GPS may be augmented with other measurement sources such as Wi–Fi (Li et al 2010), ultra wideband (UWB) (Chiu & O'Keefe 2008) ranging radios and Inertial Measurements Units (IMU). However, the performance of such systems depends on the quality of GPS measurements in addition to the availability and quality of additional measurements.

1.2 Limitation of previous work

Coherent integration times generally do not exceed the duration of a navigation data bit (20 ms) for those cases where a receiver operates in open sky conditions. Particularly, coherent integration times from 1 to 20 ms are sufficient for open sky operations where the received signal C/N_0 generally varies from 30 to 50 dB-Hz (Soloviev et al 2009). Shanmugam (2008) reports the problems of high sensitivity acquisition under weak GPS signal conditions. Increasing the coherent integration time over 20 ms has thus proven to be effective for enhancing the GPS performance in degraded environments. In Watson et al (2006b) an Assisted GPS (AGPS) approach was proposed to increase the coherent integration time of up to 10 s, providing up to 79 dB of processing gain. This amount of processing gain was achieved for a static receiver with an 8 MHz front-end bandwidth and with a precise oscillator. In more practical cases, there are some limiting factors when attempting to increase the coherent integration time, namely the clock instability (Watson et al 2006a) in static cases and motion in fading environments for dynamic cases (Broumandan et al 2010). Considering these limitations, extending coherent integration times over 1 s is not helpful for practical cases.

Another approach to increase the processing gain and alleviate multipath fading is to take advantage of a diversity scheme. The use of multiple antennas in the form of an antenna diversity system can decrease the fading problem by providing the diversity gain. A diversity scheme is established based on receiving independent signals on each diversity antenna denoted here as a diversity branch. Spatial diversity is thoroughly discussed in Haykin (2000). Colburn et al (1998) evaluate the spatial diversity performance of three different antenna configurations for the indoor 902-928 MHz

propagation channel. There is much research conducted on exploiting the diversity for different applications and frequencies.

Focusing on GNSS applications, Broumandan (2009) proposed an antenna diversity system utilizing a synthetic antenna array. It was shown that a significant improvement could be achieved by this method on the detectability of signals in dense multipath fading environments. In Zaheri (2010), diversity between antennas with different polarizations is utilized to enhance the detectability of satellite signals. Although detection performance was comprehensively analyzed by Broumandan (2009) and Zaheri (2010), performances of diversity systems in the position domain and at the measurement level have not been assessed yet. Since the ultimate goal of GNSS is estimating position, it is of interest to evaluate the performance of diversity systems in the position domain.

1.3 Objectives and Contributions

Given the lack of research directed towards the assessment of the antenna diversity performance in the position domain, the objective of this dissertation is to expand upon the work described above to a complete assessment of the antenna diversity system performance at three different levels, namely (i) signal detection, (ii) parameter estimation and (iii) navigation solution. Figure 1 illustrates these levels and corresponding metrics to be evaluated at each level.

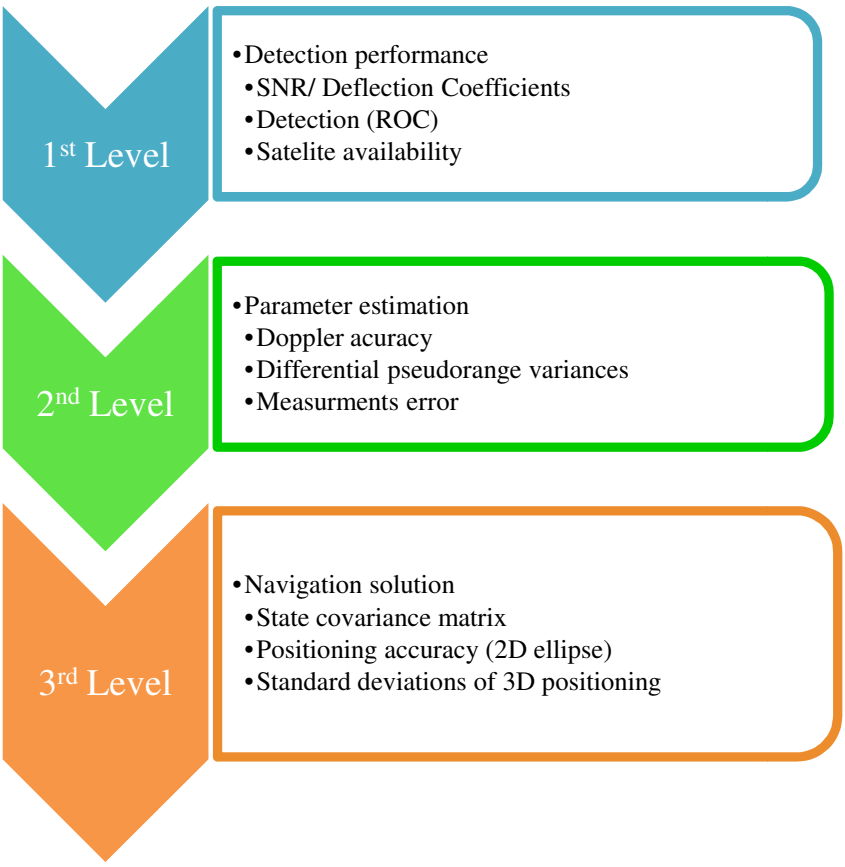

Figure 1-1 : Three levels of performance analysis of diversity algorithms

With regard to the shortcomings and challenges outlined in the previous section, the objectives of this dissertation are as follows:

1- *Channel characterization for diversity purposes.* The performance of diversity systems dramatically depends on the level of independency between branches (Turkmani 1995). Determination of the independency level between branches is a necessary task before implementing a diversity scheme. Herein, two metrics are analyzed to quantify the level of independency between branches, namely (i) the joint distribution of signal strength of branches and (ii) the correlation coefficient. Analyzing the joint distribution of branches results in a comprehensive

understanding of correlation between branches. However, this method is rarely used in the literature and a less complicated analysis approach such as correlation coefficient is preferred (Turkmani 1995). The correlation coefficient is a metric to represent the correlation between two random variables as a function of time or space.

2- *Satellite availability improvement.* Utilizing more than one branch, the probability of occurrence of fade on all branches at the same time is decreased by orders of magnitude. Moreover, combining signals from different diversity branches provides some processing gain called “diversity gain”. Alleviating the fading and achieving more processing gain result in a significant improvement in satellite availability and the probability of outage. Herein, the satellite availability enhancement achieved through utilizing different diversity combining methods is quantified. Acquiring more satellites not only enhances their availability but also reduces (hence improves) the Dilution Of Precision (DOP), which dramatically ameliorates position accuracy.

3- *Measurement accuracy enhancement.* Measurements accuracy is also enhanced through the use of different diversity systems. The measurements extracted from individual antennas are viewed as redundant measurements in Least Squares or Kalman Filter with proper covariance matrices. To analyse the enhancement achieved through implementing diversity scheme at the measurement level, a two-stage least squares approach is utilized. In the first stage, the measurements extracted from diversity branches from a given satellite are combined to enhance their precision. In the second stage, combined measurements for all available

PRN are used to estimate the position. More improvement is achieved through filter tuning for indoor situations. An analytical model is utilized to tune the filters and enhance the performance.

4- *Positioning accuracy improvement.* The integrated effect of diversity on satellite availability and measurement accuracy is realized in the position domain.

The major contributions of this dissertation can be summarized as follows:

1. Characterizing the indoor GNSS channel and finding the proper spacing for establishing the spatial antenna diversity system.
2. Characterizing Doppler measurements error sources in harsh multipath environments by developing an analytical model and verifying the theoretical finding with experimental measurements.
3. Characterizing the indoor GNSS measurements pseudorange error sources and designing novel covariance matrices for indoor measurements.
4. Implemented an antenna diversity system and tested it in different environments at three different levels.
5. Development and utilization of novel combining methods for GNSS antenna diversity.

1.4 Thesis Outline

This dissertation contains seven chapters. The remaining chapters are as follows:

Chapter Two is dedicated to review the background and system model used throughout the dissertation. It discusses indoor GPS signal behaviour and presents methods of

providing signal parameters in degraded signal environments. The A-GPS and the block processing method are described. In addition, diversity system and combining methods are discussed.

Chapter Three characterizes the indoor GNSS channel. The applicability of establishing an antenna diversity system on a hand held receiver is explored. In order to achieve this, the complex and envelope correlation coefficient between diversity branches and the joint distribution of signal strength of them are presented and analyzed.

In Chapter Four, the detection performance of the spatial antenna diversity system is analyzed. The detection performances of a single branch and different combining methods are compared in different environments using real GPS data. To this end, several metrics including Defection Coefficient, ROC curve and Satellite availability are assessed.

Chapter Five provides a detailed analysis of Doppler measurement error sources in harsh multipath environments. An analytical model based on the sphere of scatterers model considering the antenna gain pattern is developed in order to characterize the observed Power Spectral Density (PSD) by a moving antenna. The theoretical findings are verified by experimental measurements with different satellites under different conditions. The Doppler-driven velocity solution accuracy is also assessed.

Chapter Six provides a detailed analysis on the pseudorange estimation and navigation solution performance of the diversity system. Two combining approaches are examined in this chapter namely (i) combining at correlator outputs and (ii) combining at the measurement level. The performances of combining methods are compared to single branches using real GPS data. The combined pseudoranges are used for single point

positioning. At the position level, the performances of different combining methods are assessed through an analysis of different metrics including 2D error ellipses and DRMS values.

Chapter Seven summarizes the work presented in the thesis and draws conclusions based on the theoretical analysis and the empirical test results. Finally, recommendations for future work are suggested.

Chapter Two: FADING CHANNEL, BLOCK PROCESSING TECHNIQUE AND ANTENNA DIVERSITY SYSTEMS

This chapter reviews the theoretical background of GPS block processing techniques and antenna diversity systems. At first, an overview of GPS is provided along with its signal structure. The optimum detector and estimator at the acquisition level for the LOS case are formulated. An approach to detect the GNSS signal and estimate its parameters for indoor harsh scenarios named reference-rover method is discussed. Fading multipath channel along with the well-known signal distribution under multipath fading circumstances are introduced. The diversity systems are then briefly described.

2.1 Overview of GPS

Global Positioning System (GPS) is a space based navigation system that provides accurate three-dimensional Position and Velocity as well as Time (PVT) worldwide. GPS consists of three segments (Misra & Enge 2006): space segment, control segment and user segment.

2.1.1 Signal model

The signal at the output of a GPS receiver antenna can be represented as

$$r(t)=\sum_{k=1}^{K}A_k\left(\mathbf{p}(t)\right)D_k(t-\tau_k)c_k(t-\tau_k)e^{j(2\pi f_{d,k}t+\psi_k)}+\eta(t) \qquad \textbf{2-1}$$

where $A_k\left(\mathbf{p}(t)\right)$ represents the channel gain as a function of antenna position, $c_k(\bullet)$ is the pseudo-random code (PRN) corresponding to the k-th available satellite, $D(\bullet)$ is the

navigation data modulation, τ is the code offset, $f_{d,k}$ represents the frequency offset, ψ_k is the initial phase offset and *K* is the number of GPS satellites in view. The received signal is corrupted with additive noise, which has an equivalent complex baseband representation denoted by $\eta(t)$. Herein, the presence of simultaneous GPS signals will be ignored. Hence, in the remainder of the text, for notational convenience, the subscript k is omitted and the received signal is modeled as

$$\begin{aligned} r(t) &= s\ (t) + \eta(t) \\ s\ (t) &= D\ (t-\tau)\, c\ (t-\tau)\, e^{j(2\pi f_d t + \psi_k)}. \end{aligned} \qquad \textbf{2-2}$$

In the most generic case, the navigation data modulation, the code offset, the initial phase offset and the satellite vehicle number are unknown and also of interest.

The main purpose of the signal processing block of a GPS receiver is to de-spread the received signal to detect the presence of a specific satellite and to estimate the unknown parameters of the received signal. Then the estimated signal parameters, also known as measurements, are passed to the navigation-processing unit to produce a navigation solution. The signal processing block in a general form are implemented in two stages, namely acquisition and tracking.

At the acquisition stage, the presence of a satellite signal is determined and a course estimation of code phase and frequency offset is also provided simultaneously. At the tracking stage, depending on the tracking scenario, a fine estimate of some or all of unknowns is provided. Considering that the tracking stage is out of the scope of this research, in the following sections the essential theoretical background for the acquisition stage is provided.

2.2 GPS signal Acquisition

Here, the acquisition process is formulated from two points of view, detection and estimation. For both aspects, the essential theoretical background is presented and key assumptions are provided.

2.2.1 Detection in Acquisition mode

The acquisition process can be considered as a detection problem where the purpose of acquisition is to detect whether or not a signal from a given satellite is present at the receiver's input. The cell level GPS signal detection problem can be formulated as a binary hypothesis test (O'Driscoll 2006) based on a vector of observations denoted as

$$\mathbf{r} = [r(T_s), r(2T_s), ..., r(kT_s)]^{\mathrm{T}} \qquad \textbf{2-3}$$

where T_s signifies the sampling rate and $[\bullet]^{\mathrm{T}}$ is the transpose operator. Two possible hypotheses of binary detection are

$$\begin{aligned} H_1 &: \quad \mathbf{r} = \mathbf{s} + \mathbf{n} \\ H_0 &: \quad \mathbf{r} = \mathbf{n} \end{aligned} \qquad \textbf{2-4}$$

where H_1 is the hypothesis that the desired signal is present and H_0 represents the hypothesis in which the desired signal is not present. $\mathbf{s}$ is a $\mathrm{k}\times 1$ vector containing the samples of a known complex signal of $s(t)$ and $\mathbf{n}$ is also a $\mathrm{k}\times 1$ vector containing the Circular White Gaussian Noise (CWGN) samples of $\eta(t)$ which are defined as

$$\begin{aligned} \mathbf{s} &= [s(T_s), s(2T_s), ..., s(kT_s)]^{\mathrm{T}} \\ \mathbf{n} &= [\eta(T_s), \eta(2T_s), ..., \eta(kT_s)]^{\mathrm{T}} \cdot \end{aligned} \qquad \textbf{2-5}$$

The detector, therefore, will make one of the following decisions:

D_0 : The decision that H_0 is true,

D_1 : The decision that H_1 is true.

Based on the aforementioned hypotheses and decisions there are four possible outcomes for a binary hypothesis test, as tabulated in Table 2-1.

Table 2-1: Four Possible Outcomes of a Binary Hypothesis Test

	True Hypothesis	
Decision	H_0	H_1
D_0	Correct rejection	Miss Detection
D_1	False Alarm	Correct Detection

The objective of a detector is to maximize the probability of detection, P_d , for a given probability of false alarm, P_{fa} , which is referred to as the Neyman-Pearson test (Kay 1998).

The optimum Likelihood Ratio Test (LRT) yields to the D_1 decision if

$$L(x) = \frac{p(x; H_1)}{p(x; H_0)} > \gamma \qquad \textbf{2-6}$$

where γ is the threshold providing the given $P_{fa.}$. Recalling that $\mathbf{s}$ is a known complex vector and $\mathbf{n}$ is CWGN vector with elements distributed as $CN\left(0,\sigma^2\right)$, $p(x;H_0)$ and $p(x;H_1)$ can be written as

$$p(x;H_1)=\pi^{-k}\sigma^{-2k}\exp\left[-\frac{1}{\sigma^2}(\mathbf{r}-\mathbf{s})^H(\mathbf{r}-\mathbf{s})\right]$$
$$p(x;H_0)=\pi^{-k}\sigma^{-2k}\exp\left[-\frac{1}{\sigma^2}(\mathbf{r})^H(\mathbf{r})\right]. \qquad \textbf{2-7}$$

Replacing Eq. 2-7 in Eq. 2-6 and following some manipulations, [for more details refer to Kay (1998)], the test criterion can be formulated as

$$\Lambda=\mathrm{Re}\left[\mathbf{s}^H\mathbf{r}\right]>\gamma' \qquad \textbf{2-8}$$

where γ' is constrained by P_{fa} as in Eq. 2-10. Thus, the test statistic is a filter matched to the signal of interest. Hence, this approach is called the match filter approach. It can be shown that Λ is distributed as

$$\Lambda\sim\begin{cases}N\left(0,\sigma^2\,\varepsilon/2\right) & \text{under } H_0\\ N\left(\varepsilon,\sigma^2\,\varepsilon/2\right) & \text{under } H_1\end{cases} \qquad \textbf{2-9}$$

where ε is the signal energy. The performance of the match filter can be formulated as

$$P_{fa}=Q\left(\frac{\gamma'}{\sqrt{\sigma^2\,\varepsilon/2}}\right) \qquad \textbf{2-10}$$
$$P_d=Q\left(Q^{-1}\left(P_{fa}\right)-\sqrt{2\,\varepsilon/\sigma^2}\right)$$

where $Q(\bullet)$ is defined as

$$Q(x) = 1 - \Phi(x) \qquad \textbf{2-11}$$

where $\Phi(x)$ is the cumulative distribution function of a normal Gaussian distribution.

2.2.2 Estimation in Acquisition mode

The estimation problem in acquisition stage can be formulated as a coarse parameter estimation problem. Based on parameter estimation theory, presented in details in (O'Driscoll 2006), the most appropriate approach to estimate the set of unknowns in the GPS case is the Maximum Likelihood (ML) estimation.

Based on the signal model in Eq. 2-2, the GPS signal transmitted by a given satellite is received with a set of unknown parameters. Herein, by ignoring or aiding other unknowns, the set of unknowns is reduced to $\boldsymbol{\theta} = [\tau, f_d]$. Since $\mathbf{r}$, as expressed by Eq. 2-3, has *k* samples of a CWGN, the likelihood function is given by (Kay 1998)

$$f_{\mathbf{r}|\boldsymbol{\theta}}(\mathbf{r}|\boldsymbol{\theta}) = \pi^{-k} |\mathbf{C}|^{-1} \exp\left((\mathbf{r}-\boldsymbol{\mu})^{\mathbf{H}} \mathbf{C}^{-1} (\mathbf{r}-\boldsymbol{\mu})\right) \qquad \textbf{2-12}$$

where $(\bullet)^H$ denotes the complex conjugate operator and $\mathbf{C}$ is the k×k covariance matrix of the Gaussian noise samples defined by

$$\mathbf{C} \triangleq E\left[\mathbf{r}\mathbf{r}^{\mathbf{H}}\right]. \qquad \textbf{2-13}$$

Since it is assumed that the noise is white, the covariance matrix can be written as

$$\mathbf{C} = \sigma^2 \mathbf{I}. \qquad \textbf{2-14}$$

$\boldsymbol{\mu}$ is the vector containing mean values of received signals. It should be noted that the mean values of the received signals are signal component samples:

$$\boldsymbol{\mu} = E[\mathbf{r}] = \left[s(0), s(T_s), s(2T_s), ..., s((K-1)T_s) \right]^{\mathbf{T}} = \mathbf{s}(\boldsymbol{\theta}) \quad \textbf{2-15}$$

Replacing Eq. 2-15 in Eq. 2-12 the likelihood function can be written as

$$f_{\mathbf{r}|\boldsymbol{\theta}}(\mathbf{r}|\boldsymbol{\theta}) = \pi^{-k}\sigma^{-2k} \exp\left(\frac{-1}{\sigma^2} (\mathbf{r} - \mathbf{s}(\boldsymbol{\theta}))^{\mathbf{H}} (\mathbf{r} - \mathbf{s}(\boldsymbol{\theta})) \right). \quad \textbf{2-16}$$

Maximizing the likelihood function is equivalent to maximizing

$$-(\mathbf{r} - \mathbf{s}(\boldsymbol{\theta}))^{\mathbf{H}} (\mathbf{r} - \mathbf{s}(\boldsymbol{\theta})) = -|\mathbf{r}|^2 - |\mathbf{s}(\boldsymbol{\theta})|^2 + 2\,\mathrm{Re}[\mathbf{r}.\mathbf{s}(\boldsymbol{\theta})]. \quad \textbf{2-17}$$

Since the $|\mathbf{r}|^2$ is the received signal power that cannot be affected by $\boldsymbol{\theta}$, it can be eliminated from the equations. Thus, the ML estimator can be written as

$$\boldsymbol{\theta}_{ML} = \arg\max_{\boldsymbol{\theta}} \left(2\,\mathrm{Re}[\mathbf{r}.\mathbf{s}(\boldsymbol{\theta})] - |\mathbf{s}(\boldsymbol{\theta})|^2 \right). \quad \textbf{2-18}$$

It should be noted that $\boldsymbol{\theta}$ contains all of the unknown parameters of the signal to be estimated. Since the unknowns are reduced to the code phase and Doppler, and other unknowns are either ignored or aided to the estimator, Eq. 2-18 can be written as

$$\boldsymbol{\theta}_{ML} = \arg\max_{\boldsymbol{\theta}} \left(|\mathbf{r}.\mathbf{s}(\boldsymbol{\theta})|^2 \right) \quad \textbf{2-19}$$

which is similar to the optimum detector expressed as Eq. 2-8. Hence, the optimum estimator/detector needs to establish a bank of match filters each tuned on a hypothetical pairs of code phase and Doppler. This filter bank is called “search space” and the values of each matched filter is called “correlator output”. Herein, the search space is implemented using block processing technique, to be discussed in Section 2.3.

2.3 Indoor GPS challenges and methodology

In an indoor environment, multipath and signal attenuation are known as two main limitations in having an accurate and reliable GPS position. Signal attenuation occurs due to propagation through building materials, which induces attenuation of up to tens of dBs, with respect to the line of sight signals (e.g. Hu et al 2007). Multipath not only induces errors in the measurements but also causes a variation in the signal strength called "fading". Multipath phenomenon for indoor environments is discussed in more details in the next section**.** As stated above, the major challenges for a GPS receiver in indoor environments are

- Correct detection of the received signal affected by attenuation and fading
- Estimation of LOS pseudorange and Doppler

2.3.1 Multipath phenomenon in indoor circumstances

In a typical indoor GNSS propagation link, the signal arrives to the GNSS antenna via several paths. Received waves via such paths have different delays, phases and frequency offsets. At the receiver, these waves are superimposed vectorally at any given frequency resulting in an oscillating signal amplitude. The character of variations depends on the distribution of phase and energy among incoming component waves. The signal amplitude random variations are known as fading effects (Blustin & Anderson 2002).
In a general communication case, it is considered that spatial fading has three natures as follows (Blustin & Anderson 2002):

1- Path loss is considered as an overall decrease in signal strength as the distance between transmitter and receiver increases.
2- Shadowing, caused by diffractions, scattering and reflections which all show slow random variations in signal amplitude with a tendency to lognormal distribution of the signal amplitude.
3- Fast fading, caused by superimposing incoming waves in a multipath environment.

For an indoor GNSS case, the first two effects cannot be significant since path loss can be considered constant over a time interval of a few minutes and slow fading is considered to be experienced in several ten of metres intervals (Blustin & Anderson 2002). Thus, fast fading is the dominant effect for indoor GNSS situation. Fast fading can disturb the received signal's power and amplitude. In the following section, the effect of fast fading on the signal amplitude is delineated. The well-known signal amplitude distribution under fast fading circumstances are Rayleigh and Rician which are introduced here.

1- Rayleigh fading

   Rayleigh fading is a commonly used distribution to describe the signal's amplitude in fast fading scenarios. A Rayleigh distribution can be obtained mathematically as the PDF of $x = \sqrt{x_1^2 + x_2^2}$ where x_1 and x_2 are two independent Gaussian signals distributed as $N\left(0, \sigma^2\right)$. The PDF of which can be presented as

$$p(x)=\begin{cases}\dfrac{x}{\sigma^2}\exp\left(-\dfrac{x^2}{2\sigma^2}\right) & for\ x\geq 0\\ 0 & for\ x<0\end{cases} \qquad \textbf{2-20}$$

It can be shown that the PDF is maximized by $x=\sigma$. The expected value of a Rayleigh distributed signal can be calculated as

$$E[x]=\int_0^\infty xp(x)\,dx=\sigma\cdot\sqrt{\frac{\pi}{2}} \qquad \textbf{2-21}$$

Figure 2-1 shows the PDF of a Rayleigh distributed signal, with the important values being overlaid on the plot.

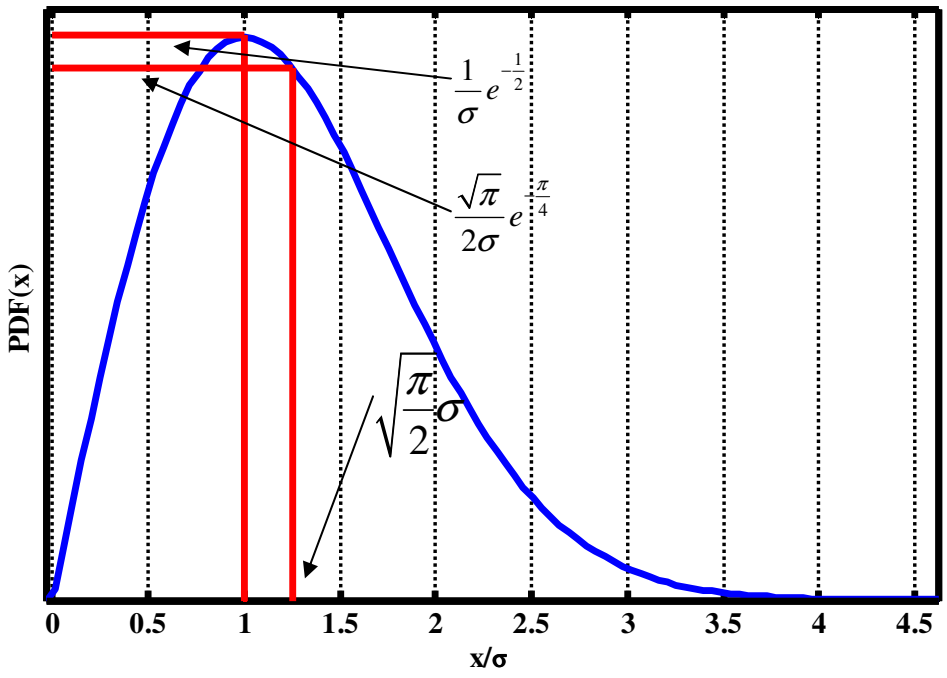

Figure 2-1: PDF of a Rayleigh distribution

2- Rician Distribution

Occasionally, in an indoor GNSS wireless channel, the line of sight (LOS) signal arrives to the antenna in addition to the multipath components. The LOS component as a dominant part of the received signal significantly affects the final received signal distribution. In this case, two quadrature components of the received signal are no longer zero mean and the resultant envelope carries a Rician distribution. Note that Non LOS dominant signals may cause the same effect as the LOS signal on amplitude distribution.

Mathematically, the PDF of $x = \sqrt{x_1^2 + x_2^2}$ where x_1 and x_2 are two independent Gaussian signals distributed as $x_1 \sim N\left(\mu_1, \sigma^2\right)$ and $x_2 \sim N\left(\mu_2, \sigma^2\right)$, is

$$p(x) = \begin{cases} \dfrac{x}{\sigma^2} \exp\left(-\dfrac{x^2 + \mu^2}{2\sigma^2}\right) \mathrm{I}_0\left(\dfrac{\mu x}{\sigma^2}\right) & for\ x \geq 0 \\ 0 & for\ x < 0 \end{cases} \qquad \textbf{2-22}$$

where $\mu^2 = \mu_1^2 + \mu_2^2$ and $\mathrm{I}_0(\bullet)$ is the modified Bessel function of the first kind and zero order, as formulated by Kay (1998).

2.3.2 Block processing

Signal processing methods that work on a block of samples without considering the rest of the data is called block processing, also called batch processing. (Uijt de Haag 1999). It is in contrast with well-known sequential data processing.

In GPS signal processing, although block processing method induces a significantly higher computational burden, it is proven to be more powerful than a sequential approach

(tracking loops) for low carrier-to-noise ratio (C/N_0) cases specifically in indoor navigation (Van Graas et al 2005). Hence, herein, a block processing approach is utilized to investigate the indoor GNSS channel and antenna diversity performance. In the following section more details on the utilized approach is presented.

2.3.3 Reference-rover processing

In order to speed-up and facilitate the block processing method, the PLAN group software receiver GSNRx-rr has been used in this research. GSNRx-rr is a modified version of the standard GSNRx (Petovello et al 2009) software receiver and allows the joint processing of several input channels.

The first channel is an open sky, called reference channel. The incoming digitized samples from the reference channel are processed sequentially to extract the navigation data bit, code phase and frequency offset. This information is the used as the aiding data for the indoor channel process. Indoor channels are subject to block processing. First local replicas for every possible code phase and frequency offset are generated as

$$\hat{s}_0^{\tau_i,\Delta f_j}(t) = D(t-\tau_i)\,c(t-\tau_i)\,e^{j(2\pi\Delta f_j t+\psi)} \qquad \textbf{2-23}$$

where τ_i is the *i*-th possible code phase and Δf_j is the *j*-th possible Doppler frequency. The replicas are correlated with the raw signal and integrated over blocks of T_c second. The correlator output for a given code phase of τ_i and Doppler frequency of Δf_j associated to the *n*-th block of data is denoted as

$$x\left[\tau_i, \Delta f_j, n\right] = \frac{1}{T}\int_{(n-1)T_c}^{nT_c} r(t)\,\hat{s}_o^{\tau_i,\Delta f_j}(t)^* dt \qquad \textbf{2-24}$$
$$= \frac{1}{T}\int_{(n-1)T_c}^{nT_c} A(\mathbf{p}(t))\, s_o(t)\hat{s}_o^{\tau_i,\Delta f_j}(t)^* dt + \frac{1}{T}\int_{(n-1)T_c}^{nT_c} w(t)\hat{s}_o^{\tau_i,\Delta f_j}(t)^* dt$$

.

Realizing the bank of correlator as introduced in Eq. 2-24, an estimation of code phase and frequency offset is achieved by choosing the correlator with the largest value:

$$\left(\Delta\hat{f}, \hat{\tau}\right)_n = \arg \max_{\Delta f_j, \tau_i} \left| \frac{1}{T}\int_{(n-1)T}^{nT} r(t)\,\hat{s}_o^{\tau_i,\Delta f_j}(t)^* dt \right|^2 \qquad \textbf{2-25}$$
$$= \arg \max_{\Delta f_j, \tau} \left| x\left[\Delta f_j, \tau, n\right] \right|^2$$

.

The procedure to estimate code phase and frequency offset is shown in Figure 2-2.

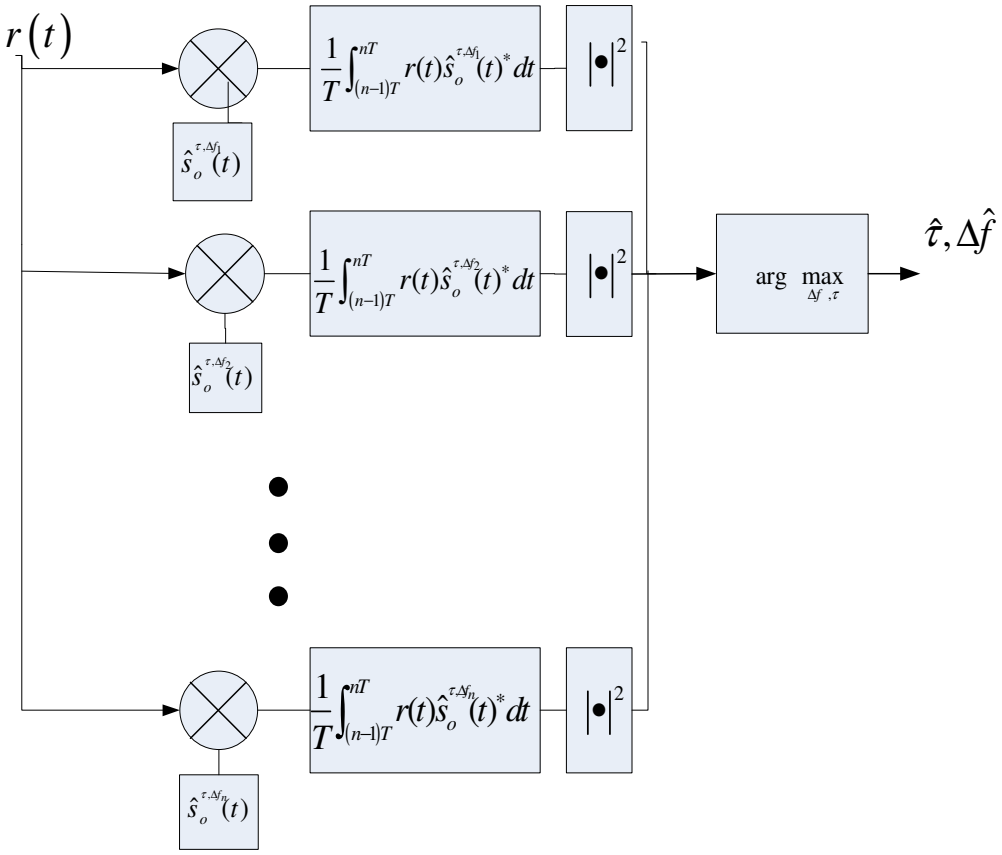

Figure 2-2: Block processing technique: a bank of matched filter is implemented and the correlator with maximum value is considered as the estimation of code phase and Doppler

To reduce the computational burden, the range of possible code and frequency offsets are reduced using the code phase and frequency offset of the reference channel. The estimated navigation data bit of the outdoor channel is also used to extend the coherent integration times beyond 20 ms. A sample correlator output is shown in Figure 2-3.

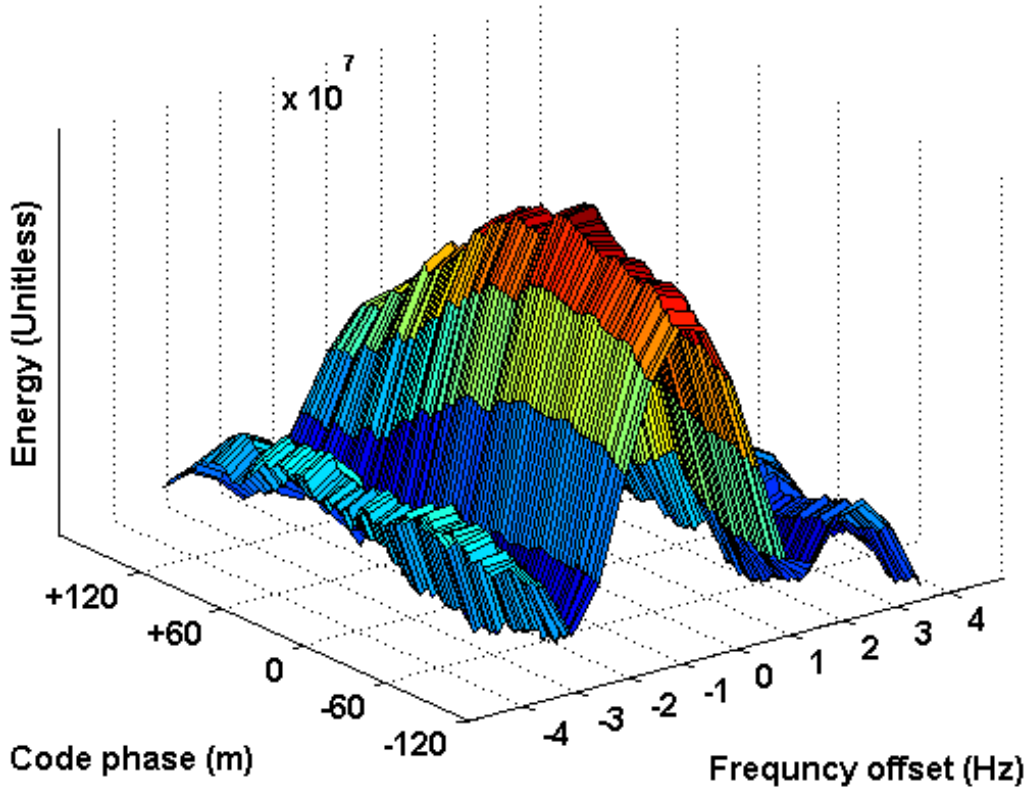

Figure 2-3: A sample correlator output for the coherent integration time of 400 ms Frequency offset and code phase are with respect to the reference channel

2.4 Diversity

The main idea behind the diversity scheme is to combine independent reception of a unique transmitted signal to enhance signal detection, parameter estimation and navigation solution performance. These independent copies are received by diversity branches. More specifically, in the antenna diversity system, several antennas with different polarizations (Zaheri et al 2009), patterns (Dietrich et al 2001) or spatial distances (Sadrieh 2011) are used to capture independent copies of the unique transmitted signal. The performance of diversity systems highly depends on the level of

independence between diversity branches (Turkmani et al 1995). The more independent the branches, the more effective the diversity scheme is. The correlation coefficient is a metric quantifying the correlation between two random variables. The correlation coefficient has been widely used to evaluate the performance of diversity systems. The complex correlation coefficient is quantified by

$$\rho_c = \frac{\mathrm{E}\left[x_1 x_2^* \right]}{\sqrt{\mathrm{E}\left[x_1 x_1^* \right] \mathrm{E}\left[x_2 x_2^* \right]}} \qquad \textbf{2-26}$$

where $\mathrm{E}[\bullet]$ is the expected value operator, and x_1 and x_2 are two complex random variables.

After receiving independent signals from diversity branches, the problem of interest is to combine these signals to enhance system's performance at all aforementioned levels. Diversity combining for GPS applications can be implemented and tested at two different levels, namely correlator outputs and measurement levels. At the correlator outputs level, the corresponding correlator outputs of each diversity branches are combined to enhance the detection, parameter estimation and navigation solution performance. A general diversity method for an *L*-branch diversity system at the correlator output level can be formulated as

$$x_d[\tau_i, n] = f\left(x_1[\tau_i, n], x_2[\tau_i, n], ..., x_l[\tau_i, n]\right) \qquad \textbf{2-27}$$

where $x_d[\bullet]$ is the combined correlator output, $x_l[\bullet]$ is the *l*-th diversity branch correlator output (i.e. 1, 2,..*L*) and n represents the processing epoch number. Note that using the block processing method, only information pertaining to a processing epoch is used at that epoch. Combining at the correlator output can enhance receiver processing

performance at all three levels (Sadrieh 2011). At the measurement level, individual branches detect the received signal and estimate the signal parameters. Then the estimated parameters (i.e. code phase and Doppler frequency) are passed to the combining unit. The combined measurements will be consequently used in the navigation solution. The diversity method for an *L*-branch diversity system at the measurement level can be formulated as

$$\hat{\tau}(n)_d = f\left(\hat{\tau}(n)_1, \hat{\tau}(n)_2, ..., \hat{\tau}(n)_l\right) \qquad \textbf{2-28}$$

where $\hat{\tau}(n)_d$ is the combined pseudorange, $\hat{\tau}(n)_l$ is the pseudorange measurement extracted from the *l*-th diversity branch (i.e. 1, 2, …, *L*), the function $f(\bullet)$ stated in Eq. 2-27 and Eq. **2-28** is an arbitrary function that can be specified by specific combining techniques. Combining at the measurement level can enhance the system performance at the measurement and position levels.

From numerous diversity combining techniques, three of them are utilized extensively, namely Equal Gain Combiner (EGC), Selection Combiner (SC) and Weighted Combiner (WC). The following section introduces these combining methods at the correlator outputs. Combining techniques at measurements level will be comprehensively discussed in Chapter 6.

2.4.1 Equal gain

In the equal gain combiner the corresponding correlator outputs of diversity branches are added to each other non-coherently. An *L*-branch EGC can be formulated as

$$x_{EG}\left[\tau_i, \Delta f_j, n\right] = \sum_{l=1}^{L} \left| x_l\left[\tau_i, \Delta f_j, n\right] \right|^2 \qquad \textbf{2-29}$$

where L is the number of diversity branches, $x_l[\bullet]$ denotes the correlator output corresponding to the l-th diversity branch and $x_{EG}[\bullet]$ represents the equal gain combined correlator output. Figure 2-4 shows the EGC block diagram.

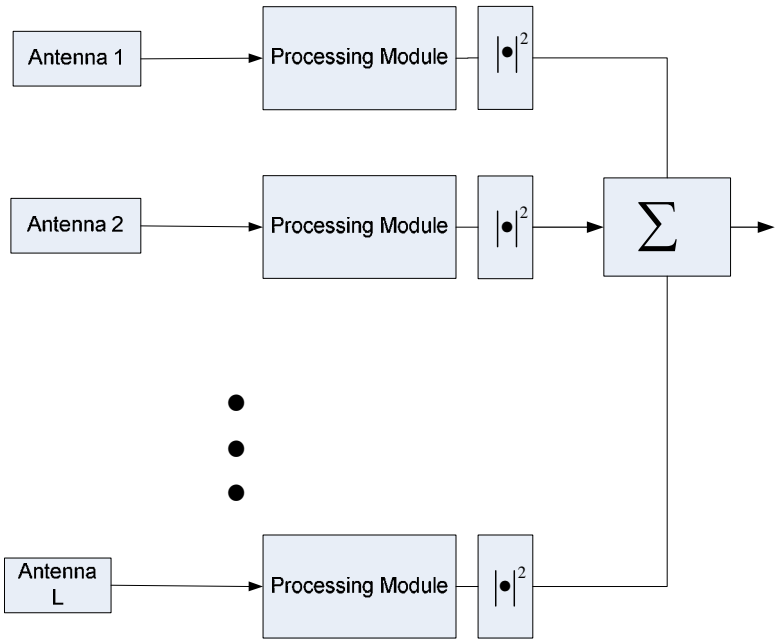

Figure 2-4: An L-branch equal gain combiner

2.4.2 Selection diversity

The selection diversity scheme chooses the "best" branch. Generally, a "best" branch is defined as the branch with the highest SNR in each processing block. The selection

diversity at the correlator outputs method in an *L*-branch diversity system can be formulated as

$$x_s\left[\tau_i,\Delta f_j,n\right]=\begin{cases} x_1\left[\tau_i,\Delta f_j,n\right] & \text{if } \mathrm{SNR}_1(n) \text{ is the highest} \\ x_2\left[\tau_i,\Delta f_j,n\right] & \text{if } \mathrm{SNR}_2(n) \text{ is the highest} \\ \bullet & \\ \bullet & \\ \bullet & \\ x_L\left[\tau_i,\Delta f_j,n\right] & \text{if } \mathrm{SNR}_L(n) \text{ is the highest} \end{cases} \qquad \textbf{2-30}$$

where $x_s\left[\bullet\right]$ is the selection combined correlator, $\mathrm{SNR}_l(n)$ is the signal-to-noise ratio associated to the *l*-th branch. Figure 2-5 presents the block diagram of an *L*- branch selection combiner.

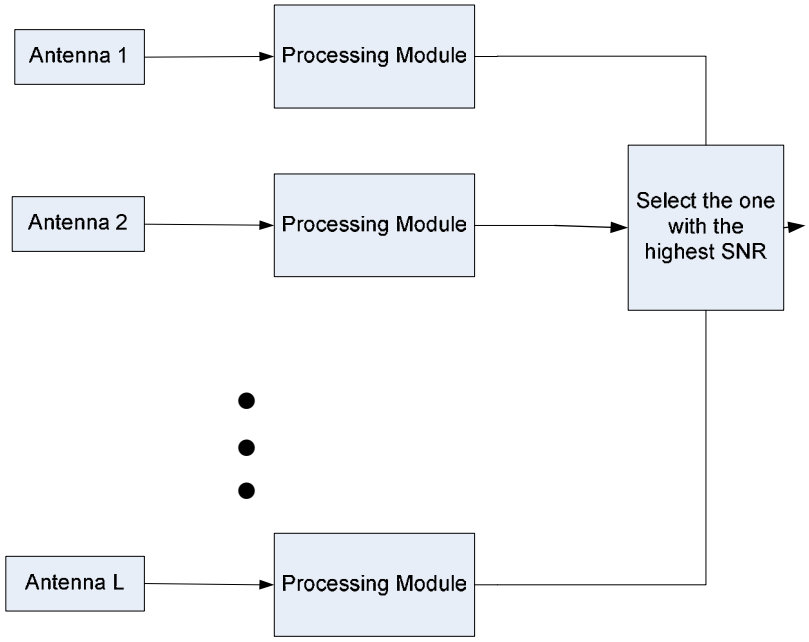

Figure 2-5: An L-branch selection combiner

2.4.3 Weighted combiner

In this method, the correlator outputs of each branch are multiplied by a weighting function to consider the quality of each branch, and then weighted branches are added together non-coherently. Therefore, branches with better qualities have higher shares in combined signal. The weights can be generated using different metrics. Nevertheless, SNR is the most sophisticated metric commonly utilized. The weighted combiner at the correlator outputs can be formulated as

$$x_W\left[\tau_i, \Delta f_j, n\right] = \sum_{l=1}^{L} \left| w_l(n) x_l\left[\tau_i, \Delta f_j, n\right] \right|^2 \qquad \textbf{2-31}$$

where $x_W[\bullet]$ is the weighted combined correlator output and w_l is the weighting function for the *l*-th branch. Figure 2-6 presents a block diagram showing the weighted combining method's procedure for an *L*-branch diversity system.

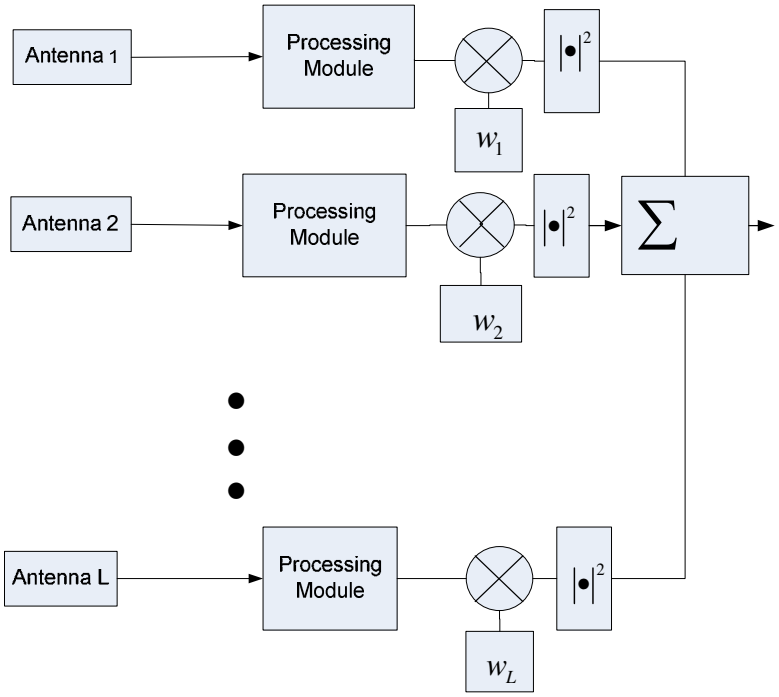

Figure 2-6 An *L*-branch weighted combiner

Chapter Three: INDOOR MULTIPATH GNSS CHANNEL CHARACTERIZATION

Channel characterization is known as the art of analyzing the behaviour of a wireless propagation channel through experiments. Here, the communication channel is treated as a black box with unknown transfer function and characteristics. The output of the channel is analyzed using pre-defined input signals such rectangular pulses or sinusoids at a pre-defined frequency to determine the channel input-output relationship (Jost & Wang 2009, Steingass & Lehner 2003). In this research, signals transmitted by GPS satellites are exploited to analyze indoor and dense multipath GPS channels. Exploitation of real GPS signals has two main advantages (i) the channel characterization situation matches the practical situation that a typical user may face indoors in terms of frequency band and signal strength (ii) test hardware for transmitting the test signal is eliminated. On the other hand, due to tremendous attenuation and fading, acquiring the GPS signal in the indoors is a significant challenge. To solve this problem, A-GPS technology is used, as described in the previous chapter. In an indoor GNSS communication link, the signal transmitted by a satellite vehicle experience path loss, atmospheric effects and time/space varying fading phenomena before arriving at the GNSS antenna. In this research work, it is of specific interest to characterize the indoor communication channel to determine the spatial and temporal correlation of the indoor channel in order to explore the possibility of establishing an effective diversity scheme. For the aim of this research several metrics are analyzed namely (i) temporal and spatial correlation coefficients, (ii) joint signal strength distribution and (iii) signal amplitude statistics.

3.1 Characterization methodology

Indoor GNSS signal reception in multipath environments is degraded by signal attenuation and fading. Signal attenuation is accrued due to propagation through building materials up to 30 dB with respect to line-of-sight signals (Hu et al 2007). In indoor wireless GNSS links, the signal typically propagates from satellites to a receiver over reflective paths with a random variation in the amplitude of the received complex signal called fading. Acquiring GNSS signals in such environments is itself a challenge. In order to overcome these limitations, several approaches have been described in the literature to characterize the GPS communication channel. Existing GPS characterization methods to overcome signal attenuation and fading can be classified into three groups (Satyanarayana 2011):

- **Off-the-shelf high sensitivity receivers**: There are several commercially available high sensitivity receivers capable of tracking weak GPS signals. Some of them are capable of tracking signals of the order of -160 dBm. Utilization of an off-the-shelf technology eases up the channel characterization methodology. On the other hand, there are several disadvantages associated with adopting these technologies. First, using a commercial receiver, only metrics provided by the manufacturer can be analyzed. Second, typically this type of receivers needs to be initiated outdoors. At last and not least, the measurements made with these receivers in highly attenuated environments are very noisy, which might negatively influence the characterization.
- **Pseudolites and channel sounding**: In this method, pseudo-satellite transmitters capable of broadcasting GPS-like signals, called pseudolites, are used. Pseudolites

use very high gain transmitters in order to overcome the high level of attenuation caused by building materials (Jost & Wang 2009). Here GPS-like transmitters are placed outside the building on either a fixed pole or a crane. The high level of SNR results in accurate measurements, which is the main advantage of this method. Very expensive equipment is the main disadvantage of this method. Beside this primary disadvantage, the frequency band and signal shape are slightly different from real GPS specifications.

- **A-GPS**: In this method, a pair of synchronized receivers is utilized. Here, the first receiver (reference) is placed in an open sky environment nearby the second receiver, which is placed in a harsh environment. An aiding package extracted from the reference receiver enables the indoor process to extend the coherent integration time to hundreds of ms. (Peterson et al 1997, Lakhzouri et al 2005). The theoretical and practical considerations associated with this method were elaborated in the previous chapter.

Considering the cons and pros of these approaches, the reference-rover approach is opted for this research work.

3.2 Correlation coefficient

Antenna diversity techniques are established based on receiving statistically independent signals on each diversity antenna denoted as a diversity branch (Sadrieh et al 2010). Hence, the level of independency of branches should be evaluated in order to establish an effective diversity scheme. Correlation coefficient can be used as a metric to explore the

possibility of establishing an effective diversity system in different fading environments (Broumandan et al 2010, Colburn et al 1998). The correlation coefficient is a metric representing the correlation of two random variables as a function of time or space. In the following section, a brief review of the correlation coefficient theoretical background is first presented then theoretical findings are examined by experimental tests.

3.2.1 Correlation coefficient theoretical background

The correlation coefficient between two received signals can be characterized by using either the envelope or complex forms of the input signals. Assuming that the received signals have a Rayleigh distributed envelope and uniformly distributed phase, the envelope and complex correlation coefficients are associated to each other as (Gao 2007)

$$\left|\rho_c\right|^2 = \rho_e \,. \qquad \textbf{3-1}$$

Narayanan et al (2004) quantify both complex and envelope correlation coefficient and report an approximately similar behaviour for both complex and envelope correlation coefficients. The complex and envelope correlation coefficients of two complex random variables can be expressed as follows (Colburn et al 1998):

$$\rho_c = \frac{\mathrm{E}\left[x_1 x_2^*\right]}{\sqrt{\mathrm{E}\left[x_1 x_1^*\right]\mathrm{E}\left[x_2 x_2^*\right]}} \qquad \textbf{3-2}$$

$$\rho_e = \frac{\mathrm{E}\left[e_1 e_2\right]}{\sqrt{\mathrm{E}\left[e_1^2\right]\mathrm{E}\left[e_2^2\right]}} \qquad \textbf{3-3}$$

where $E[\bullet]$ is the expected value operator, x_1 and x_2 represent two complex zero mean random variables. e_1 and e_2 are the zero-mean envelope of x_1 and x_2 respectively. In most previous research (e.g. Colburn et al 1998, Dietrich et al 2001), x_i vectors are extracted from different antennas that are separated by a specific distance. Hence, the calculated correlation coefficient is representing the corresponding correlation coefficient of that distance. With this method, the correlation coefficient is calculated only for a specific distance. Hence, for calculation of correlation coefficients for several distances, the data collection should be repeated with different antenna spacings. These repetitions can be very time consuming. In the GNSS case, this procedure not only is time consuming but is not feasible since satellites are visible for a limited time. Herein, in order to mitigate these practical problems another method is considered whereby x_i vectors are extracted for a single antenna with certain time shifts. These shifts can be interpreted as either a time shift for the static antenna or a spatial/temporal shift for the moving antenna. By applying this method to a moving case, both spatial and temporal de-correlations will be sensed together but in static case, only temporal de-correlation will be measured. Using this method, the complex correlation coefficient can be written as

$$\rho_c(lT) = \frac{\mathrm{E}\left[x_1[\mathbf{k}] x_1^*[\mathbf{k}-l] \right]}{\sqrt{\mathrm{E}\left[x_1[\mathbf{k}] x_1^*[\mathbf{k}] \right] \mathrm{E}\left[x_1[\mathbf{k}-l] x_1^*[\mathbf{k}-l] \right]}} \qquad \textbf{3-4}$$
$$\mathbf{k} = [l+1, l+2, ..., N]$$

where T is the coherent integration time, lT is the time shift to be assessed and N is the number of epochs. Hence, TN is the total observation time. This approach can be expanded for the envelope correlation coefficient as follow

$$\rho_c(lT) = \frac{\mathrm{E}\left[e_1[\mathbf{k}] e_1[\mathbf{k}-l] \right]}{\sqrt{\mathrm{E}\left[e_1[\mathbf{k}] e_1[\mathbf{k}] \right] \mathrm{E}\left[e_1[\mathbf{k}-l] e_1[\mathbf{k}-l] \right]}} \qquad \textbf{3-5}$$
$$\mathbf{k} = [l+1, l+2, ..., N]$$

.

Considering the fact that both e_1 and x_1 are zero mean, the dominator in Eq. 3-4 and Eq. 3-5 can be replaced by the variance of x_1 and e_1 respectively. Thus, Eq. 3-4 and Eq. 3-5 can be reduced to

$$\rho_c(lT) = \frac{\mathrm{E}\left[x_1[\mathbf{k}] x_1^*[\mathbf{k}-l] \right]}{\mathrm{var}(x_1)} \qquad \textbf{3-6}$$
$$\mathbf{k} = [l+1, l+2, ..., N]$$

$$\rho_c(lT) = \frac{\mathrm{E}\left[e_1[\mathbf{k}] e_1^*[\mathbf{k}-l] \right]}{\mathrm{var}(e_1)} \qquad \textbf{3-7}$$
$$\mathbf{k} = [l+1, l+2, ..., N]$$

.

Assuming a Rayleigh faded environment and uniformly distributed angles of arrivals, Broumandan (2009) has quantified the spatial correlation coefficients as a function of the antenna separation over wavelength with angle spread of ϕ and mean of incident of θ as shown in Figure 3-1.

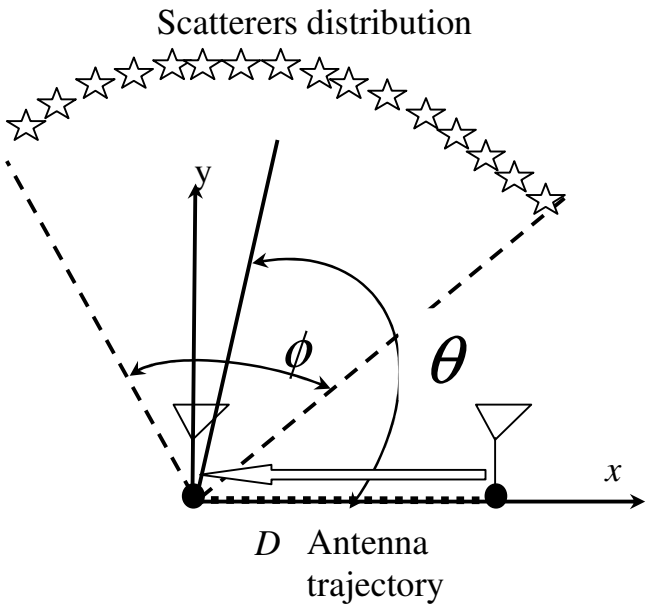

Figure 3-1: Antenna trajectory with respect to scatterers distribution

Figure 3-2 shows the correlation coefficient for some sample combinations of ϕ and θ. Note that for $\phi = 360^{o}$, the assumptions will match the assumptions of Clark's rings of scatterers (Van trees 2002). Here, the complex correlation coefficient for the rings of scatterers model is written as

$$\rho_c = \mathrm{J}_0\left(\frac{2\pi D}{\lambda}\right) \qquad \textbf{3-8}$$

where $\mathrm{J}_0(\bullet)$ is the zero-order Bessel function of the first kind and D is the separation of two branches. It is observable from Figure 3-2 that complex correlation will drop to zero with less than half a wavelength separation of branches.

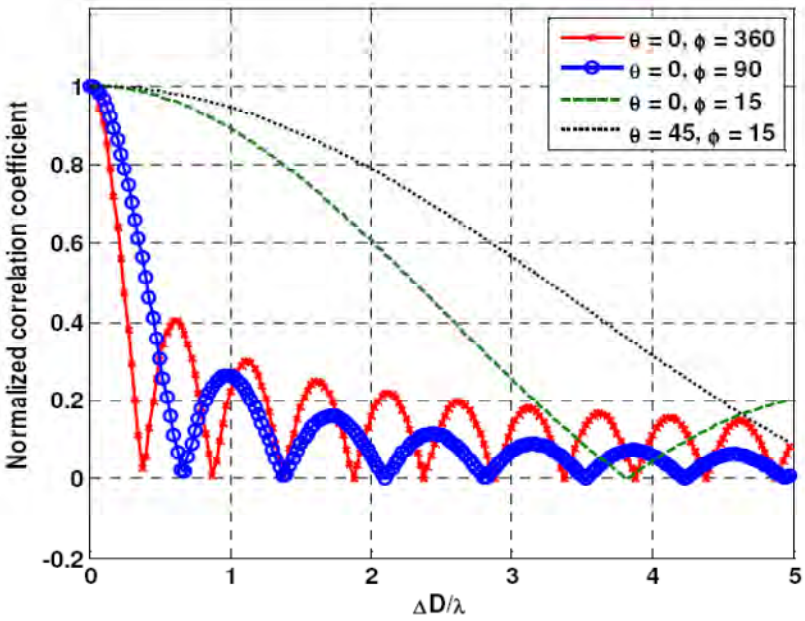

Figure 3-2: Correlation coefficient for some sample combinations of ϕ and θ

Another parameter that can affect the correlation coefficient is the presence or absence of a dominant path (e.g. LOS). Having a dominant path, Rayleigh distribution assumption will not be valid anymore and the Rician distribution can be assumed instead. In such cases, higher correlation with respect to Rayleigh distributed cases will be expected.

3.2.2 Empirical measurement setup

Data collections were performed in three different environments, namely a typical North American wooden frame house, a laboratory with concrete walls and a large workshop. Figure 3-3 shows the data collection locations and settings.

During data collections, an active GPS antenna was mounted on a moving table to collect spatial/temporal raw GPS data samples. In addition to the moving antenna, another antenna was placed near the same location to collect static GPS data samples. An outdoor reference antenna was also used to collect open sky GPS samples. In each data set, GPS

L1 C/A signals of all three aforementioned antennas were captured by a National Instruments ^{TM} (NI) PXI-5661 system composed of three front-ends, able to operate in a synchronous mode. More details of the data collection settings are presented in Table 2. Sixteen-bit digitized samples from the front-end were stored in an external hard drive and post-processed with the University of Calgary reference-rover GNSS software receiver (GNSRx-rr^{TM}). The detailed processing method was presented in Chapter 2.

(a) **(b)**

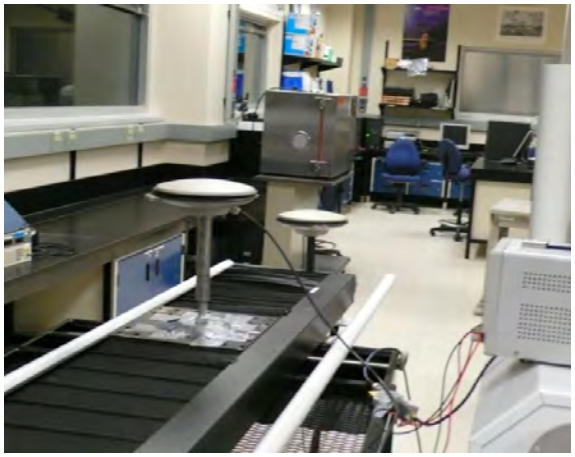

(c)

Figure 3-3: Data collection locations and setup (a) Wooden frame house (b) Workshop (c) Laboratory

Table 2: Data collection setting

Data set	Data set name	Type of building	available PRNs	Speed of moving antenna	Coherent integration time
1	Wooden frame house	Wooden	5,15,16,18, 21,24, 29	4 cm/s	100 ms
2	Laboratory	Concrete	18, 21, 26	2 cm/s	200 ms
3	Workshop	Concrete	2, 4, 12, 30	2 cm/s	200 ms

3.2.3 Spatial versus temporal coefficient

As mentioned before, the static antenna experienced temporal de-correlation and the moving antenna experienced both temporal and spatial de-correlation. Hence, correlation coefficient measurements extracted from the static antenna are only representing the temporal characterization of the fading channel whereas the correlation coefficient measurements of the moving antenna express the joint temporal/spatial characteristics. Comparing the temporal and spatial/temporal de-correlations can provide a valuable

insight into spatial de-correlation. Figure 3-4: shows the complex and envelope correlation coefficient of a sample PRN in the wooden frame house.

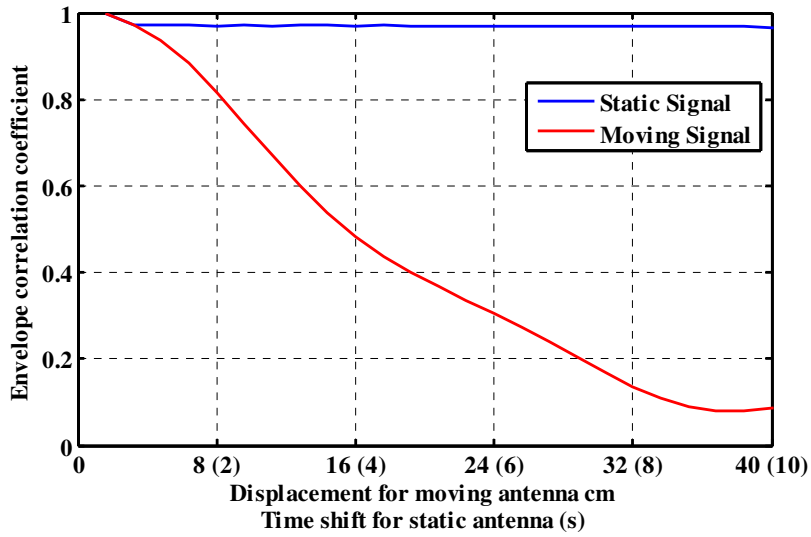

(a)

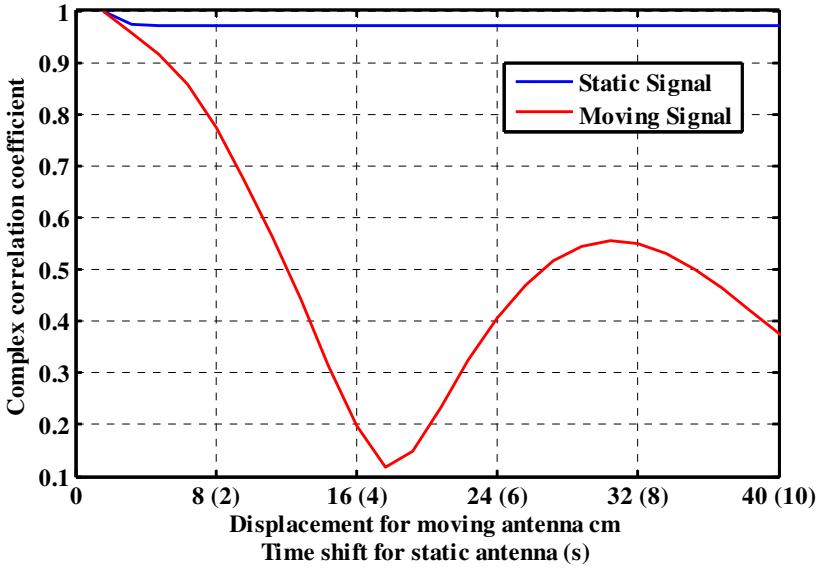

(b)

Figure 3-4: (a) Envelope and (b) Complex correlation coefficient of PRN 5 in the wooden frame house

Figure 3-5 shows the complex and envelope correlation coefficient of a sample PRN in the laboratory with concrete walls and ceiling.

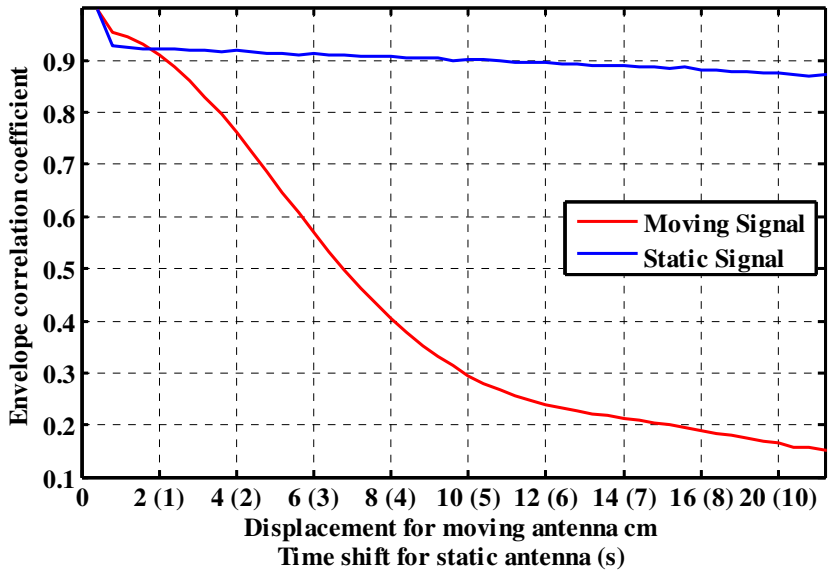

(a)

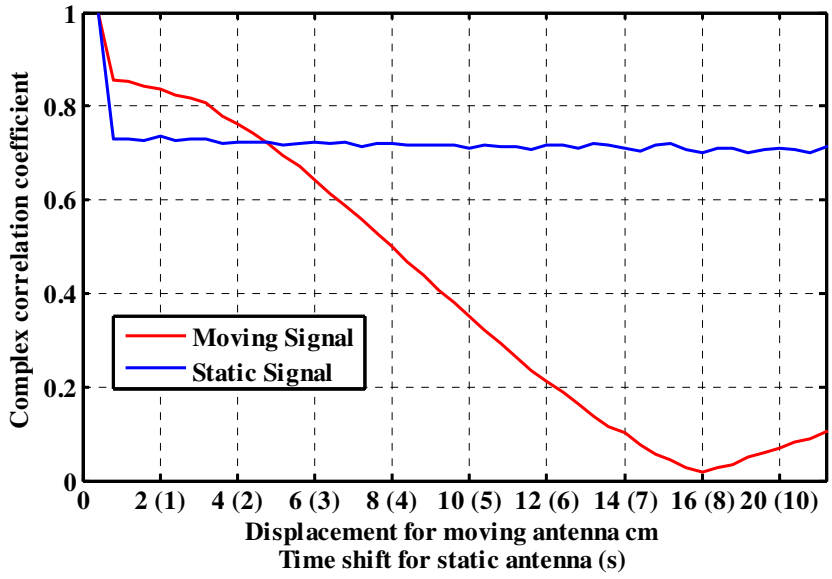

(b)

Figure 3-5: (a) Envelope and (b) Complex correlation coefficient of PRN 18 in the laboratory

In both locations and for both complex and envelope correlation coefficients, temporal de-correlation is significantly lower than joint spatial/temporal de-correlation. Hence, the temporal de-correlation effect can be ignored with respect to the spatial de-correlation.

3.2.4 Noise effect of correlation coefficient measurements

It is expected that the correlation coefficient for the smallest time shift (100 ms; l=1 and T=100 ms) remains approximately unity especially for the static antenna. However, a significant drop of correlation coefficient measurements for all PRNs in all locations with the smallest non-zero shift is observed (e.g. Figure 3-4: and Figure 3-5). This drop is more significant in the low SNR situations (e.g. Figure 3-5 in the laboratory). Considering the signal model, the correlator output consists of both signal and noise components:

$$x_1 = s_1 + v_1 \qquad \textbf{3-9}$$

where s_1 represent the signal component of the correlator output and v_1 is its noise component. Replacing Eq. 3-9 in Eq. 3-7, the correlation coefficient measurement can be expressed as

$$\rho_c^p(lT) = \frac{E\left[s_1[\mathbf{k}]s_1^*[\mathbf{k}-l]\right] + E\left[v_1[\mathbf{k}]v_1^*[\mathbf{k}-l]\right]}{E\left[s_1[\mathbf{k}]s_1^*[\mathbf{k}]\right] + E\left[v_1[\mathbf{k}]v_1^*[\mathbf{k}]\right]} \qquad \textbf{3-10}$$
$$\mathbf{k} = [l+1, l+2, ..., N]$$

where ρ_c^p is the measured complex correlation coefficient and lT is the time shift. Since v_1 is modeled as a white random variable, $E\left[v_1[\mathbf{k}]v_1^*[\mathbf{k}-l]\right]$ will be zero for every non-zero shifts. In the case of l=0, Eq. 3-10 results in unity whereas due to presence of

additive noise term in the denominator, the measured correlation coefficient values drops for non-zero shifts. This degradation can be modeled by a scale factor as

$$\rho_c^p = \rho_c^r \left[\frac{1}{\left(1+\left(\frac{\mathrm{var}(v)}{\mathrm{var}(s_1)}\right)\right)} \right] = \rho_c^r \left[\frac{1}{\left(1+\frac{1}{PSNR}\right)} \right] \qquad \textbf{3-11}$$

where ρ_c^r is the complex correlation coefficient in the ideal noiseless situation, which is actually of interest, and *PSNR* is the correlator output's signal to noise ratio, called Post-SNR. Figure 3-6 shows the measured complex correlation coefficients of the smallest time shift as a function of their measured SNR for different PRNs in different data sets for static antenna. The scale factor proposed by Eq. 3-11 is also overlaid, to enhance the comparison.

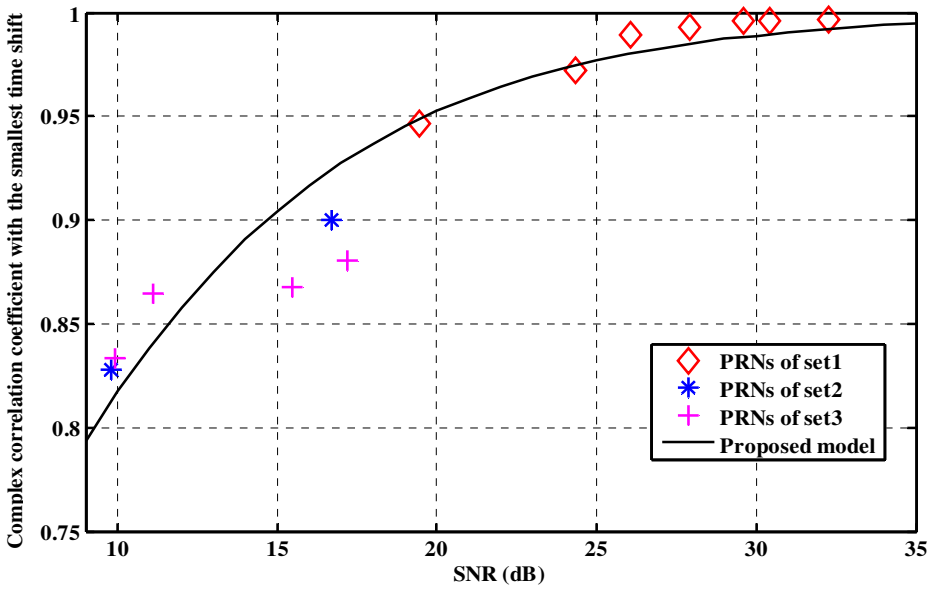

Figure 3-6: Correlation coefficient of the smallest time shift as a function of their measured SNR and the proposed scale factor

It can be concluded from Figure 3-6 that the scale factors proposed by Eq. 3-11 can justify the correlation coefficient drop for the smallest time shift. Having a reliable Post-SNR estimator, the noise effect can be modeled and removed. Hence, pure spatial or temporal correlation may be analyzed. Figure 3-7 shows the correlation coefficients for a sample PRN in the laboratory with the corresponding rescaled values.

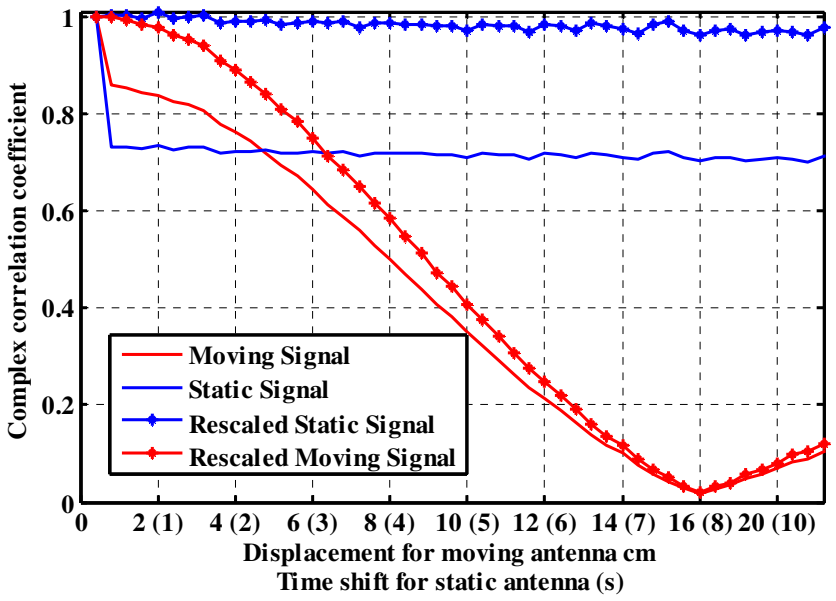

Figure 3-7: Correlation coefficients for PRN 18 in the laboratory with the rescaled correlation coefficients

3.2.5 Spatial correlation coefficient

As discussed previously the temporal de-correlation, provided by a few seconds of time shift, is negligible with respect to the spatial one. Hence, all de-correlations experienced by the moving antenna can be associated with spatial de-correlation and noise. Since the noise effect can be modeled and removed using Eq. 3-11, the spatial de-correlation due to the antenna displacement can be computed accordingly. Assessment of spatial correlation

is the ultimate aim of channel characterization in order to determine the possibility of establishing a spatial diversity system on a handheld device. In order to carry out this assessment, both the complex and envelope correlation coefficients for two different spatial spacings, namely (i) 5 cm and (ii) 10 cm, will be assessed. Considering the GPS L1 wavelength these spacing are approximately equal to a quarter and half of a wavelength, respectively. In the following parts, complex and envelope correlation coefficient measurements of all PRNs in all data sets for 5 cm and 10 cm spacings are provided.

3.2.5.1 Correlation coefficient measurements with 5 cm spacing

Figure 3-8 shows the envelope and complex correlation coefficients of all available PRNs in different locations for 5 cm spacing. The complex correlation coefficients remain above 0.5 even in harsh multipath environments such as a workshop and a laboratory. In the envelope case, the de-correlation is more significant especially in harsh environments. In the workshop, the envelope correlation coefficient goes down to 0.3, which shows sufficient de-correlation for implementing an efficient diversity scheme.

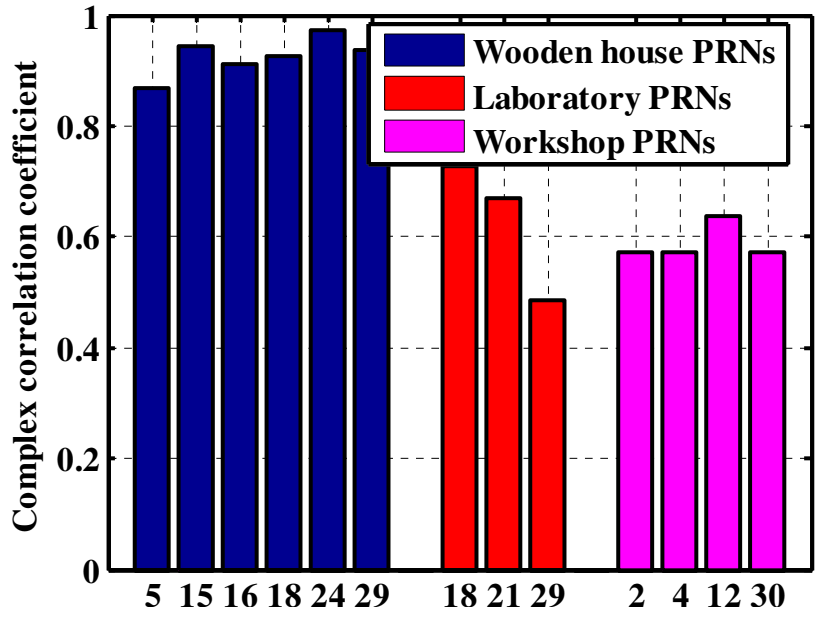

(a)

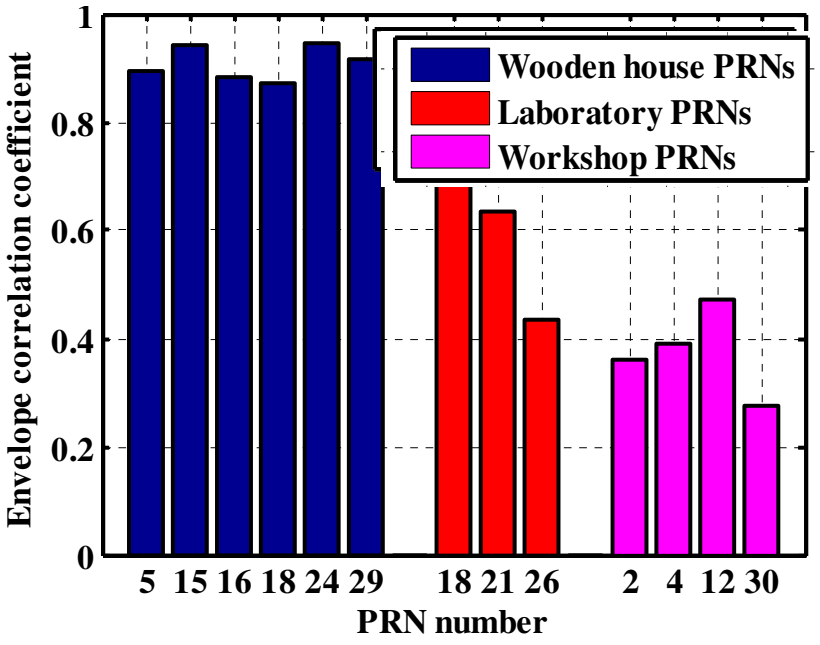

(b)

Figure 3-8 Complex correlation coefficients for different PRNs in three different locations for 5 cm spacing

3.2.5.2 Correlation coefficients with 10 cm spacing

In Figure 3-9, the complex and envelope correlation coefficient measurements for different PRNs with a 10 cm antenna separation are shown.

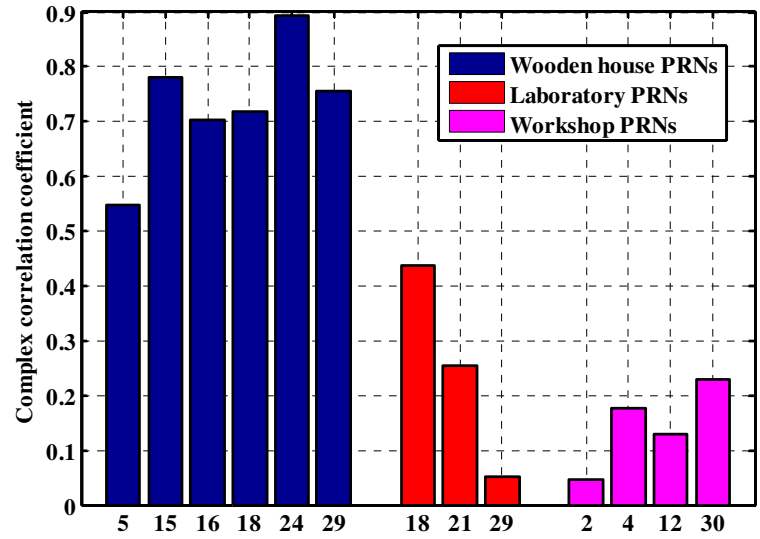

(a)

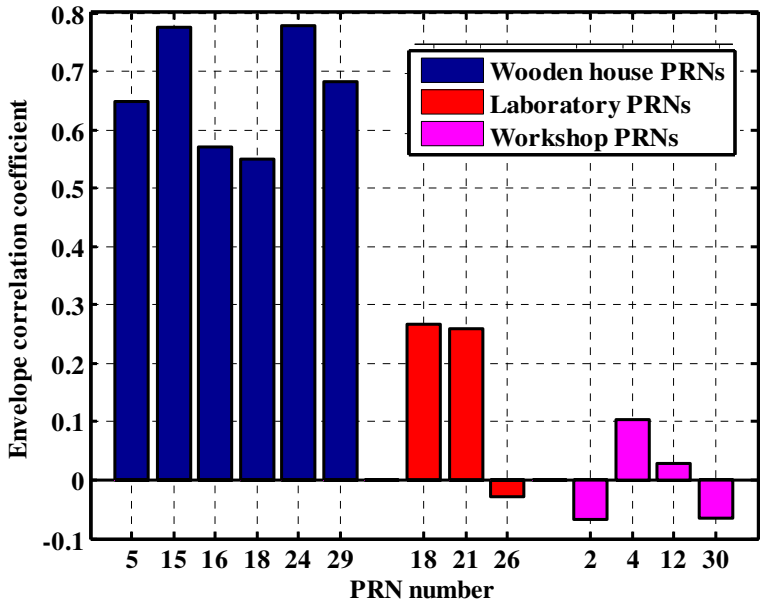

(b)

Figure 3-9 Envelope correlation coefficients of all the available PRNs in all the locations for 10 cm spacing

As shown in Figure 3-9, both complex and envelope correlation coefficient measurements degrade with an approximately half a wavelength spacing in harsh environments whereas in the wooden frame house case, the correlation coefficients are still significant. These observations support well the theoretical findings, which predict a significant de-correlation by half a wavelength spacing for Rayleigh faded environments with the ring of scatterers model.

3.3 Joint distribution of signal strength

Although correlation coefficients effectively characterize the correlation level of two random variables and are widely used in literature, the joint distribution of signal amplitude or signal strength can better visualize their independency and/or correlation. Figure 3-10 shows the joint distribution of measured C/N_0 values of two antennas spatially separated by 3 cm in the laboratory.

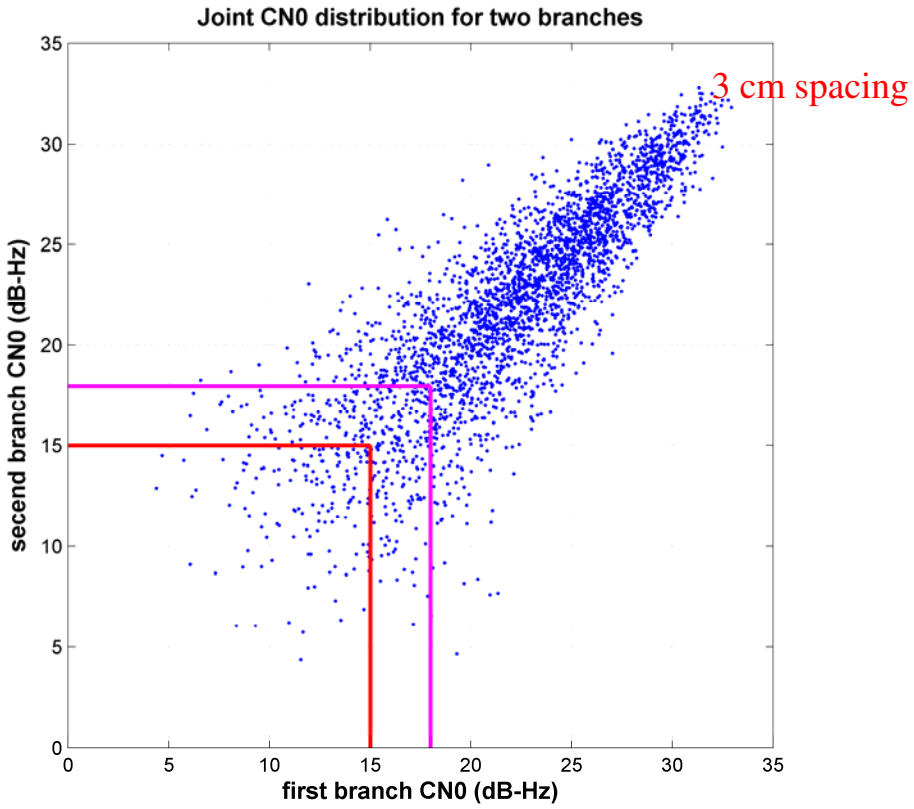

Figure 3-10: Joint distribution of signal strengths of two antennas spatially separated by 3 cm in the laboratory

It can be observed from Figure 3-10 that the two branches are significantly correlated to each other. Although the figure does not quantify the correlation level between branches, it provides a valuable insight into the correlation of branches. Figure 3-11 shows the corresponding results for branches with 9 cm spacing.

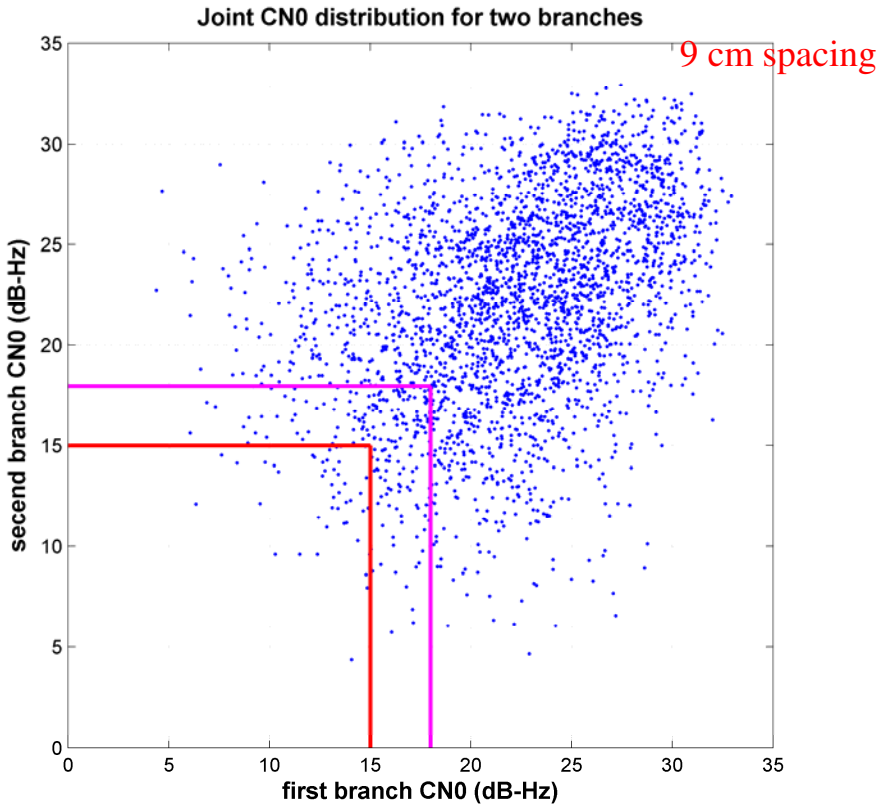

Figure 3-11: Joint distribution of signal strengths of two antennas spatially separated by 9 cm in the laboratory

It can be observed from Figure 3-11 that C/N_0 of two branches with 9 cm spacing is fairly independent. Again, the joint distribution does not quantify the level of independency and simply visualize the independency of branches.

3.4 Signal amplitude statistic

As shown previously the correlation coefficient measurements in the laboratory and the workshop follow the theoretical values provided by Eq. 3-8, whereas the correlation coefficients of the available PRNs in the wooden frame house do not follow the aforementioned values. One of the effective parameters on the correlation coefficient

measurements is the presence or absence of Line Of Sight (LOS) signal component or any dominant component.

The theoretical values shown for the correlation coefficient are based on the Rayleigh fading model in the absence of LOS or any dominant signal component. Thus, in the presence of LOS or any dominant signal, the aforementioned theoretical values are no longer appropriate. In this section, the signal distribution of a sample PRN in each location is analysed. Comparing the signal distribution with Rayleigh and Rician and normal distributions, a valuable insight about the presence or absence of LOS in each location is provided. Rician PDF describes the multipath fading signal distribution in the presence of a dominant path. A Rician PDF will reduce to a Rayleigh PDF if a dominant path is not present. On the other hand, if multipath energy is negligible with respect to the dominant path's energy, a Rician PDF can be approximated by a Normal distribution.

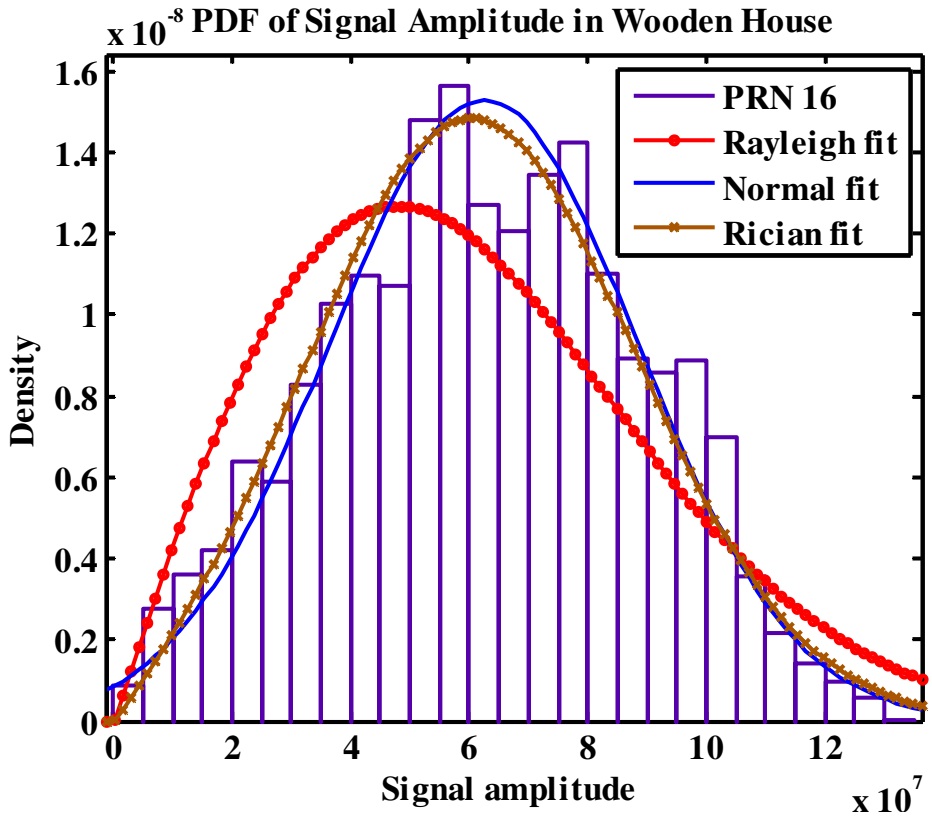

Figure 3-12: PDF of signal amplitude in wooden frame house and three different fits

Observations from Figure 3-12 are as follows:

1- The Rayleigh model is not a suitable fit for signal amplitude distribution in this case. Hence, theoretical values for the correlation coefficient provided by Eq. 3-8, which is calculated based on a Rayleigh distributed signal, are not appropriate for the wooden frame house situation.

2- The significant discrepancy between Rayleigh and Rician fits and the similarity of Rician and normal fits indicate the presence of a dominant path (probably the LOS signal).

Figure 3-13 and Figure 3-14 show the same plot for the laboratory and workshop respectively. In contrast with the wooden frame house case, it is visible from these figures that the Rayleigh distribution fits the signal amplitude distribution well. The similarity of Rayleigh and Rician fit indicates that there is not any significant LOS component in the laboratory or workshop locations.

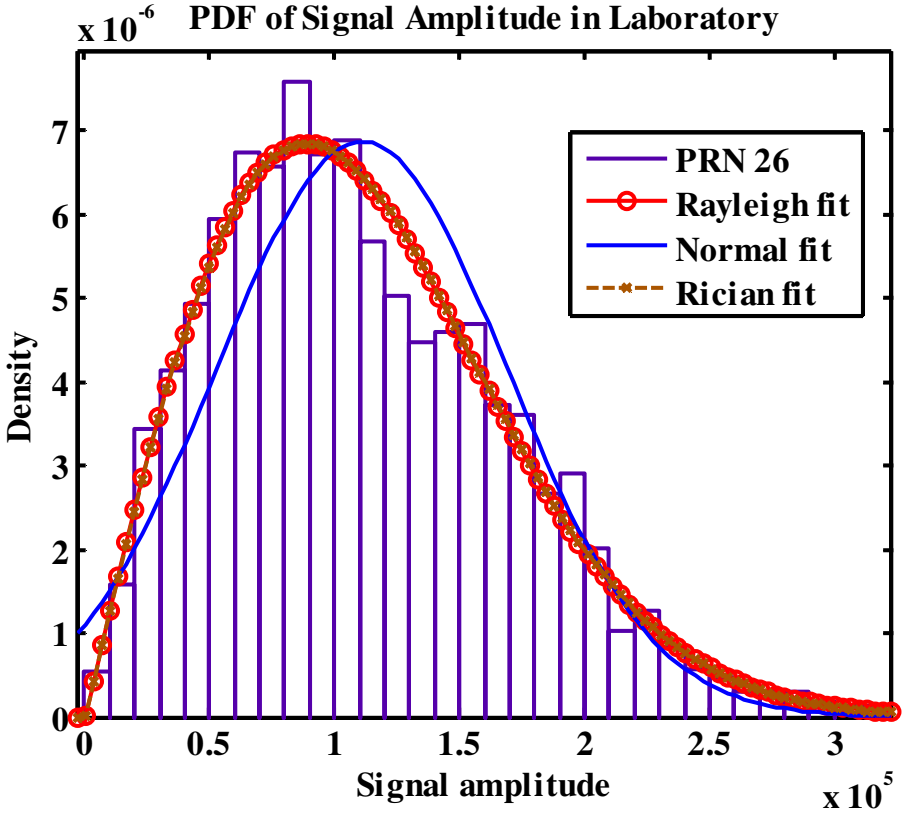

Figure 3-13 PDF of signal amplitude in the laboratory and three different fits

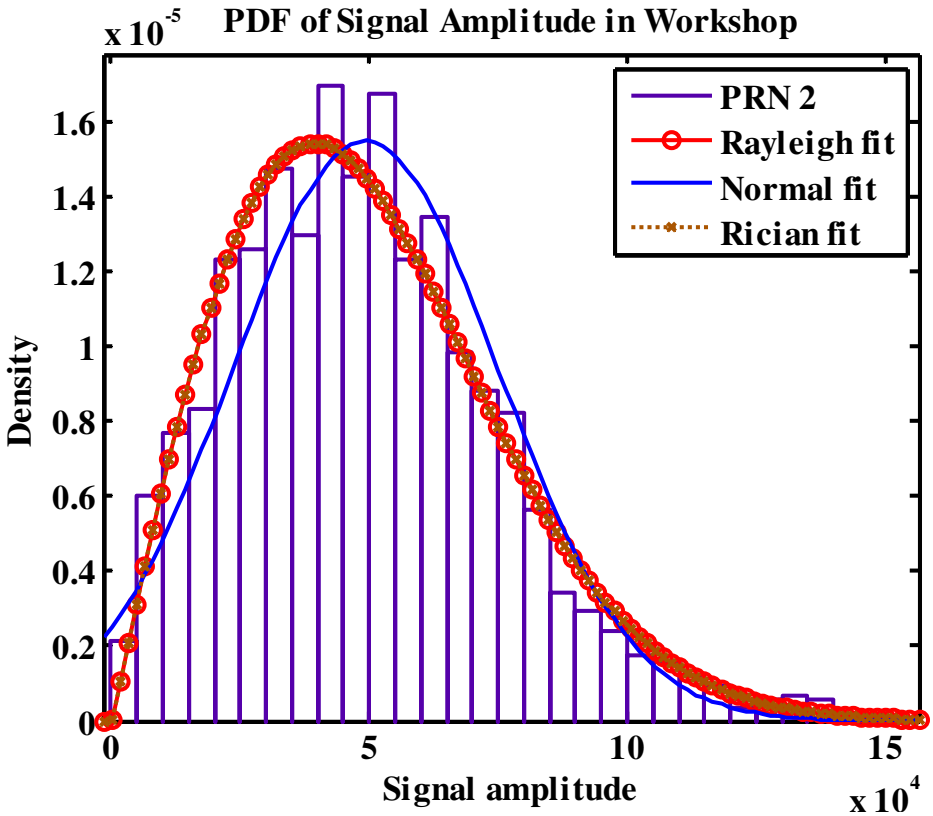

Figure 3-14: PDF of signal amplitude in the workshop and three different fits

3.5 Conclusions

In this chapter, the spatial/temporal indoor GNSS channel characterization based on measuring correlation coefficients was analyzed. After a theoretical background review, empirical complex and envelope correlation coefficients were measured in three different indoor environments. Temporal and joint temporal and spatial de-correlation for a static and a moving antenna were evaluated. The effect of noise on scaling the correlation coefficients was mathematically analyzed. Based on these analyses, a scale factor to remove the effect of noise on correlation coefficient measurements was proposed and tested. As shown in the static antenna cases, signals remain highly correlated during the observation time. However, signal de-correlates considerably faster spatially. Hence, all

de-correlation experienced by the moving antenna can be associated with spatial de-correlation. By modeling and removing the noise effect on correlation coefficients, the pure spatial de-correlation is analysed in three environments. It was shown that in harsh multipath Rayleigh faded environments, signals received by antennas separated by ½ wavelength become approximately uncorrelated. However, for cases with a dominant signal path (e.g. wooden frame house), received signals that are spatially separated by half a wavelength remain considerably correlated.

Chapter Four: DETECTION PERFORMANCE OF THE SPATIAL ANTENNA SYSTEM

As discussed in the previous chapter, antennas with half wavelength spacing capture independent signals. Combining these independent receptions can enhance the receiver performance in acquiring satellites, estimating signal parameter and positioning. In this chapter, the detection performance of spatial diversity systems is assessed. The assessment is carried out both theoretically and empirically and by analyzing different metrics such as the deflection coefficients, ROC curve and satellite availability. The remainder of this chapter is organized as follows. Section 4.1 presents the different combining strategies. In Section 4.2, the theoretical background of combining methods is reviewed and a practical method is introduced. In Section 4.3, performance of diversity system composed of spatially separated antennas is assessed through two experiments in different indoor locations.

4.1 Combining strategies

Having collected independent GPS signals by spatially separated antennas, the problem of interest is to combine them. Signal of diversity branches can be combined at different stages, namely correlator outputs, measurement and position level (Sadrieh et al 2012). Figure 4-1 shows a GNSS receiver block diagram and three different stages at which signal from multiple antennas can be combined. In the following part, these stages will be briefly introduced.

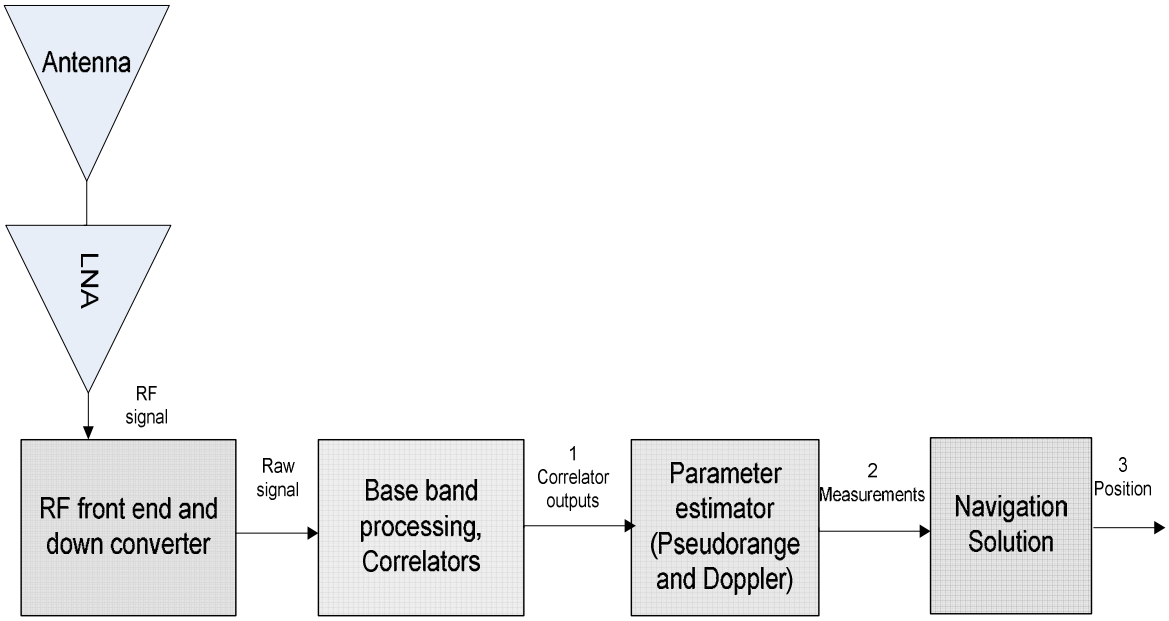

Figure 4-1: Three different stages at which signal of multiple antennas can be combined

1- **Correlator outputs**: At the correlator output level, the corresponding correlator outputs of diversity branches are combined to enhance detection, parameter estimation and navigation solution performance. Recalling the correlator outputs introduced in Eq. 2-24, a general diversity method for a *M*-branch diversity system at the correlator output level can be formulated as

$$x_D\left[\tau_i,\Delta f_j,n\right]=f(x_1\left[\tau_i,\Delta f_j,n\right],x_2\left[\tau_i,\Delta f_j,n\right],...x_M\left[\tau_i,\Delta f_j,n\right]) \qquad \textbf{4-1}$$

where $x_D\left[\tau_i,\Delta f_j,n\right]$ is the combined correlator output, $x_l\left[\tau_i,\Delta f_j,n\right]$ is the *l*-th diversity branch correlator output (i.e. 1, 2,…, *M*), *n* represents the processing epoch number and *M* is the number of diversity branches. *f* is an arbitrary function to be designed.

2- **Measurement level**: At the measurement level, individual branches detect the received signal and estimate the signal parameters (i.e. code phase and Doppler frequency). Then the estimated parameters are passed to the combining unit. Recalling the estimated parameters introduced by Eq. 2-25, the diversity method for a *M*-branch diversity system at the measurement level can be formulated as

$$\left(\Delta\hat{f},\hat{\tau}\right)_n^C = f\left(\left(\Delta\hat{f},\hat{\tau}\right)_n^1,\left(\Delta\hat{f},\hat{\tau}\right)_n^2,...,\left(\Delta\hat{f},\hat{\tau}\right)_n^M\right) \qquad \textbf{4-2}$$

where $\left(\Delta\hat{f},\hat{\tau}\right)_n^C$ represents the combined measurements, and $\left(\Delta\hat{f},\hat{\tau}\right)_n^l$ represents the measurements extracted from the *l*-th diversity branch. The combined measurements will be consequently used in the navigation solution. Combining at the measurement level can enhance system performance at the measurement and position levels.

3- **Position level**: At the position level, individual branches detect the received signal, estimate the signal parameters and establish their own navigation solution. Then estimated positions are passed to the combining unit to produce a combined position. Combining at the position domain for a *M*-branch diversity system can be formulated as

$$\begin{pmatrix}\phi\\ \lambda\\ h\end{pmatrix}_n^C = f\left(\begin{pmatrix}\phi\\ \lambda\\ h\end{pmatrix}_n^1,\begin{pmatrix}\phi\\ \lambda\\ h\end{pmatrix}_n^2,...,\begin{pmatrix}\phi\\ \lambda\\ h\end{pmatrix}_n^M\right) \qquad \textbf{4-3}$$

where ϕ represents the estimated latitude, λ is the estimated longitude and h the estimated height. $(\bullet)_n^C$ is the combined position of the n-th epoch and $(\bullet)_n^i$ is the position estimated by the i-th diversity branch of that epoch. Combining at the position level can enhance the positioning performance.

As alluded before, performance of combining methods can be assessed at different levels. Figure 4-2 shows the combining levels and their corresponding performance assessment scheme.

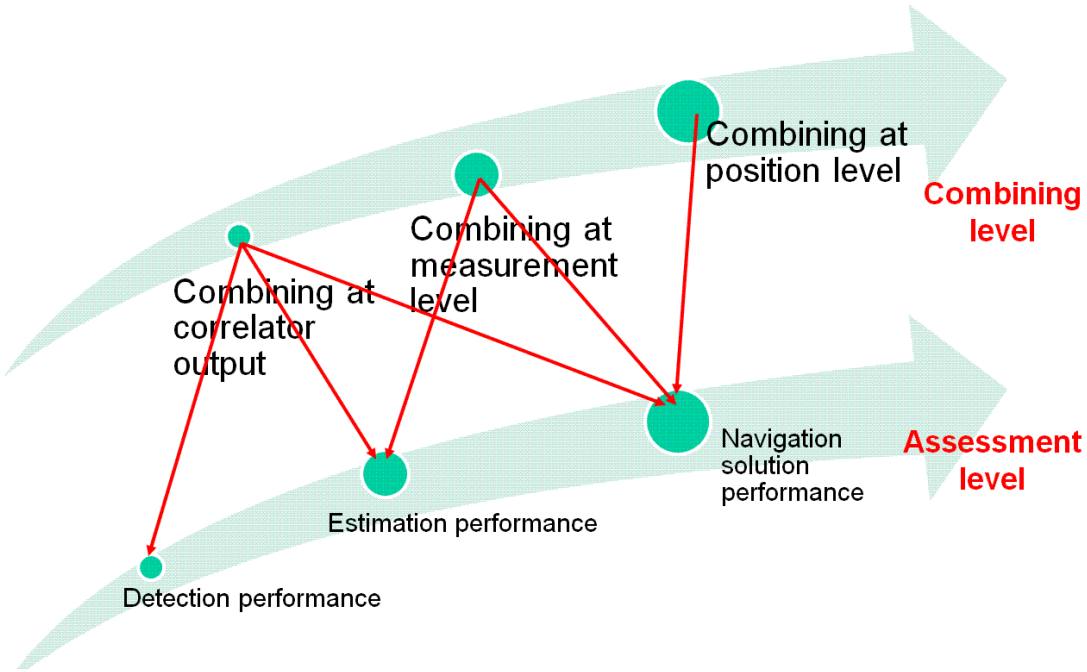

Figure 4-2: Combining levels and their corresponding assessment levels

Recalling the aim of this chapter, which is enhancement of the signal detection performance, herein the combining methods at the correlator outputs level are studied. Combining at the measurement level will be studied in Chapter 6.

4.2 Detection theoretical background

The cell level GPS signal detection problem can be formulated as a binary detection problem. Here, the detector includes two hypotheses, namely the null hypothesis and the alternative hypothesis, herein referred as H_0 and H_1 respectively. H_1 is the hypothesis in which the desired signal is present and H_0 represents the hypothesis in which the desired signal is not present. It should be noted that in the GPS case, since the signal of a satellite in view is always present, H_1 represents the hypothesis in which the received signal and local replica are synchronized and H_0 represents the hypothesis in which the received signal and local replica are not synchronized. The detection problem is to distinguish between these two conditions and make one of the following decisions:

D_0 : The decision that H_0 is true

D_1 : The decision that H_1 is true

As mentioned in Chapter 2, two types of errors may happen in the detector, namely deciding D_0 where the H_1 is the case (miss) and deciding D_1 where the H_0 is the case (false alarm). It is not possible to reduce both errors together. The appropriate approach in order to design an optimum detector is to keep the probability of false alarm fixed and reduce the probability of miss or equivalently increase the probability of detection. This approach is referred as the Neyman-Pearson approach (Kay 1998).

4.2.1 Likelihood Ratio Test (LRT)

Herein, in order to enhance the signal detection performance, the correlator outputs extracted from diversity branches will be combined. Hence, the observation vector contains the correlator outputs of *M* diversity branches as

$$\mathbf{x}=\left[x_1,x_2,...,x_M\right]^{\mathrm{T}}. \qquad \textbf{4-4}$$

where *M* is the number of diversity branches and x_i is the correlator output of the *i*-th diversity branch. Two possible hypotheses of binary detection can be listed as

$$\begin{aligned} H_1:&\quad \mathbf{x}=\mathbf{s}+\mathbf{n} \\ H_0:&\quad \mathbf{x}=\mathbf{n} \end{aligned}. \qquad \textbf{4-5}$$

where $\mathbf{s}$ is a $M\times 1$ vector containing the samples of the Complex Normal (CN) signal of $\mathbf{s}$. Herein, it is assumed that $\mathbf{s}$ is distributed as $CN\left(0,\mathbf{C_s}\right)$ where $\mathbf{C_s}$ is a $M\times M$ covariance matrix of $\mathbf{s}$. A complex normal signal distribution is widely assumed for signal distribution in dense multipath environments. More specifically, in the GNSS case, the complex normal assumption in harsh multipath environment was verified by Broumandan (2009). $\mathbf{n}$ is a $M\times 1$ vector containing samples of a complex normal white noise which are distributed as $CN\left(0,\sigma^2\mathbf{I}\right)$:

$$\begin{aligned} \mathbf{s}&=[s_1,s_2,...,s_M]^{\mathrm{T}} \\ \mathbf{n}&=[n_1,n_2,...,n_M]^{\mathrm{T}} \end{aligned} \qquad \textbf{4-6}$$

where s_i and n_i represents the signal and noise components of the *i*-th correlator output. In order to detect the presence of the signal of interest, the Likelihood Ratio Test (LRT) function is utilized. The detector yields to the D_1 decision if

$$L(x) = \frac{p(x;H_1)}{p(x;H_0)} > \gamma \qquad \textbf{4-7}$$

where $p(x;H_i)$ is the probability distribution function of *x* under the H_i condition and γ is the threshold for a given P_{fa} which can be calculated from

$$P_{fa}(\gamma) = \int_{x=\gamma}^{\infty} p(x;H_0)dx \qquad \textbf{4-8}$$

.

Considering that $\mathbf{s}$ is distributed as $CN(0,\mathbf{C_s})$ and $\mathbf{n}$ is distributed as $CN(0,\sigma^2\mathbf{I})$ and by assuming that $\mathbf{n}$ and $\mathbf{s}$ are independent, the signal distribution under H_1 and H_0 can be denoted as

$$\begin{aligned} p(x;H_1) &= CN(0,\mathbf{C_s}+\sigma^2\mathbf{I}) \\ p(x;H_0) &= CN(0,\sigma^2\mathbf{I}) \end{aligned} \qquad \textbf{4-9}$$

.

Inserting Eq. 4-9 in Eq. 4-7 and performing some manipulations, the test criterion can be formulated as

$$L(\mathbf{x}) = \mathbf{x}^H\mathbf{C_s}(\mathbf{C_s}+\sigma^2\mathbf{I})^{-1}\mathbf{x} \qquad \textbf{4-10}$$

.

In a general case, received signals from diversity branches may be correlated. In order to simplify the test criterion of Eq. 4-10, a system modal matrix of **V**, a $M \times M$ matrix composed of the eigenvectors of $\mathbf{C_s}$, is used to de-correlate the input signal:

$$\begin{aligned} \mathbf{y} &= \mathbf{V}^T \mathbf{x} \\ \mathbf{\Lambda_s} &= \mathbf{V}^H \mathbf{C_s} \mathbf{V} \end{aligned} \qquad \textbf{4-11}$$

where $\mathbf{y}$ is a $M \times 1$ vector. $\mathbf{\Lambda_s}$ is a $M \times M$ matrix where the diagonal elements are eigenvalues of $\mathbf{C_s}$ which is formed as

$$\mathbf{\Lambda_s} = \begin{bmatrix} \lambda_{s1} & 0 & \bullet & \bullet & \bullet & 0 \\ 0 & \lambda_{s2} & & & & 0 \\ \bullet & & \bullet & & & \bullet \\ \bullet & & & \bullet & & \bullet \\ \bullet & & & & \bullet & \bullet \\ 0 & 0 & \bullet & \bullet & \bullet & \lambda_{sm} \end{bmatrix}. \qquad \textbf{4-12}$$

Therefore, the covariance of **y** under the H_1 hypothesis can be calculated as

$$\begin{aligned} \mathbf{C_y} &= E\left[\mathbf{y}\mathbf{y}^H\right] = \mathbf{V}^T \mathbf{C_x} \mathbf{V} \\ &= \mathbf{V^H}\left(\mathbf{C_s} + \sigma_w^2 \mathbf{I}\right)\mathbf{V} \\ &= \mathbf{\Lambda_s} + \sigma_w^2 \mathbf{I} \end{aligned} \qquad \textbf{4-13}$$

.

After some manipulation [for more details refer to Kay (1998)], the test criterion in Eq. 4-10 can be written as

$$L(\mathbf{y} = \mathbf{V}^T \mathbf{x}) = \sum_{l=1}^{M} \frac{\lambda_{sl}}{\lambda_{sl} + \sigma_w^2} y_l^2 \qquad \textbf{4-14}$$

where λ_{sl} denotes the eigenvalue of the signal covariance matrix and σ_w^2 is the variance of the additive noise. This detector is known as the Estimator Correlator (EC).

4.2.2 Weighted combining method

Although in a general case received signals from different diversity branches can be correlated, herein by considering enough spacing between branches, in a dense multipath environments the received signals can be assumed to be uncorrelated. Hence, the covariance matrix will be a diagonal matrix as

$$\mathbf{C_s} = \begin{bmatrix} \lambda_{s1} & 0 & \bullet & \bullet & \bullet & 0 \\ 0 & \lambda_{s2} & & & & 0 \\ \bullet & & \bullet & & & \bullet \\ \bullet & & & \bullet & & \bullet \\ \bullet & & & & \bullet & \bullet \\ 0 & 0 & \bullet & \bullet & \bullet & \lambda_{sm} \end{bmatrix} \qquad \textbf{4-15}$$

where λ_{sl} represents the variance of signal components of the *l*-th diversity branch and can be replaced by σ_{sl}^2. Thus, Eq. 4-10 can be written as

$$L(\mathbf{x}) = \sum_{l=1}^{m} w_l x_l^2 \qquad \textbf{4-16}$$

where

$$w_l = \frac{\sigma_{sl}^2}{\sigma_{sl}^2 + \sigma_w^2} = \frac{SNR_l}{SNR_l + 1} \qquad \textbf{4-17}$$

where SNR_l is the signal to noise ratio of the *l*-th diversity branch. To generate the weights of Eq. 4-17, two approaches can be considered:

1- Using a limited number of samples to generate the weights and use the weights for the entire data. This approach is more suitable for stationary channels.

2- By utilizing an epoch-by-epoch SNR estimator, weights can be generated for each epoch. Although this approach induces more computational burden, it is more suitable for non-stationary multipath channels.

Herein, based on the non-stationary nature of indoor GNSS channel, the epoch-by-epoch approach is opted. In order to generate the weight vector, an epoch-by-epoch SNR estimator is utilized, which consists of separate signal and noise variance estimators. The signal power estimator takes L_1 consecutive complex correlator outputs observed over $T=L_1.T_c$ seconds denoted as

$$\left[x_1, x_2, ..., x_{L_1}\right]^T \qquad \textbf{4-18}$$

T is restricted by the coherence time of the channel. Considering the results presented in Chapter 3, T is set to 400 ms. The noise power estimator takes L_2 consecutive complex correlator outputs for a non-existing PRN, which represents the noise samples denoted as

$$\left[x_{ext,1}, x_{ext,2}, ..., x_{ext,L_2}\right]^T \qquad \textbf{4-19}$$

where $x_{ext,.}$ represents the correlator output of the non-existing PRN. Assuming the noise process to be stationary, L_2 may be set to greater than L_1 and yield a more accurate estimation of noise. Then the ML estimation of SNR is obtained as (Groves 2005)

$$SNR = \frac{\left(\left|\frac{1}{L_1}\sum_{k=1}^{L_1} x_k\right|\right)^2}{\frac{1}{2\left(L_2-1\right)}\sum_{m=1}^{L_2}\left|x_{ext,m}\right|^2} \qquad \textbf{4-20}$$

Although using the non-existing PRN correlator removes the signal component from the correlator outputs, some small signal components may still leak into the correlator outputs. This leakage is due to the non-zero cross correlation of PRNs. The small signal components, called residual biases, can affect the SNR estimator performance. Satyanarayana et al (2012) proposed a new method in order to alleviate the effect of residual biases in noise variance estimator. This modified estimator is referred as the Modified ML (MML) and formulated as

$$SNR = \frac{\left(\left|\frac{1}{L_1}\sum_{k=1}^{L_1} x_k\right|\right)^2}{\frac{1}{2(L_2-1)}\sum_{m=1}^{L_2}\left|x_{ext,i} - \frac{1}{L_2}\sum_{k=1}^{L_2} x_{ext,k}\right|^2} \qquad \textbf{4-21}$$

Herein, by setting T= 400 ms and experiencing C/N_0 values between 15-30 dB-Hz based on the analysis presented in (Satyanarayana et al 2012) the resultant SNR will be accurate within 2 dB for 95% of the time. Note that although in MML L_1 consecutive correlators are used, utilizing a sliding window approach, the update rate of SNR will be one per epoch. Figure 4-3 shows the SNR estimator block diagram [more details about the SNR estimator can be found in Satyanarayana et al 2012].

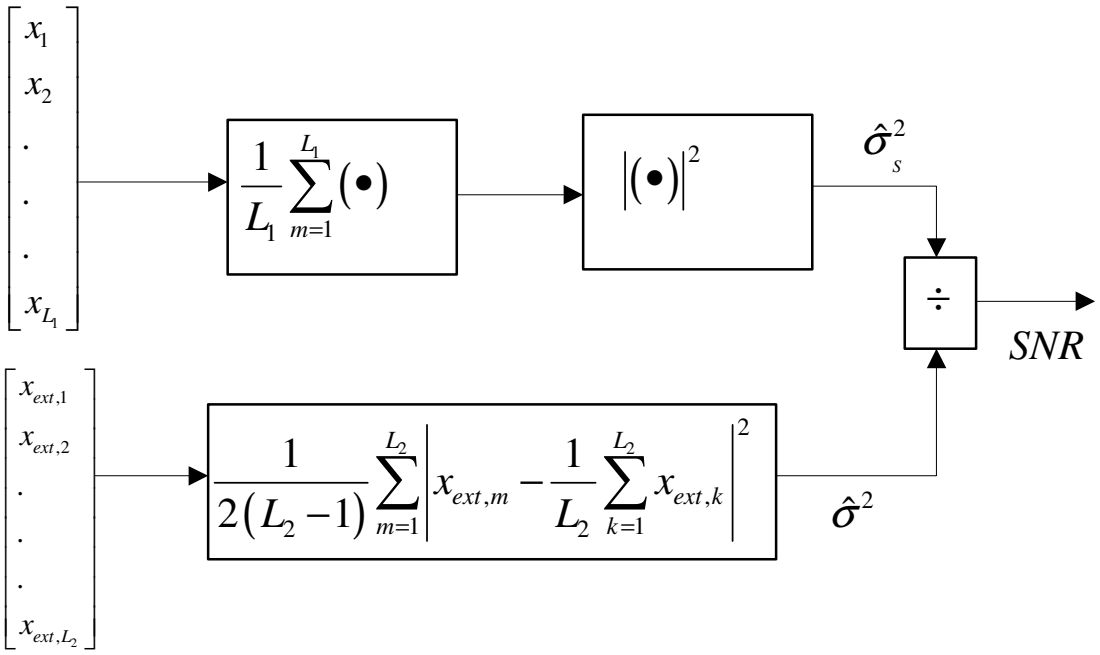

Figure 4-3: SNR estimator block diagram

Opting an epoch-by-epoch approach and utilizing the epoch-by-epoch SNR estimator the weights can be written as

$$w_l(n)=\frac{\sigma_{sl}^2(n)}{\sigma_{sl}^2(n)+\sigma_w^2(n)}=\frac{SNR_l(n)}{SNR_l(n)+1} \qquad \textbf{4-22}$$

where n is the epoch number, $SNR_l(n)$ represents the signal to noise ratio of the l-th diversity branch at the n-th epoch. Utilizing epoch-by-epoch weights, the combining method can be formulated as

$$T(\mathbf{x})=\sum_{l=1}^{m}\frac{\sigma_{sl}^2(n)}{\sigma_{sl}^2(n)+\sigma_w^2(n)}x_l^2(n) \qquad \textbf{4-23}$$

Herein, this method is called Weighted Combiner (WC).

4.3 Diversity performance assessment

In this section, the performance of the weighted combiner will be compared to the Equal Gain combiner (EGC) and Selection combiner (SC) as well as single branches. The comparison is carried out using real GPS L1 data collected in two indoor harsh environments.

4.3.1 Test setup

To assess the performance of diversity schemes two data collections were performed. The first data set was collected in a large workshop located in the CCIT building of the University of Calgary. The second data set was collected in a Laboratory in the same building. The building has concrete walls and metallic structure. Hence, both locations can be considered as extremely harsh multipath and highly attenuated environments. The received signal C/N_0 ranged from 15 to 30 dB-Hz. In order to acquire GPS signals in such indoor environments, an Assisted-GPS (A-GPS) approach was utilized. In this approach, the aiding information includes navigation data bit, and an epoch-by-epoch estimate of code phase and Doppler provided by a nearby outdoor antenna. The data bits estimated from an outdoor antenna is utilized to wipe off the navigation data bit from the indoor process. Therefore, the indoor process is enabled to increase the coherent integration times beyond the 20 ms data bit period. The measured code phase and Doppler from the outdoor antenna is utilized as a reference for the indoor process. Hence, it can be determined whether the indoor process can detect the signal of interest properly or not. In the first data set, four indoor antennas are used as the diversity branches

whereas in the second data set, two indoor antennas are utilized as diversity branches. In both cases, the indoor antennas were separated by 10 cm to capture approximately independent signals in such dense multipath environments. The indoor antennas were mounted on a linear motion table in order to capture independent samples. Figure 4-4 shows the data collections settings and locations.

(a)

(b)

Figure 4-4: Data collections settings and locations (a) first data set (b) second data set

The L1 C/A signal of the reference outdoor antenna and all (four for first and two for second data set) indoor (rover) antenna signals were captured by a National Instrument (NI) system, composed of front-ends working in a synchronized mode. All frontends shared the same reference oscillator. Hence, they experienced the same clock drift.

In order to speed-up and facilitate the block processing method, the PLAN group software receiver, GSNRx-rr, was used. GSNRx-rr is a modified version of the standard GSNRx (O'Driscoll et al 2010) software receiver and allows the joint processing of several input channels. The first channel is the outdoor reference channel, which provides the aiding information. For each of the other channels, GSNRx-rr provides correlator outputs for each processing epoch. There is also an option file to manage the correlation process in terms of correlator ranges in code phase and Doppler, correlator spacing and coherent integration time. Table 4-1 tabulates some information about data collection and processing setups.

Table 4-1: data collection and processing specifications

Data set	location	Number of Available outdoor PRNs	Speed of moving antennas	Coherent integration time	Number of epochs
1	Laboratory	11	5 cm/s	200 ms	500
2	Workshop	8	25 cm/s	400 ms	500

4.3.2 Fading mitigation

One of the metrics that can be used to characterize the detection performance is the Deflection Coefficient (DC), which is quantified as

$$DC = \frac{\left(E\left[x;H_1\right] - E\left[x;H_0\right]\right)}{\mathrm{var}\left[x;H_0\right]} \qquad \textbf{4-24}$$

where $E\left[\bullet\right]$ is the expected value operator, $\mathrm{var}\left[\bullet\right]$ is the variance operator, $(x;H_1)$ represents the correlator output when the received signal and the replica are synchronized (presence of signal of interest); in contrast $(x;H_0)$ represents the correlator output when the received signal and the replica are not synchronized (absence of signal of interest).

The deflection coefficient can be interpreted as the distance between $E\left[x;H_1\right]$ and $E\left[x;H_0\right]$ normalized with respect to the spread (variance) of the $\left(x;H_0\right)$.

The deflection coefficient fully characterizes the detection performance where the signal distributions under both H_0 and H_1 hypotheses are Gaussian. However, it also may be used for non-Gaussian cases, which presents useful information about detection performance (Kay 1998).

Herein, the deflection coefficient is utilized to depict the ability of diversity schemes for signal fading mitigation. Figure 4-6 shows the time series of the deflection coefficient of a sample PRN for single branches and two combining methods in the first data set.

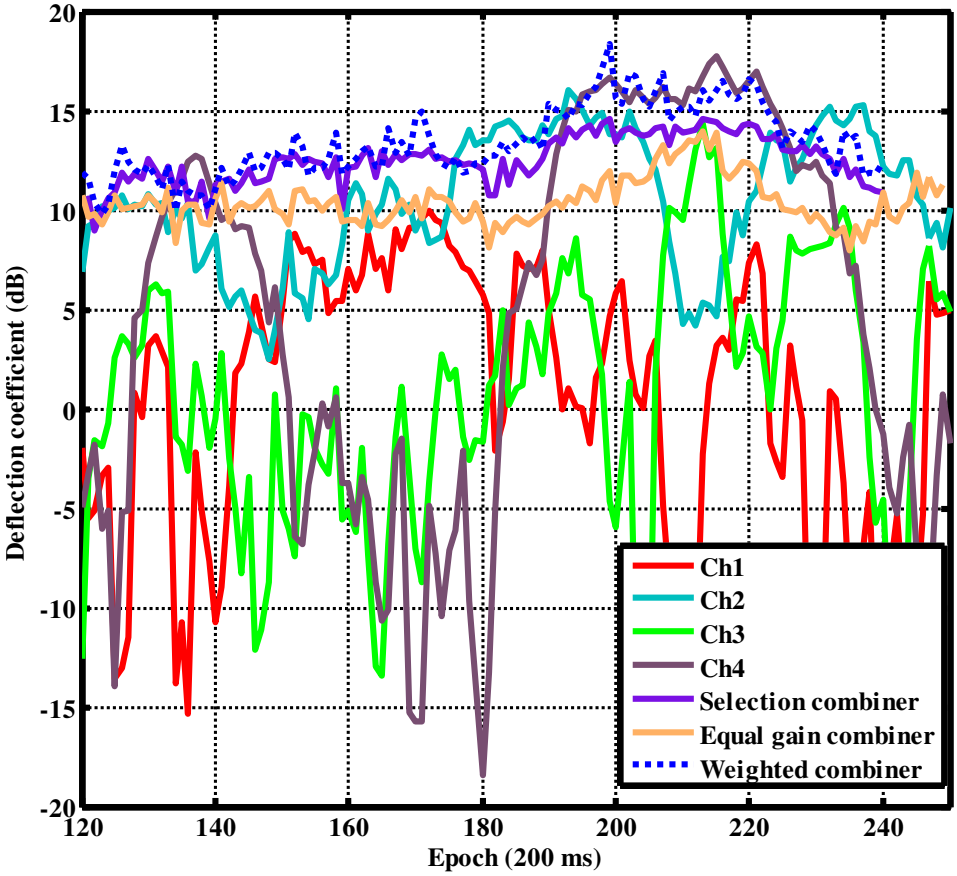

Figure 4-5: Time series of the Deflection Coefficient of a sample PRN for single branches and two combining methods in the first data set

Figure 4-5 indicates the ability of a diversity scheme to mitigate the fading. Although all single branches experienced considerable fades, all diversity schemes effectively alleviate the fading. Figure 4-5 shows time series of the deflection coefficient of single branches

and diversity schemes for a sample PRN in the second data set. Figure 4-6 shows that applying a diversity scheme can effectively mitigate the fading.

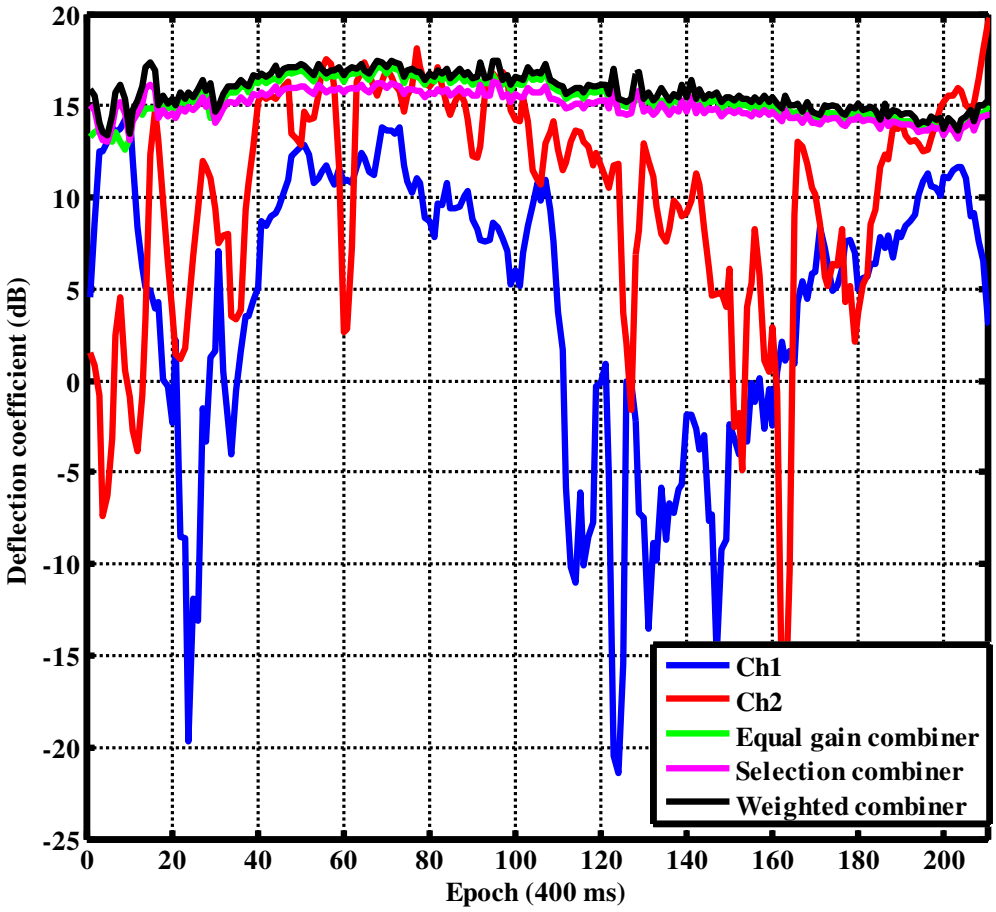

Figure 4-6: Time series of Deflection Coefficient of a sample PRN for single branches and two combining methods in the second data set

4.3.3 ROC curve

Although different metrics have been utilized to assess the performance of different diversity methods, a more quantitative analysis can be carried using Receiver Operating Characteristics (ROC) curves. A ROC curve is a plot of the probability of detection as a function of the probability of false alarm (Kay 1998). Figure 4-9 shows the ROC curves of single branches and different diversity combining methods for a sample PRN in the first data set.

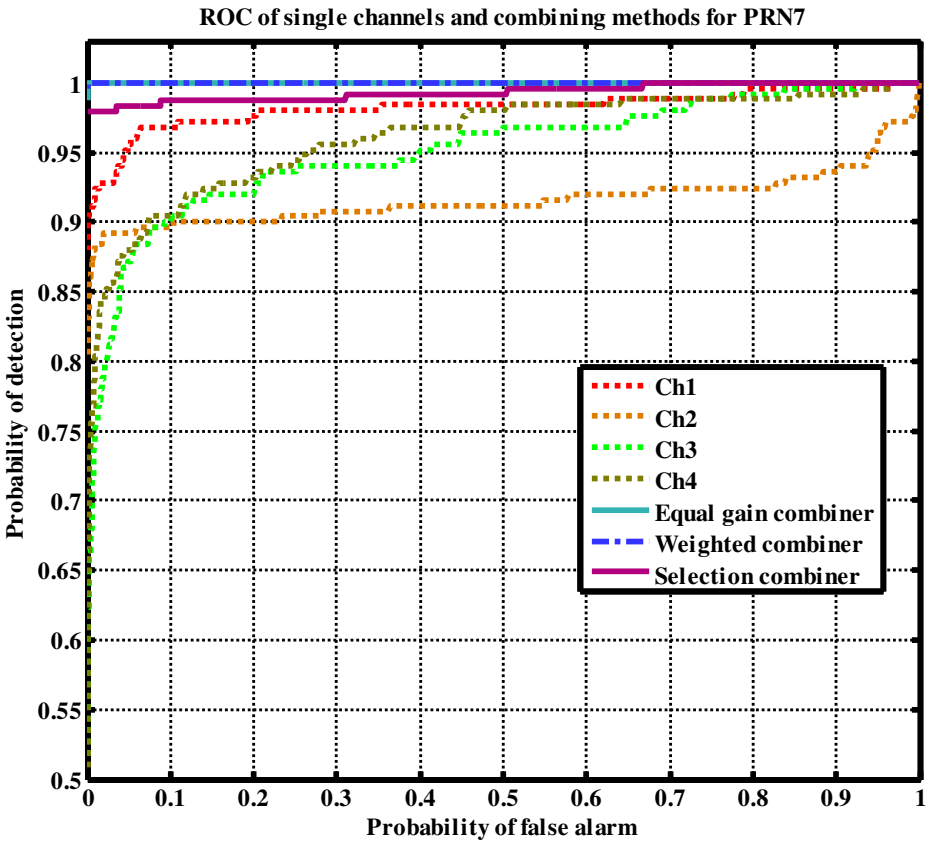

Figure 4-7: ROC curves of single branches and different diversity combining methods for a sample PRN in the first data set

The most important observation from Figure 4-7 is the tremendous enhancement in detection performance by applying either of the combining methods. Figure 4-8 shows the same plot for a satellite with relatively poor quality.

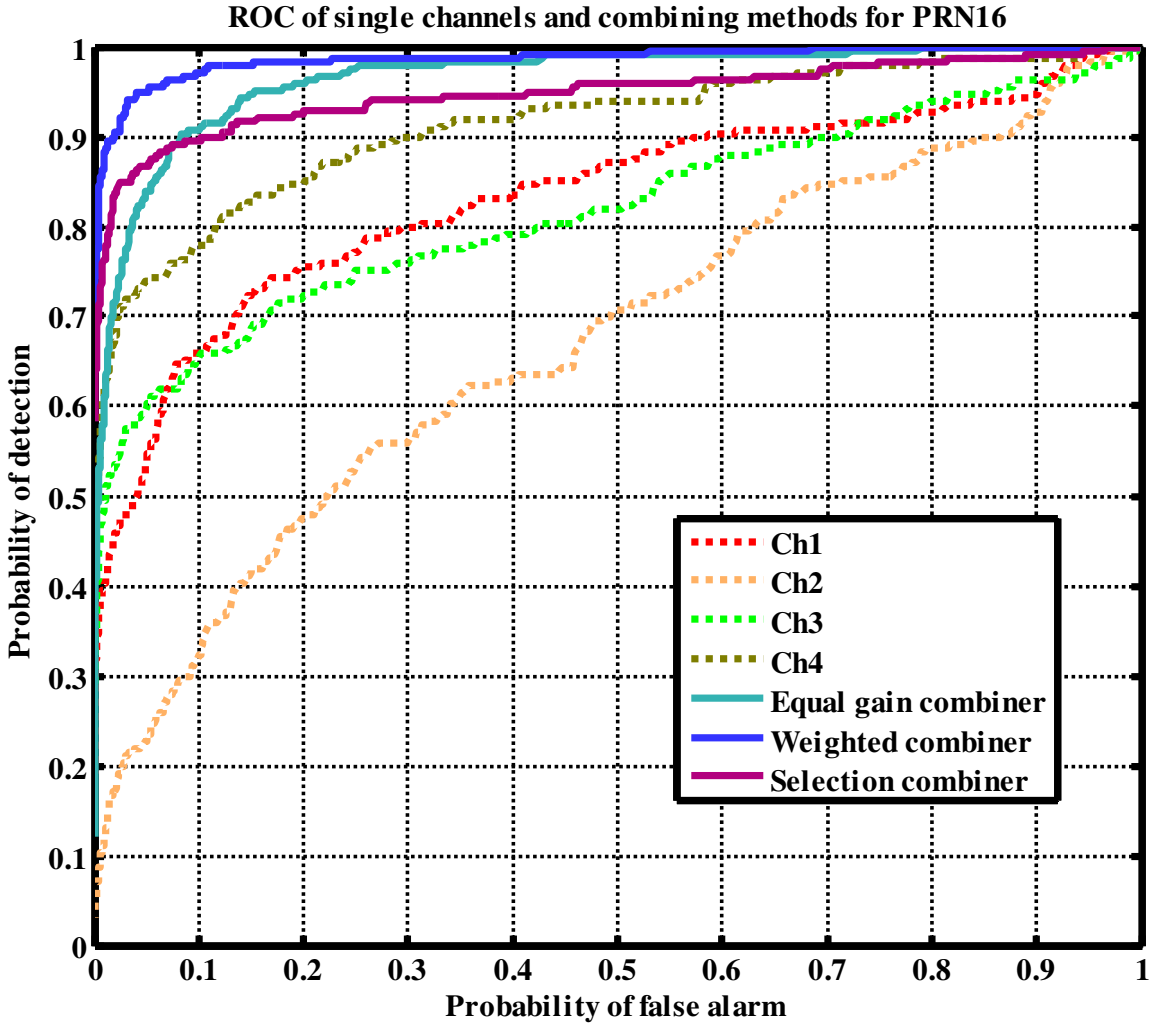

Figure 4-8: ROC curves of single branches and different diversity combining methods for a sample PRN in the first data set

It can be seen in Figure 4-8 that having branches with different signal qualities, the performance of EGC degrades significantly, as expected. In such cases, EGC might perform worse than selection combining, which is the case in Figure 4-8.

Figure 4-9 and Figure 4-10 shows the ROC curves of different combining methods for sample PRNs in the second data set. The ROC curves of individual diversity branches are

also overlaid for comparison. In the second data set, just two diversity branches were available to be combined.

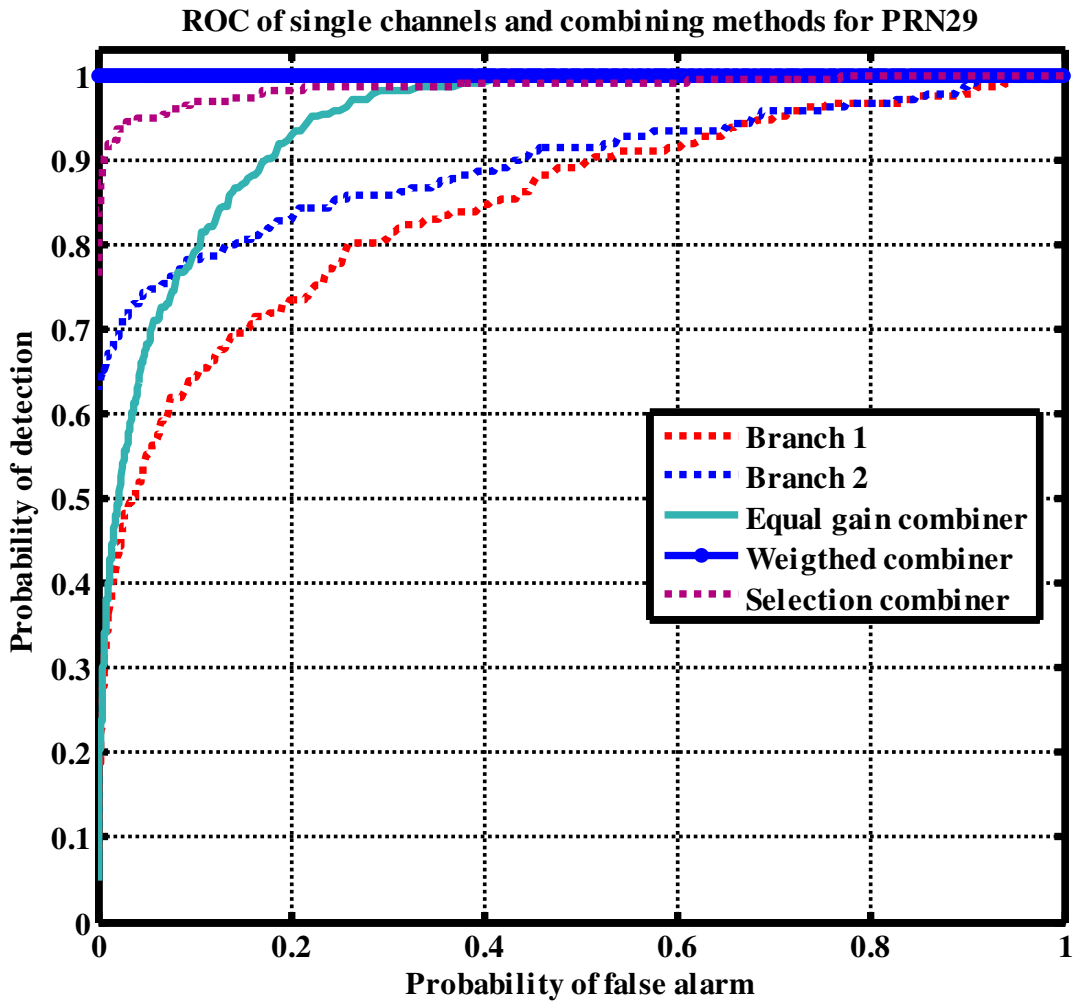

Figure 4-9: ROC curves of single branches and different diversity combining methods for a sample PRN in the second data set

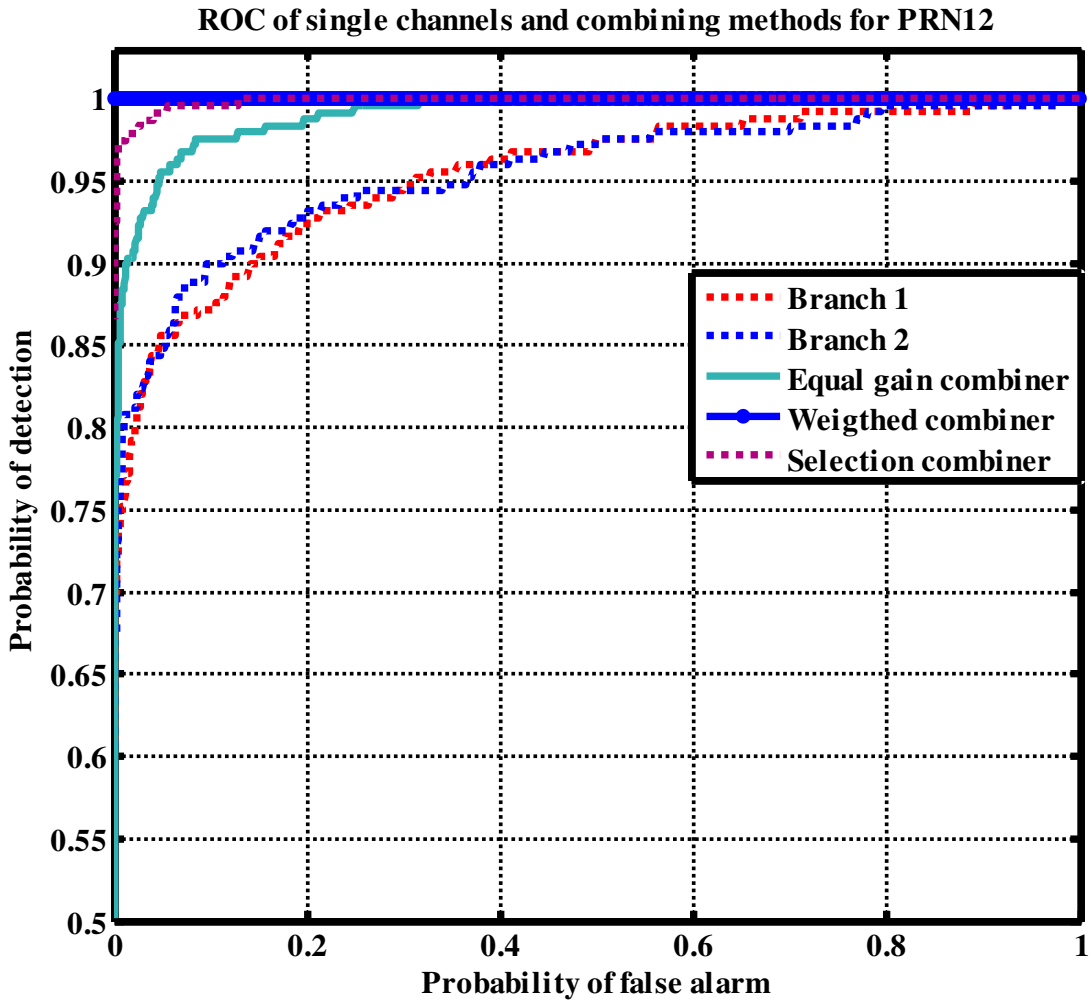

Figure 4-10: ROC curves of single branches and different diversity combining methods for a sample PRN in the second data set

It can be concluded from these figures that all combining schemes significantly enhanced the detection performance. Analyzing Figure 4-7 to Figure 4-10 the following conclusions can be drawn:

1- Diversity schemes, in general, enhance the detection performance.

2- Since the weighted combining method uses more information and combines the diversity channels considering their individual instantaneous qualities, this method outperforms all of the other diversity combining methods.
3- EGC is vulnerable to discrepancy of the diversity branches qualities. EGC performance varies from weighted combining (where channels have approximately the same qualities) to even below some of single branch performance (Figure 4-8 and Figure 4-9).
4- Although selection combining uses the instantaneous quality information, because of its very basic combining algorithm (Pick the best) performs below weighted combining.

In order to quantify the enhancement achieved through establishing a diversity scheme, satellite availability is used to quantify the detection performance of different diversity methods and single branches in the next section.

4.3.4 Satellite availability

Enhancement in signal detectability improves satellite availability, which is one of the critical problems in dense multipath environments (Watson et al 2006b).

Herein for each satellite, based on the noise distribution a threshold is considered which provides a P_{fa} of 0.002. It should be noted that considering the total 500 epochs, a P_{fa} of 0.002 is the least possible non-zero probability. Then the signal levels of all available satellites in each processing epoch are compared to the threshold. The number of available satellites for a given epoch is measured as the satellite availability of the given

epoch. Figure 4-11 shows the Cumulative Distribution Function (CDF) of satellite availability for single branches and different combining methods in the first data set.

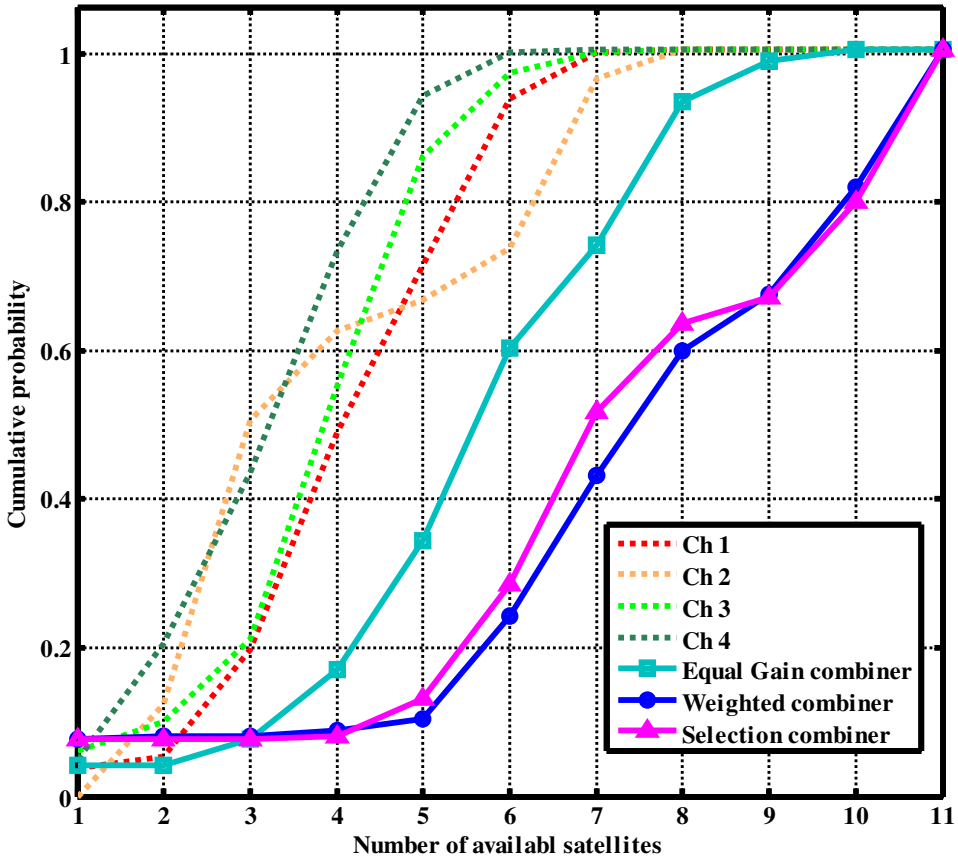

Figure 4-11: Cumulative Distribution Function (CDF) of satellite availability for single branches and different combining methods in the first data set

Significant improvement in satellite availability by using diversity methods is observable from Figure 4-11. Among diversity methods, EGC performs the worst. The degraded performance of EGC could be predicted based on Figure 4-7 to Figure 4-10. Weighted Combining performs slightly better than Selection Combining.

To have a position solution at least four satellites are necessary at each processing epoch in the general case. Having less than four correctly acquired satellites in a processing

epoch, which results in no position solution for the epoch, is defined as an outage in the corresponding epoch. The most important enhancement achieved by the diversity schemes is the reduction of the probability of an outage. The probability of an outage is defined as the ratio between the number of epochs in which a position solution cannot be achieved over the total number of epochs. The probability of outages decreased from more than 50% for single branches to less than 10% for diversity methods. In addition, acquiring more satellites will decrease the Dilution of Precision (DOP) and consequently enhances satellite geometry and positioning accuracy.

Figure 4-12 shows the CDF of satellite availability for single branches and different combining methods in the second data set.

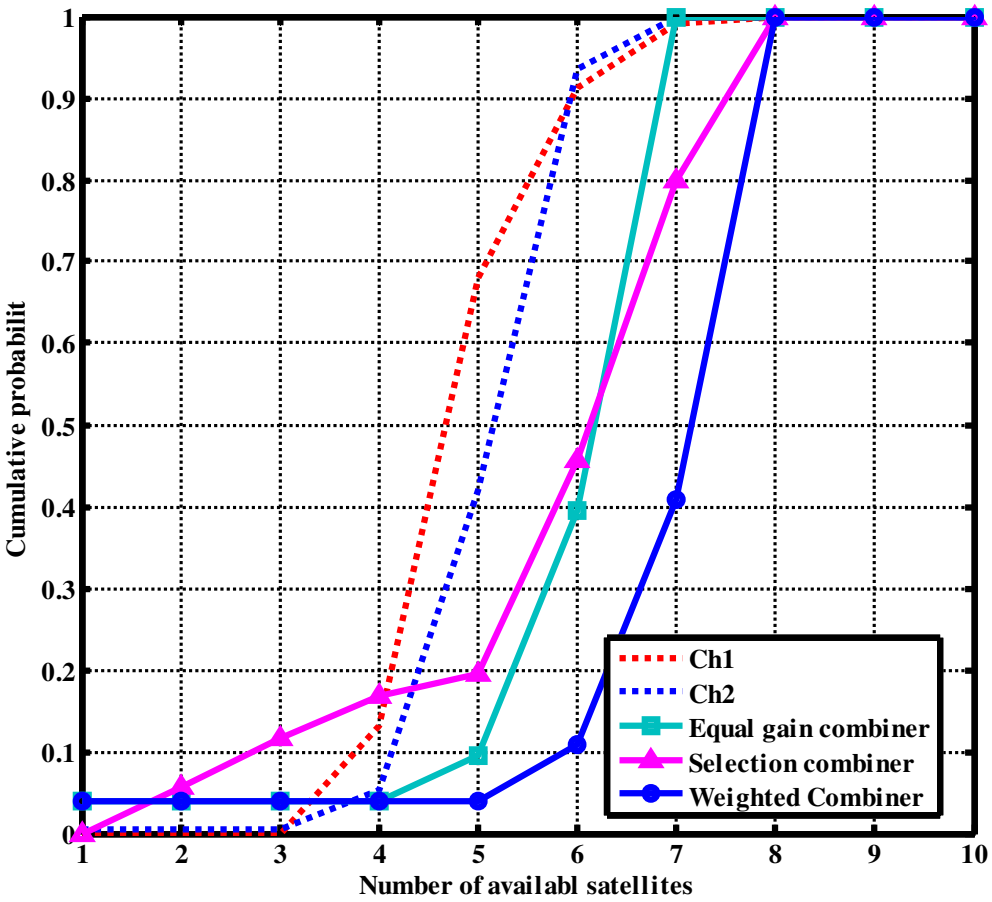

Figure 4-12: Cumulative Distribution Function (CDF) of satellite availability for single branches and different combining methods in the second data set

Although a significant enhancement of satellite availability can be observed from Figure 4-12, the enhancement achieved through diversity schemes decreased with respect to the first data set. Causes of this degradation can be as follows:

1- Decreased number of diversity branches. Having less diversity branches the expected improvement by applying diversity scheme is decreased specifically in selection combining which picks the best branch among all available branches. Thus, reduction of number of branches degrades the achievable improvement.

2- Higher speed of motion and longer coherent integration time. Using higher integration time and higher speed somehow filters the spatial samples of fading. Thus single branches experienced fewer deep fades with respect to cases with shorter integration time or lower motion speed. Thus, having single branches with better qualities, the enhancement may be achieved through diversity scheme will reduce.

4.4 Summary

In this chapter, the performance of diversity systems composed of spatially separated antennas was analyzed. Three different stages in which signals of diversity branches can be combined were introduced. The correlator outputs stage was selected as the only stage in which combining the signal of diversity branches can enhance the detection performance. After introducing Estimator Correlator for combining the correlator outputs, by utilizing an epoch-by-epoch SNR estimator a modified version of the Estimator Correlator, called weighted combiner, was devised. The performance of the weighted combiner, equal gain combiner and selection combiner were compared with single branches through two different experiments. By analyzing deflection coefficients, it was shown that diversity schemes are able to effectively alleviate fading. A ROC curve analysis revealed a considerable enhancement through diversity schemes. It was also shown that equal gain combiner is vulnerable to discrepancy of diversity branches qualities. In such cases, it is recommended to use selection or weighted combining instead. Finally, satellite availability was assessed as the most quantifying measure for

the enhancement achieved through diversity schemes for GNSS applications in the detection stage. It was shown that by applying a diversity scheme, the probability of outage can be reduced substantially, namely from 50% to less than 10% in the tests performed.

Chapter Five: DOPPLER MEASUREMENTS CHARACTERIZATION IN MULTIPATH ENVIRONMENTS FOR GNSS APPLICATIONS

In the previous chapter, the detection performance of diversity systems composed of spatially separated antennas was assessed. It was shown that by utilizing spatially separated antennas and establishing diversity schemes the detection performance will be enhanced and the probability of outage will be reduced. Detecting GPS satellites and parameter estimation is the next step toward a positioning solution. Two main parameters, namely pseudorange and Doppler, are investigated in this thesis. In this chapter, Doppler estimation in harsh multipath environments will be analyzed. This analysis is carried out in order to investigate the use of Doppler measurements for indoor positioning. More specifically, their application in diversity systems is of interest. The remainder of the chapter is organized as follows. Section 5.1 introduces the Doppler measurements and their error sources in harsh multipath environments. In Section 5.2 after presenting the signal model, the Power Spectral Density (PSD) measurement method using the block processing technique is described. Section 5.3 describes different multipath propagation models and theoretical Doppler spread characteristics. The effect of the antenna gain pattern on PSD is also considered in this section. Section 5.4 describes the measurement set up and the data collection scenarios. The experimental results and practical considerations are also given in this section. Finally, conclusions are presented in Section 5.5.

5.1 Doppler measurements application in harsh multipath environments

A receiver can observe the carrier frequency of the received GPS signal by generating a replica carrier wave. Based on the Doppler effect, the observed frequency differs from the transmitting frequency (e.g. L1 or any other carrier frequencies) emitted from the satellites. This frequency shift is due to the relative motion between the receiver and the satellite. Moreover, a possible frequency mismatch between transmitter and receiver due to clock offset and drift can affect the frequency shift. The actual frequency shift observed by the receiver is called the Doppler measurement. Knowing the Doppler measurements, satellite velocity and the satellite-receiver unit vector, one can determine the receiver velocity and clock drift. Besides velocity estimation, the Doppler measurements are commonly used for aiding inertial navigation systems (INS). Conventionally, a GPS/INS integrated system utilizes pseudorange measurements to aid the INS. Raw Doppler measurements (Petovello 2003) or the velocity information extracted from them (Moafipoor et al 2008) have also been used to update the INS drift. Doppler measurements have also been used in signal attenuated circumstances to improve the relative position estimation utilizing the velocity solution (Borio et al 2011) or to update inertial navigation systems (INS) in urban and multipath environments (Aminian 2011).

5.1.1 Doppler characterization

The accuracy of Doppler measurements plays a critical role in velocity estimation, relative positioning and GPS/INS applications. Hence, Doppler measurement characterization is problem of interest for GNSS applications. Previous work on GPS

Doppler characterization e.g. (Van Grass & Soloviev 2004), (Aminian et al 2010) has focused on open sky conditions and in urban environments where multipath components affect the line of sight signals. In Aminian et al (2010) a practical method to characterize the Doppler and velocity measurements in the indoor environments based on the block processing technique is proposed. However, the experiments were limited to North American residential houses. A comprehensive theoretical framework for velocity estimation has been developed in Borio et al (2011) to investigate the impact of the tracking loop parameters such as bandwidth, integration time and loop order as well as Carrier-to-Noise ratio (C/N_0) and user dynamics on the accuracy of the Doppler and velocity measurements in attenuated signal environments. However, the Doppler measurements have not been fully characterized for indoor pedestrian navigation scenarios with the propagation channel represented by a Rayleigh fading model. Since this research focuses on harsh multipath environments with the Rayleigh fading model, it is crucial to characterize the Doppler measurements in such environments. With the ultimate goal of using Doppler measurements for positioning purposes in mind, it should be determined whether Doppler measurements are convenient observables in such circumstances or not.

When a mobile receiver is moving in multipath fading environments, the multipath components arrive at the receiver antenna from different paths, giving rise to randomly distributed Doppler shifts. The width of the distribution of the Doppler shifts is related to the Doppler spread. Souden et al (2009) defined the Doppler spread as the standard deviation of the Doppler shifts and explained the relation between the Doppler spread and the received signal Power Spectral Density (PSD).

This chapter characterizes PSD of the received signal and consequently the Doppler estimation accuracy in harsh multipath GPS channels due to the user motion. Controlled experiments with constant known antenna motion are used to determine the resulting Doppler spread. Experimental measurements with different satellites under different conditions have been utilized to verify the theoretical findings. The effect of the receiver antenna pattern on Doppler estimation and Doppler spectrum are theoretically and experimentally characterized.

5.2 Signal model

Consider a mobile receiver scenario where the receiver is travelling along an arbitrary path in a dense multipath environment. The complex baseband signal representation of the received signal at the antenna output is denoted as $r(t)$. The signal component of $r(t)$ emanating from the *k*-th satellite is denoted as $s_k\left(t,\mathbf{p}(t)\right)$, which is a function of time t and antenna position $\mathbf{p}(t)$. As introduced in Chapter 2, this signal can be expressed as

$$\begin{aligned} s_k\left(t,\mathbf{p}(t)\right) &= A_k\left(\mathbf{p}(t)\right) s_{0_k}(t) \\ s_{0k}(t) &= D_k(t-\tau)c_k(t-\tau)e^{j(2\pi\Delta f_k t+\psi_k)} \end{aligned} \qquad \textbf{5-1}$$

where $c_k(t)$ is the pseudo-random code (PRN) corresponding to the *k*-th satellite, $D(t)$ is the navigation data modulation, τ is the code offset, Δf_k represents the frequency offset and ψ_k is the initial phase offset. $A_k\left(\mathbf{p}(t)\right)$ is the multipath channel response to the incident signal at the antenna position $\mathbf{p}(t)$. The received signal is corrupted with additive noise, which has an equivalent complex baseband representation denoted by

$w(t)$. It is assumed that $w(t)$ is a complex normal random process, independent of the signal and has a power spectral density that is constant within the bandwidth of the received signal. Hence, the representation of $r(t)$ can then be expressed as

$$r(t) = S(t) + w(t) \qquad \textbf{5-2}$$

where

$$S(t) = \sum_{k=1}^{K} A_k(\mathbf{p}(t)) D_k(t-\tau_k) c_k(t-\tau_k) e^{j(2\pi\Delta f_k t + \psi_k)}. \qquad \textbf{5-3}$$

K is the number of GPS satellites in view. Here, the presence of simultaneous GPS signals will be ignored. Hence, in the remainder of the text, for notational convenience, the subscript k is eliminated and the received signal is modeled as

$$r(t) = A(\mathbf{p}(t)) s_o(t) + w(t) \qquad \textbf{5-4}$$

where $s_0(t) = D(t-\tau) c(t-\tau) e^{j(2\pi\Delta f t + \psi)}$ is known to the receiver except for the navigation data, the code phase, the Doppler frequency and the initial phase offset ψ. Herein, the block processing technique described in Chapter 2 is utilized to investigate the Doppler spread and Doppler estimation accuracy. As alluded in Chapter 2, in the block processing method, the receiver generates the replica signal for all possible values of Doppler and code phases and realizes a bank of correlators for each processing epoch. The signal snapshot of $r(t)$ is collected by the receiver de-spread by the locally generated replica of $\hat{s}_0^{\tau_i,\Delta f_j}(t) = D(t-\tau_i) c(t-\tau_i) e^{j(2\pi\Delta f_j t + \psi)}$ for given code phase τ_i and Doppler frequency Δf_j. The de-spread signal is then coherently integrated over a snapshot interval of $t \in [(n-1)T, nT]$. For the epoch number n the correlation process

results in an output variable denoted by $x\left[\tau_i, \Delta f_j, n\right]$ corresponding to $\tau_i, \Delta f_j$. Correlator outputs are expressed as

$$\begin{aligned} x\left[\tau_i, \Delta f_j, n\right] &= \frac{1}{T}\int_{(n-1)T}^{nT} r(t)\,\hat{s}_o^{\tau_i,\Delta f_j}(t)^* dt \\ &= \frac{1}{T}\int_{(n-1)T}^{nT} A(\mathbf{p}(t))\, s_o(t)\hat{s}_o^{\tau_i,\Delta f_j}(t)^* dt + \frac{1}{T}\int_{(n-1)T}^{nT} w(t)\hat{s}_o^{\tau_i,\Delta f_j}(t)^* dt \end{aligned} \qquad \textbf{5-5}$$

.

Here, the Doppler frequency characterization in the multipath environments has been considered. Hence, it is assumed that the true code phase and the navigation data bits are known. The Doppler component observed by a moving receiver to the first order contains three terms, namely: the Doppler frequency caused by the satellite motion, Doppler due to the receiver clock drift and Doppler due to the receiver motion. Since in this work the Doppler frequency induced by the receiver motion is of interest and to reduce the range of the Doppler search and computational burden in the block processing method, other Doppler components are wiped off. This has been done by aiding the moving receiver process by a reference nearby receiver collecting synchronous signals under open sky static conditions. Hence, considering the aiding process the correlator outputs can be expressed as

$$x\left[\tau_i, \Delta f_j, n\right]\Big|_{\tau_i=\tau} = \frac{1}{T}\int_{(n-1)T}^{nT} A(\mathbf{p}(t))\, s_o(t)\hat{s}_o^{\tau,\Delta f_j}(t)^* dt + \eta \qquad \textbf{5-6}$$

where $\eta = \frac{1}{T}\int_{(n-1)T}^{nT} w(t)\hat{s}_o^{\tau,\Delta f_j}(t)^* dt$. Since the code phase is known, the correlator outputs can be written as

$$x\left[\Delta f_j, n\right] = G\int_{(n-1)T}^{nT} A\left(\mathbf{p}(t)\right) e^{-j2\pi(\Delta f_j - \Delta f)t} dt + \eta \qquad \textbf{5-7}$$

where G is the correlation gain. Eq. 5-7 can be considered as the noisy samples of the Short Time Fourier Transform (STFT) of the windowed channel response between $\left[(n-1)T, nT\right]$. Adding the square of absolute values of the correlator outputs for the consecutive windows reduces the noise effect on Fourier transform samples. Thus, the PSD can be expressed as

$$\mathrm{PSD}\left[\Delta f_j\right] = \sum_{n=1}^{N} \left| x\left[\Delta f_j, n\right] \right|^2 \qquad \textbf{5-8}$$

where NT is the total observation time.

As mentioned before, by aiding the true code delay, the Doppler frequency estimation is reduced to sinusoidal frequency estimation in noise (Borio et al 2011). Thus, the Maximum Likelihood (ML) frequency estimation can be expressed as

$$\begin{aligned} \Delta\hat{f}(n) &= \arg \max_{\Delta f_j} \left| \frac{1}{T} \int_{(n-1)T}^{nT} r\left(t\right) \hat{s}_o^{\tau,\Delta f_j}(t)^* dt \right|^2 \\ &= \arg \max_{\Delta f_j} \left| x\left[\Delta f_j, n\right] \right|^2 \end{aligned} . \qquad \textbf{5-9}$$

Figure 5-1 shows the Doppler estimation block diagram based on the block processing method.

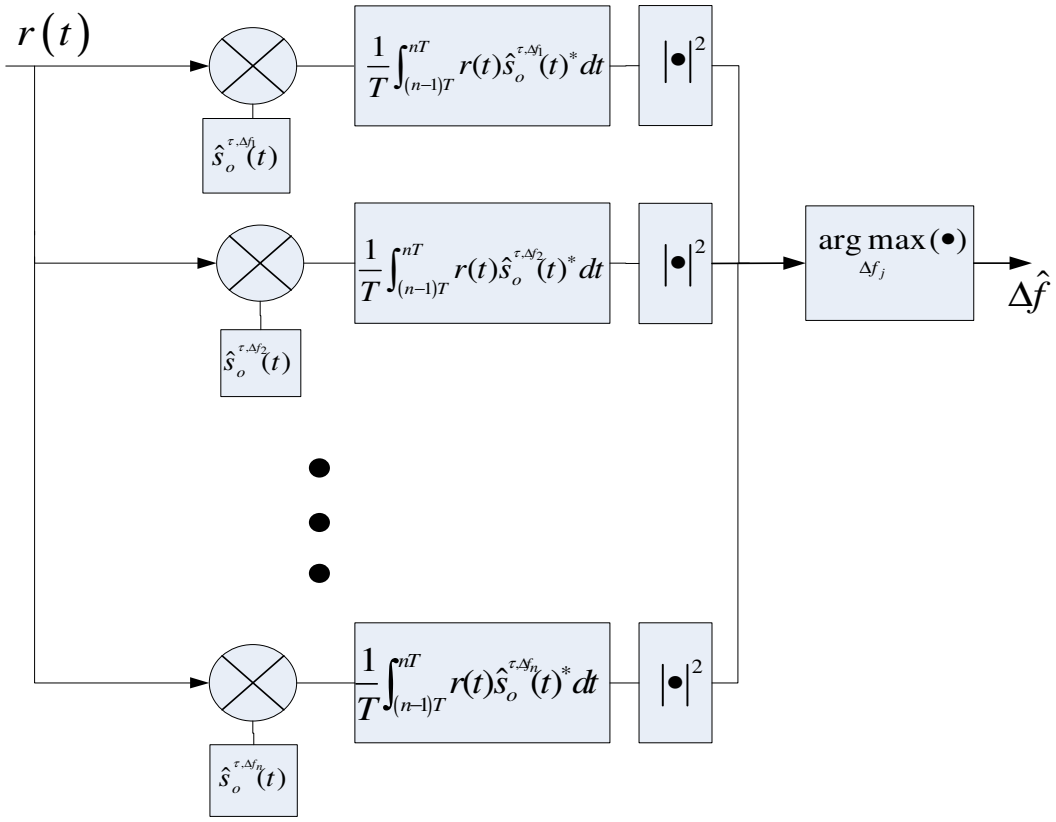

Figure 5-1: : Doppler estimation using block processing method

5.3 Doppler Characteristics in Multipath Fading

In the multipath GNSS channel, propagation between a satellite and a receiver is not only through the direct Line-Of-Sight (LOS) path, but also by many other paths through scattering by reflections from or diffraction around buildings and terrain. Hence, the signal received by the receiver consists of a large number of plane waves whose amplitudes, phases, and angle of arrivals relative to the motion direction are random. Any changes in the scatterers' geometry will change the resulting plane wave incident on the receiver. Hence, in dense multipath environments, the received frequency consists of contributions from many reflected signals, each shifted in frequency by a Doppler shift

commensurate with the motion along the corresponding path. In indoor environments, these paths may be assumed to be arriving from the surface of a sphere whose radius is large compared to the signal wavelength (Blaunstein & Anderson 2002). Frequencies associated to these paths are confined to the Doppler spread around the transmitted frequency (Van Trees 2002). This model is called the sphere of scatterers' model. Measurement results given in Broumandan et al (2010) and Dehghanian et al (2010) have shown that the indoor GNSS channels can be characterized by the sphere of scatterers model. Hence, this model has been considered here. Consider a GNSS receiver traveling with a constant speed of $|v|$ in a 3D coordinate system characterized by the sphere of scatterers model as shown in Figure 5-2. The Doppler shift associated to a path is related to its Angle Of Arrivals (AOA) and can be denoted as

$$f = f_m \cos(\alpha + \alpha_0)\cos(\beta + \beta_0) \qquad \textbf{5-10}$$

where α and β are the azimuth and elevation angles of the incident path and α_0 and β_0 are the azimuth and elevation angles of the motion direction. f_m is the maximum Doppler shift which is defined by

$$f_m = \frac{|v|}{\lambda} \qquad \textbf{5-11}$$

where λ signifies the carrier wavelength.

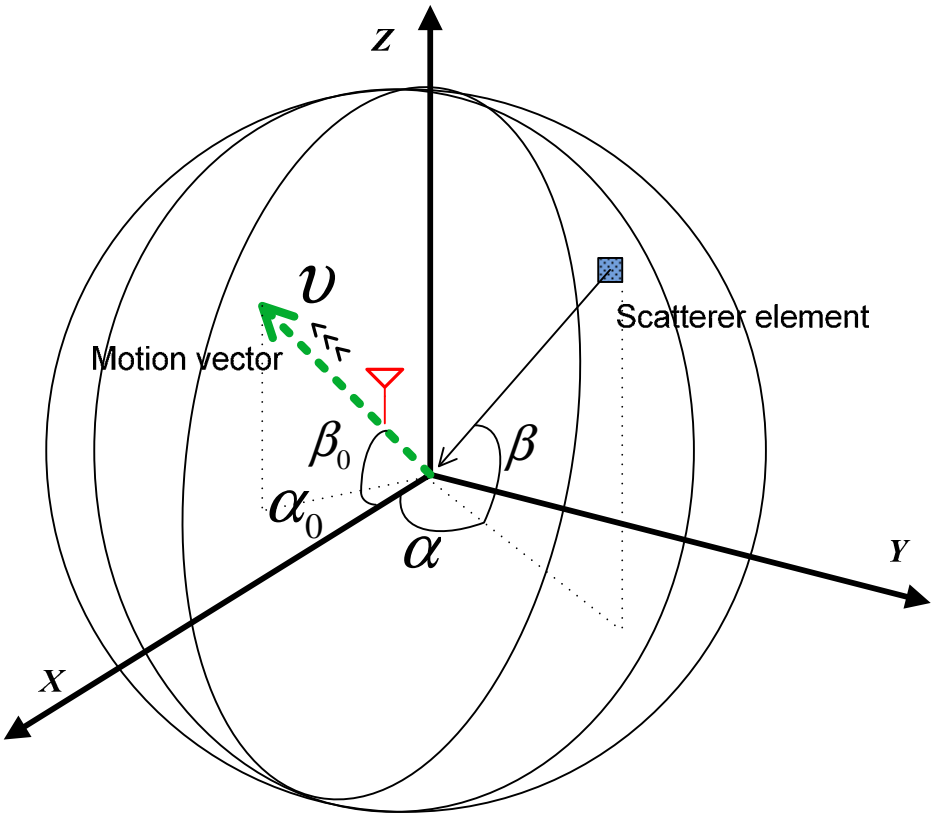

Figure 5-2: GNSS receiver traveling in a multipath environment

The total power of the plane waves arriving from the surface element of $d\alpha d\beta$, denoted here as the surface element, received by a non-isotropic antenna and correct polarization is denoted by

$$S_{d\alpha d\beta}(f) = \frac{1}{B_{LPF}}\operatorname{sinc}\left(\frac{\left(f_m\cos(\alpha+\alpha_0)\cos(\beta+\beta_0)-f\right)}{B_{LPF}}\right)p(\alpha,\beta)G(\alpha,\beta)\cos(\beta)\,d\alpha d\beta \qquad \textbf{5-12}$$

where B_{LPF} is the bandwidth of the low pass filter, $p(\alpha,\beta)$ represents the scatterers' distribution, and $G(\alpha,\beta)$ is the 3D antenna gain pattern relative to the isotropic antenna. The sinc function represents the effect of the coherent integration time's windowing in the frequency domain where B_{LPF} is defined as

$$B_{LPF} = \frac{1}{T} \qquad \textbf{5-13}$$

where T is the coherent integration time. The total power spectrum can be obtained by summing the contributions of all paths. This expression is denoted as

$$S(f) = \int_{-\frac{\pi}{2}}^{\frac{\pi}{2}}\int_{0}^{2\pi} \frac{1}{B_{LPF}} \operatorname{sinc}\left(\frac{\left(f_m \cos(\alpha+\alpha_0)\cos(\beta+\beta_0)-f\right)}{B_{LPF}}\right) p(\alpha,\beta)G(\alpha,\beta)\cos(\beta)\,d\alpha d\beta. \qquad \textbf{5-14}$$

If the coherent integration time is large enough, Eq. 5-14 can be rewritten as

$$S(f) = \int_{-\frac{\pi}{2}}^{\frac{\pi}{2}}\int_{0}^{2\pi} \delta\left(f_m \cos(\alpha+\alpha_0)\cos(\beta+\beta_0)-f\right) p(\alpha,\beta)G(\alpha,\beta)\cos(\beta)\,d\alpha d\beta \qquad \textbf{5-15}$$

where $\delta(t)$ is the delta Dirac function. Equations 5-14 and 5-15 in their general forms are too complicated to result in a close form expression and should be calculated numerically. By considering some assumption on the scatterers' distribution, the PSD formulation can be simplified. Assuming that the distribution of the scatterers in the horizontal plane is independent from their distribution in the vertical plane, $p(\alpha,\beta)$ can be written as

$$p(\alpha,\beta) = p(\alpha)\,p(\beta). \qquad \textbf{5-16}$$

Considering the same assumption for the antenna gain pattern, $G(\alpha,\beta)$ can be written as

$$G(\alpha,\beta)=G(\alpha)G(\beta). \qquad \textbf{5-17}$$

Replacing Eq. 5-16 and Eq. 5-17 in Eq.5-14 and setting α_0,β_0 to zero, Eq. 5-14 can be rewritten as

$$S(f)=\int_{-\frac{\pi}{2}}^{\frac{\pi}{2}} p(\beta)G(\beta)\int_0^{2\pi} p(\alpha)G(\alpha)\delta(f_m\cos(\alpha)\cos(\beta)-f)\cos(\beta)d\alpha d\beta \qquad \textbf{5-18}$$

.

In the following, one widely used scatterers model that results in closed form expressions for PSD has been considered.

5.3.1 Clark's ring of scatterers model.

Assuming the 2D uniform horizontal distribution of scatterers where $p(\beta)=\frac{1}{2\pi}$ and $p(\beta)=\delta(\beta)$, Eq. 5-18 for an isotropic antenna can be simplified to

$$S(f)=\int_0^{2\pi}\frac{1}{2\pi}\delta(f_m\cos(\alpha)-f)d\alpha=\frac{1}{f_m 2\pi\left|\sin\left(\cos^{-1}\frac{f}{f_m}\right)\right|} \qquad \textbf{5-19}$$

where $\sin\left(\cos^{-1}\left(\frac{f}{f_m}\right)\right)$ can be written as

$$\sin\left(\cos^{-1}\frac{f}{f_m}\right)=\pm\sqrt{1-\frac{f}{f_m}}. \qquad \textbf{5-20}$$

Replacing Eq. 5-20 in Eq. 5-19, the PSD for the ring of scatterers model can be written as

$$S(f)=\frac{1}{f_m 2\pi\sqrt{1-\left(\frac{f}{f_m}\right)^2}} \qquad \textbf{5-21}$$

which is the well-known U shaped PSD (Clarke 1968).

Considering different assumptions on $p(\alpha,\beta)$ and $G(\alpha,\beta)$, different theoretical PSDs can be obtained. Herein, the theoretical PSD curves under three different circumstances are numerically calculated utilizing Eq. 5-15. Figure 5-3 shows the normalized PSD curves for a ring of scatterers and a sphere of scatterers models. This figure also shows the effect of the antenna gain pattern on the observed PSD in the sphere of scatterers environments observed by a non-isotropic GNSS antenna. Since in the experimental section the Novatel 702 GG antenna is used, in Figure 5-3 its gain pattern (Novatel Inc 2011a) is considered to calculate the theoretical PSD curve. The Novatel 702 GG antenna gain pattern and its orientation with respect to the motion direction are shown in Figure 5-4.

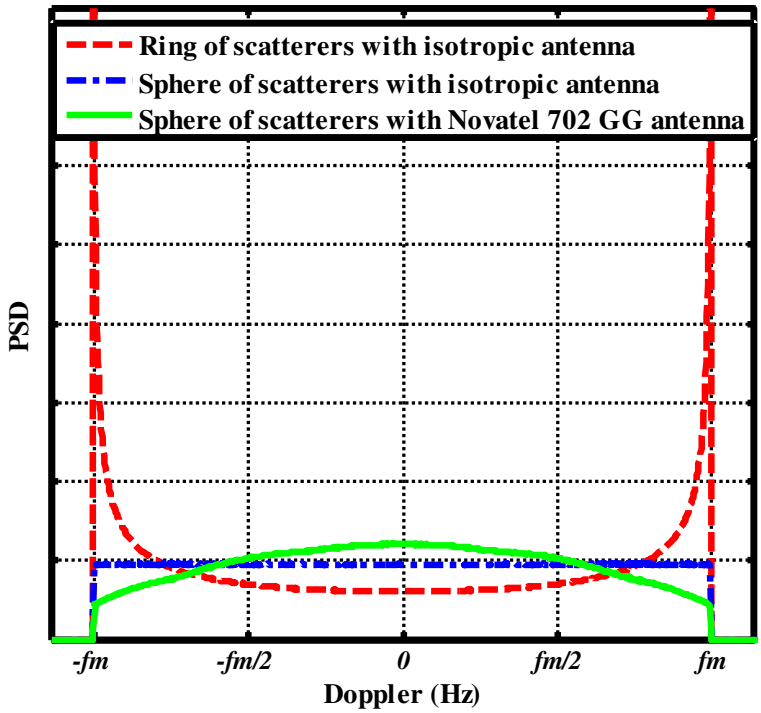

Figure 5-3:Theoretical PSD of ring and sphere of scatterers are compared with that of a sphere of scatterers observed by a directional antenna

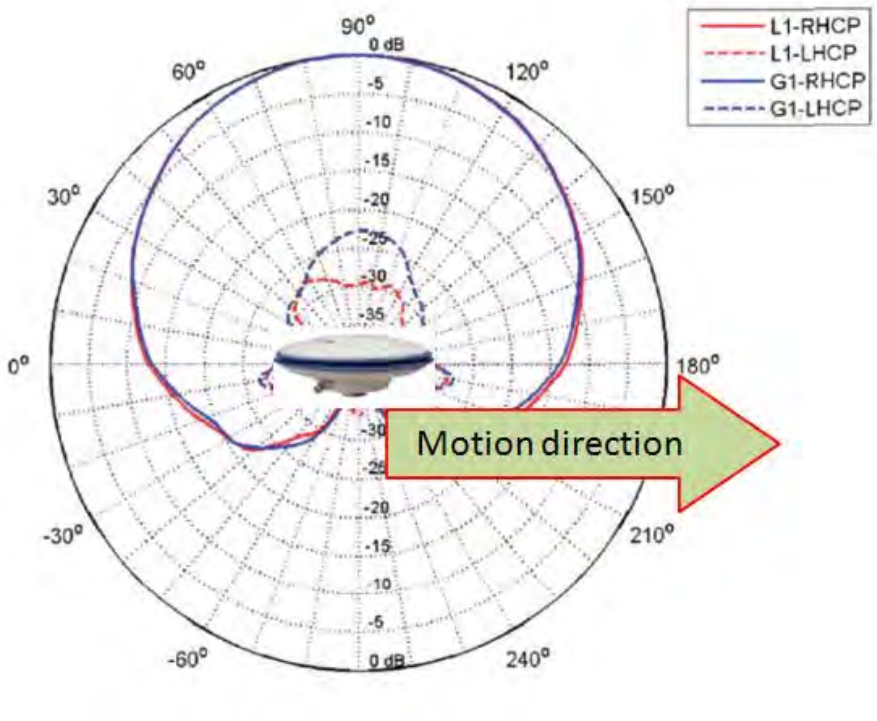

Figure 5-4:Novatel 702 GG antenna gain pattern (Novatel Inc 2011a) and its orientation with respect to the motion direction

5.4 Experimental Results

In the previous sections, PSD and Doppler characteristics in various multipath environments based on commonly used diffuse multipath models were analyzed. In this section, live GPS signal measurements in a dense indoor fading environment are considered to verify the theoretical findings. In addition, the velocity solution utilizing the Doppler measurements is characterized in this section.

5.4.1 Data collection setting and setup

Data collection was performed in a laboratory located at the University of Calgary. The laboratory has concrete walls and metallic structure considered an extremely harsh multipath environment. Figure 5-5 shows the data collection setup and location.

In order to acquire GPS signals in such an environment, an Assisted GPS (A-GPS) approach was utilized. The aiding information consisting of navigation data bits, the code phase and the Doppler frequency were provided by a nearby outdoor static reference receiver. To investigate the effect of the antenna gain pattern on the Doppler spectrum, two NovAtel 702 GG antennas with different orientations were utilized as shown in Figure 5-5. GPS L1 signals from the outdoor and indoor antennas were captured using a three-channel front-end operating in a synchronized mode. All the three channels were connected to a reference oscillator. During the data collection process, the indoor antennas were mounted on a precise linear motion table moving at the speed of 50 cm/s in order to emulate user motion. With such a velocity, the maximum Doppler shift due to the indoor antenna motion is about 2.6 Hz at the GPS L1 frequency. The indoor antennas were located 50 cm apart in order to minimize the mutual coupling effect (Allen & Ghavami 2005). One of the antennas was erected vertically (the antenna gain pattern was perpendicular to the motion direction), while the other antenna was aligned to the motion direction. Herein, two data sets were captured. In the first set, the moving table was aligned with the east–west direction. One of the antennas was mounted such that the maximum antenna gain pattern was directed toward zenith (as shown in Figure 5-5). Another antenna was mounted east facing aligned with the motion direction where the maximum antenna gain pattern was directed to horizon. In the second data set, the

moving table was placed in the north–south direction as shown in Figure 5-6. In this data set, the second indoor antenna was mounted toward north. In addition to the indoor antennas a tactical grade IMU was mounted on the moving table to provide the reference Doppler measurements. The tactical grade SPAN–LCI IMU was used (Novatel Inc 2011b).

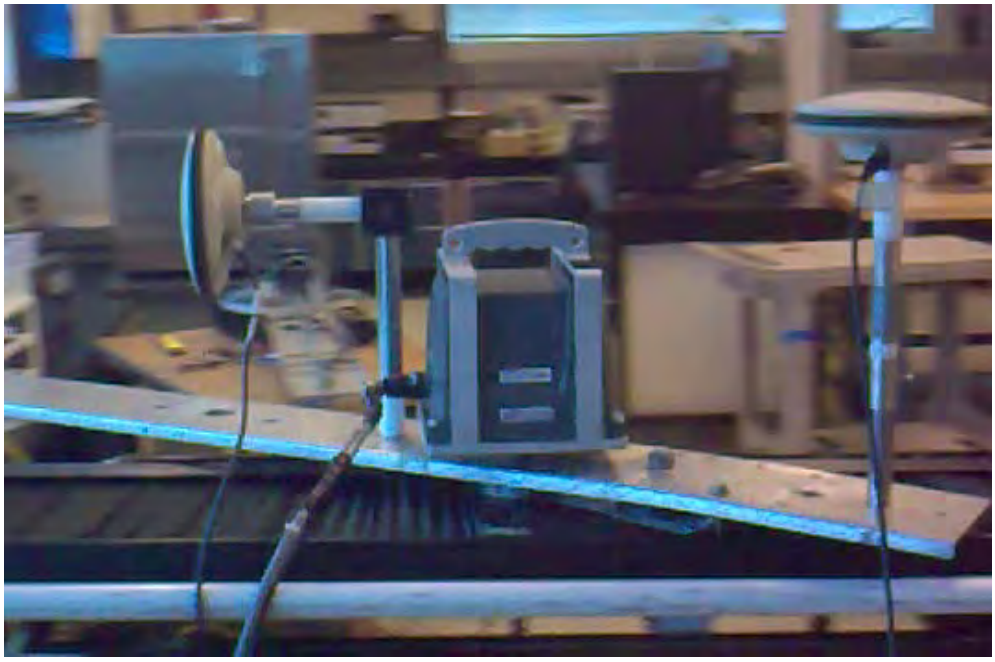

Figure 5-5: Data collection location and setup of two differently oriented antennas (up facing and east facing) with an IMU are mounted on a moving table

Aiding the indoor receiver process with the outdoor receiver Doppler frequency results in a remaining indoor Doppler frequency associated with the indoor receiver motion. The moving table forward-backward motion creates two Doppler frequencies associated with these motions. These two Doppler frequencies have the same value and opposite signs. For the sake of illustration, the backward motion is eliminated using the reference Doppler measurements extracted from the IMU measurements. This elimination yields to

a pure eastward motion for the first data set and a pure southward motion for the second data set with the constant speed of 50 cm/s.

To evaluate the Doppler frequency characterization in the indoor fading environments a search space of ± 5 Hz centered on the outdoor antenna Doppler frequency was selected. The captured data was processed with the GSNRx-rr^{TM} software receiver (O'Driscoll et al 2010). The correlation outputs are calculated using three different coherent integration times namely 200 ms, 400 ms and 800 ms. Different coherent integration times were utilized to investigate the effect of the coherent integration time on the observed PSD and the Doppler estimation accuracy. The correlation outputs then passed to a processing function to estimate the Doppler and velocity solution characteristics.

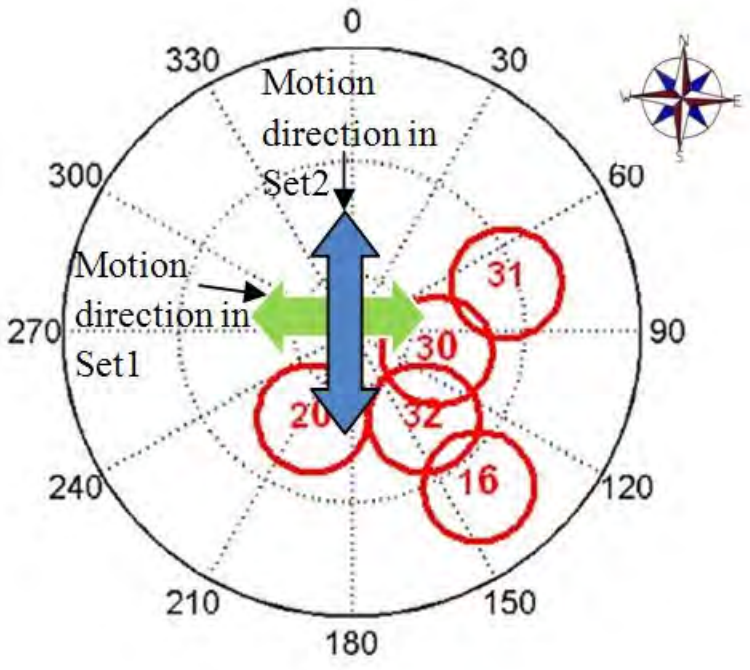

Figure 5-6: Sky plot shows the available GPS PRNs (red circles) and the motion direction of each set

5.4.2 Power Spectral Density characteristics of the indoor GPS channels.

As mentioned in the theoretical section, different multipath models have been proposed to characterize the PSD of the received signal in different multipath environments. Moreover, the effect of the antenna gain pattern on the received signal PSD was analyzed. Herein the PSD measurements for several PRNs in a harsh environment can be compared with the theoretical PSD values derived from the sphere of scatterers' model. The theoretical PSD curves are calculated utilizing the nominal antenna gain pattern calculated numerically using Eq. 5-15. The Novatel 702 GG antenna gain pattern is shown in Figure 5-4.

Figure 5-7 shows the measured PSD curves for different PRNs in the first data set. For comparison, the theoretical PSD curves based on the sphere of scatterers' multipath model considering the utilized antenna gain pattern are overlaid. The theoretical Doppler values due to the LOS signals using Eq. 5-10 are also shown with vertical arrows.

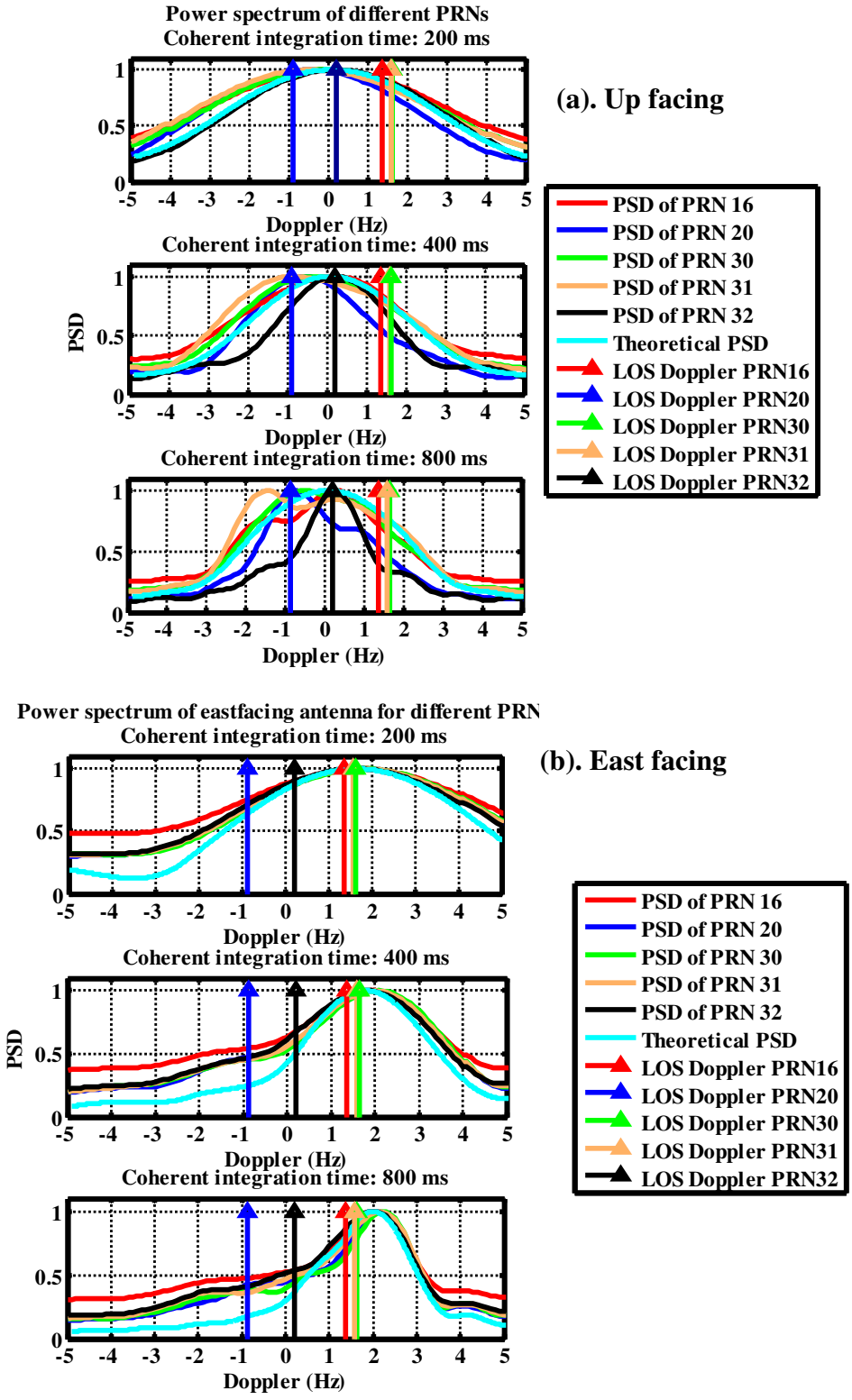

Figure 5-7: PSD curves for data set 1: (a) up facing antenna(b) east facing antenna

The PSD curves are measured based on adding the correlation outputs for all processing epochs in the frequency domain for 1000 s of captured data.

Figure 5-8 shows the theoretical and measured PSD curves for Data Set 2. Considering the results of Figure 5-7 and Figure 5-8, several observations can be made. In the case of the east and north facing antennas where the results are shown in Figure 5-7(b) and Figure 5-8(a), the PSD curves for all PRNs follow the theoretical fit. The peaks of the PSD curves are located close to the maximum Doppler shift of 2.6 Hz for a speed of 50 cm/s. This is due to the fact that in the north and east facing cases the antenna pattern has a maximum gain in the motion direction. Hence, the antenna gain pattern amplifies signals arriving from the horizon. The measurement results clearly show that the antenna gain pattern shapes the PSD pattern. Increasing the coherent integration time sharpens the measured PSD curves; however it does not improve the accuracy of the measurements. In the up-facing antenna cases where the results are shown in Figure 5-7(a) and Figure 5-8(b), although the theoretical fit are still acceptable, the goodness of fit is reduced with respect to the north or east facing cases. The measured PSD curves for some PRNs (e.g. PRN 20, PRN 32) do not match the theoretical curves. This phenomenon is more observable by increasing the coherent integration time in the case of higher elevation satellites. This observation indicates that there are dominant components on higher elevation PRNs. The presence of the dominant components in fact disrupts the sphere of scatterers model and causes the observed PSD curves to deviate from the theoretical one.

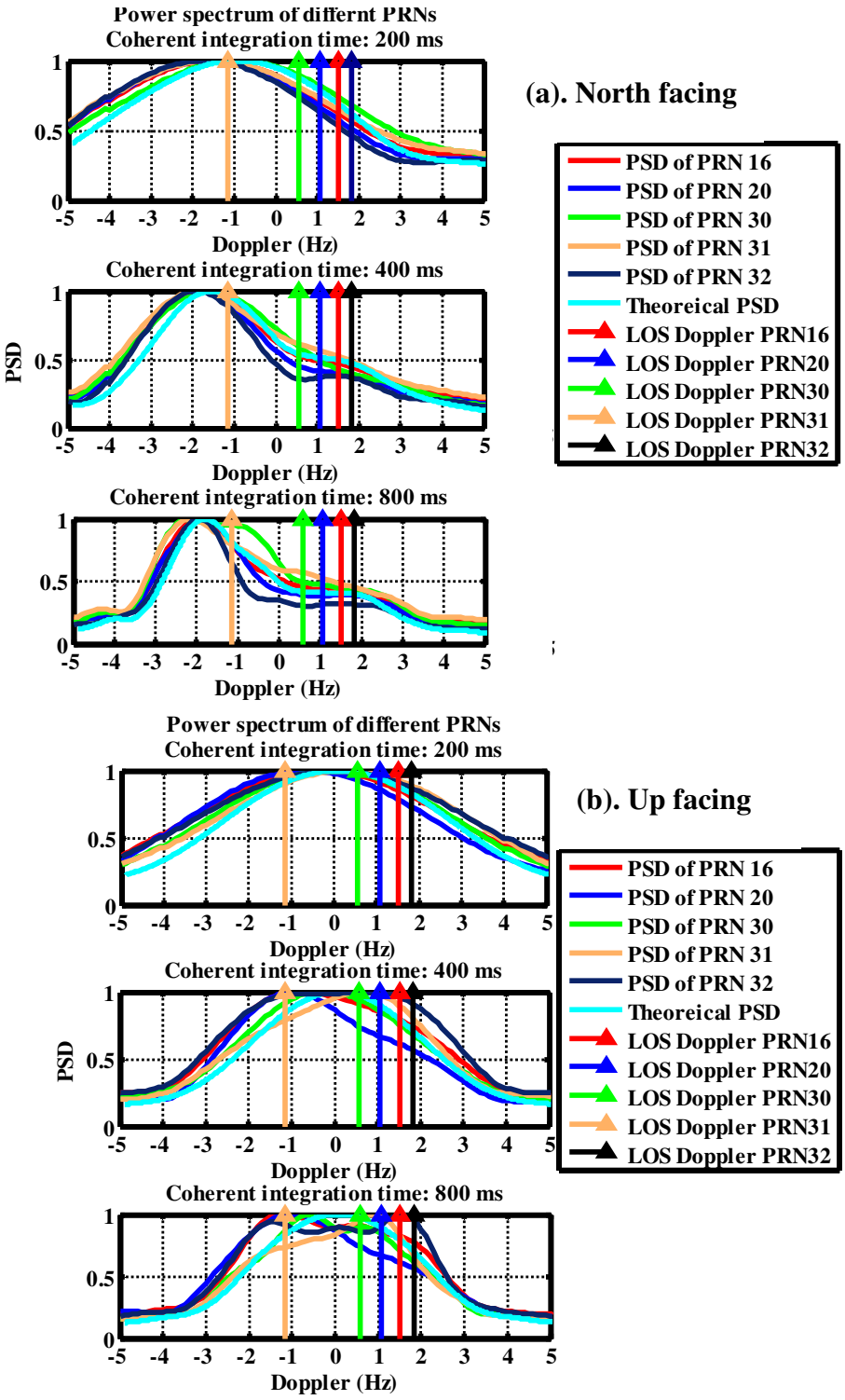

Figure 5-8: PSD curves for Data Set 2: (a) north facing antenna (b) up facing antenna

It should be mentioned that the presence of such dominant components on higher elevation PRNs is also reported in (Keshvadi et al 2012) where some data collections were performed in the same location. Although these components are dominant in the up facing cases, they are not strong enough to overcome the 10 to 15 dB attenuation due to the antenna gain pattern in the east or north facing cases. It should be mentioned that although some of these dominant components are representing the LOS Doppler values (e.g. PRN 32 and 20 in the first dataset), others are expressing the Doppler frequency of the reflected dominant paths (e.g. PRN 31 in both datasets). As a closing remark, since the PSD measurements of differently oriented antennas (up facing vs. north or east facing) are significantly different it can be concluded that the antenna gain pattern and the orientation of the antenna has a significant effect on the measured PSD curves in dense multipath environments.

5.4.3 Doppler estimation characteristics

In order to proceed further with the analysis and investigate the Doppler estimation characteristics in multipath fading environments, an epoch-by-epoch Doppler estimation method is exploited. In this method, the peak value of the correlator outputs at each processing epoch was considered as the estimated Doppler. Figure 5-9 shows the experimentally measured Probability Density Functions (PDF) of the estimated Doppler frequencies for the up facing and the east facing antennas in the first data set. The Doppler values due to the LOS components are also shown in Figure 5-9.

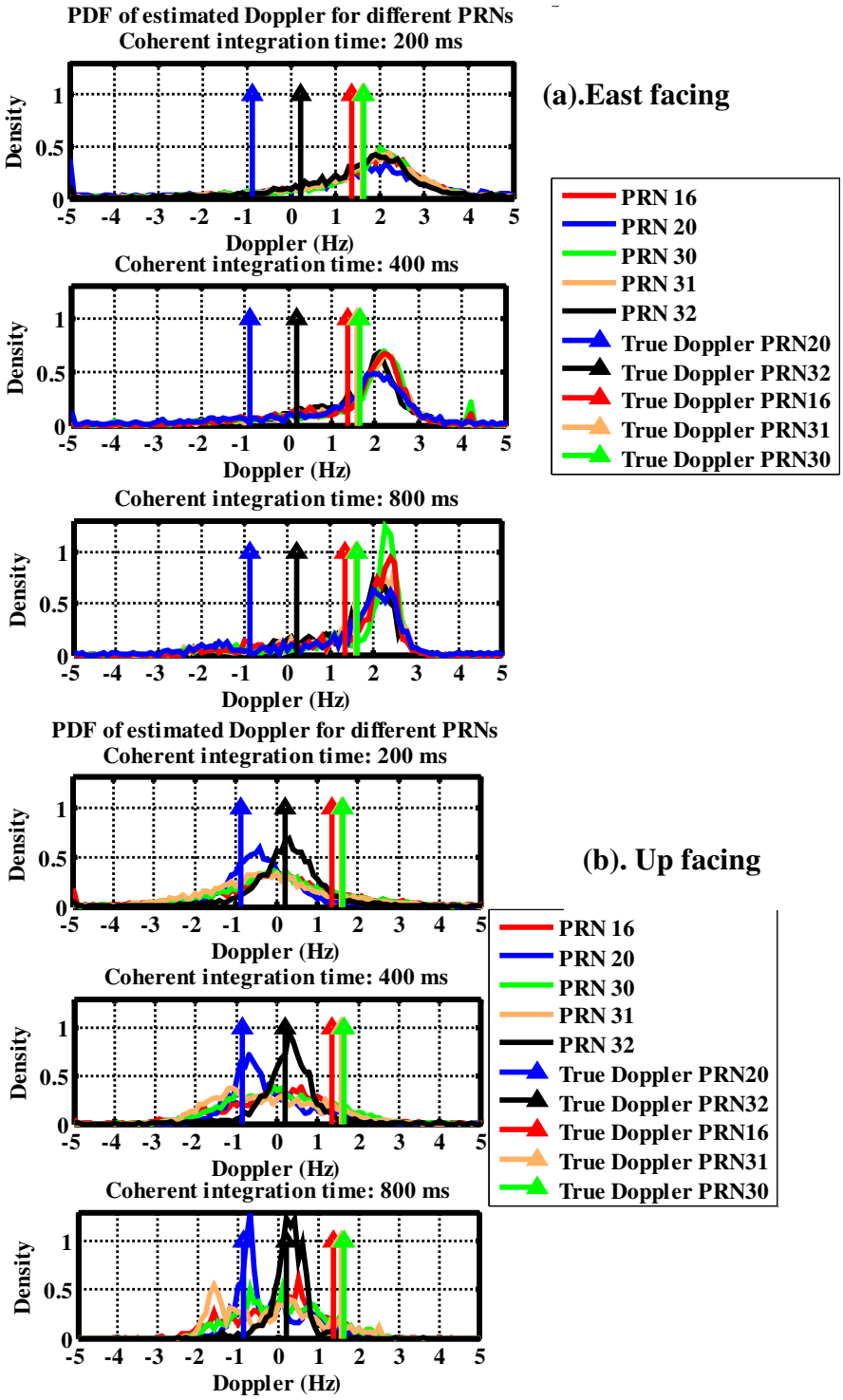

Figure 5-9: PDF of estimated Doppler values in the first data set: (a) east facing (b) up facing

Figure 5-10 shows the measured PDFs extracted from the up facing and north facing antenna in the second data set.

In the east or north facing cases (Figure 5-9(a) and Figure 5-10(a)), the estimated Doppler frequencies for all available PRNs follow the same pattern. As expected from the theoretical results (Figure 5-7 and Figure 5-8), in the multipath fading environments the Doppler measurements extracted from the antennas aligned with the motion direction are more likely to be around the maximum Doppler shift.

The measurement results in the up facing antenna cases reveal that for most PRNs the estimated Doppler values are distributed around zero. This phenomenon agrees with the theoretical findings provided in the previous section. This is due to the fact that in such cases the antenna's maximum gain pattern is perpendicular to the motion direction. The experimental measurements provided here are in agreement with the measurement results of (He et al 2012) where an up-facing antenna in different indoor locations was used.

In some circumstances (e.g. PRN 20 and PRN 32) where the satellites are located at higher elevation angles, the estimated Doppler frequencies follow the LOS Doppler values. As discussed in the previous section, this is due to the existence of dominant paths. These dominant components are however attenuated by the antenna gain pattern in the east or north facing cases. Hence, their effect is not noticeable on these cases. Increasing the coherent integration time reduces the Doppler estimation errors in cases where the LOS signal is the dominant component. It can be concluded that the measured PSD curves shown in Figure 5-7 and Figure 5-8 follow the estimated Doppler frequencies pattern shown in Figure 5-9 and Figure 5-10.

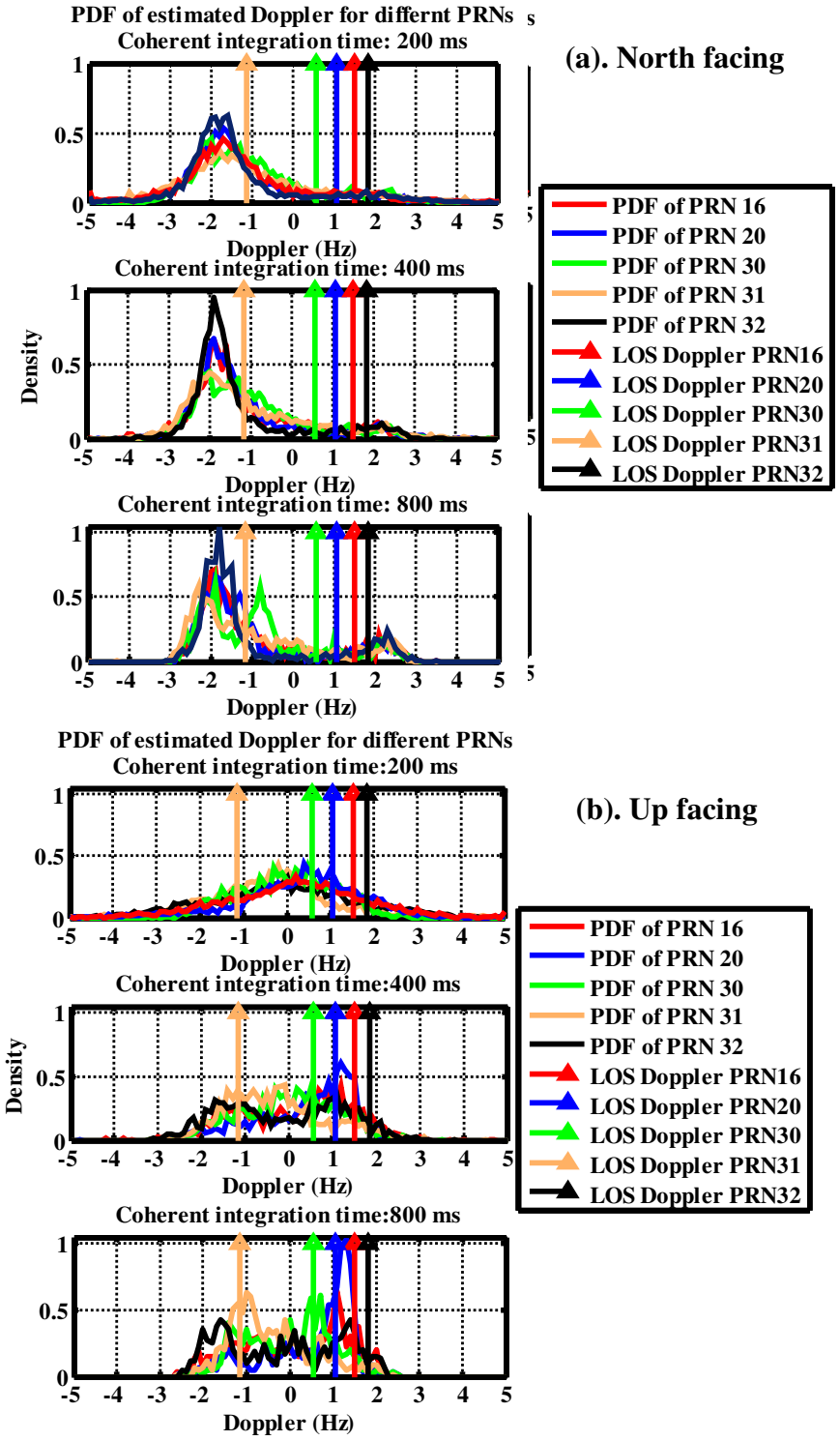

Figure 5-10: PDF of estimated Doppler values in the second data set: (a) north facing (b) up facing

5.4.4 Discussion and comparison with attenuated signal situations

In Borio et al (2011) a theoretical bound for the Doppler estimation standard deviation (STD) using the block processing method for attenuated signal circumstances is given. The theoretical bound on the Doppler STD is given as

$$\sigma_{Doppler} = \frac{1}{2\pi T_c}\sqrt{\frac{6/T}{C/N_0}} \quad \text{[Hz]} \qquad \textbf{5-22}$$

where C/N_0 represents the carrier-to-noise ratio and T is the coherent integration time. Experimental results in (Borio et al 2011) have shown that in attenuated signal environments the measurement results utilizing the block processing techniques agrees with the theoretical findings given in Eq. 5-22. It should be noted that the theoretical STD in Eq. 5-22 was derived under the attenuated LOS circumstances where the multipath effect on the Doppler estimation was not considered. To investigate the effect of multipath propagation on the Doppler estimation accuracy in diffuse multipath environments, the empirically measured Doppler STDs extracted from different antennas are shown in Figure 5-11. The theoretical STD curves based on Eq. 5-22 for different C/N_0 and coherent integration times are also overlaid to compare with the empirical STD values.

Since the measured Doppler STD values are significantly higher than the theoretical STD values, it can be concluded that the multipath propagation in dense multipath environment is the main source of error. It should be mentioned that the multipath phenomenon not only significantly increases the Doppler measurement STD but also induces a bias on the Doppler measurements, which is clearly noticeable in Figure 5-9 and Figure 5-10.

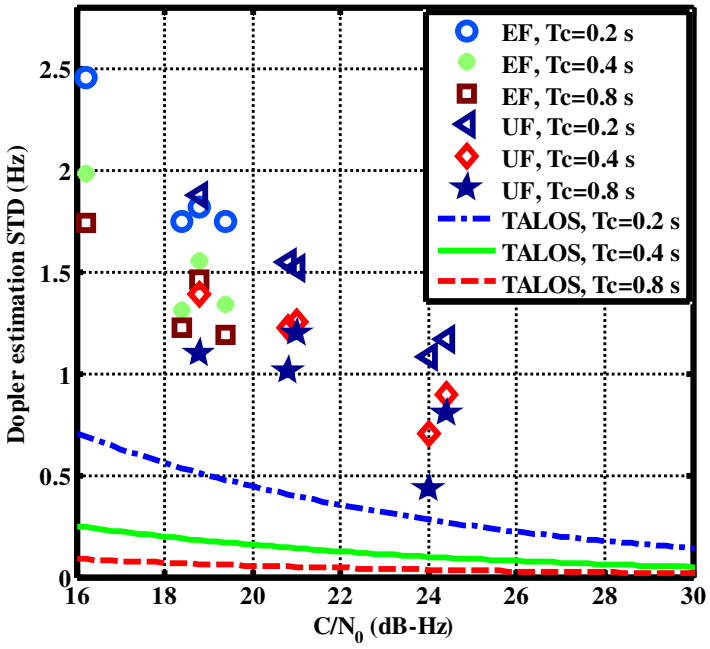

(a)

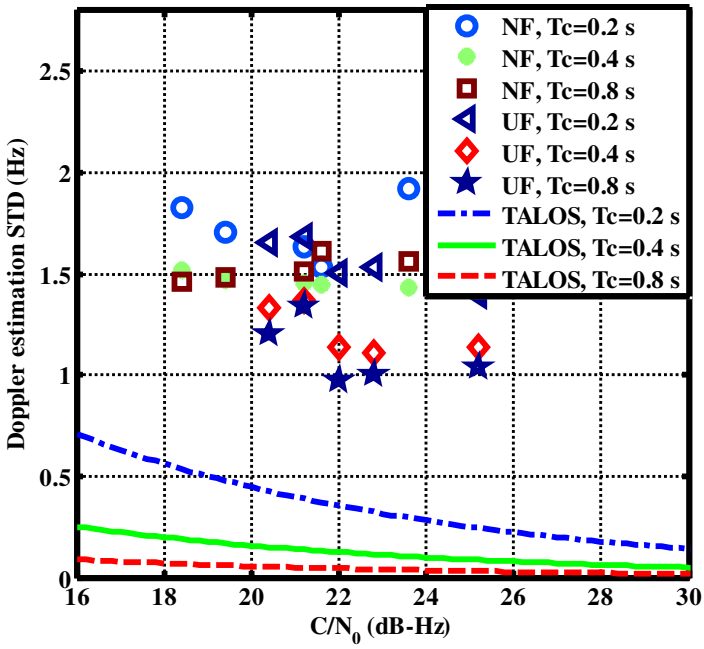

(b)

Figure 5-11: Doppler estimation STD (a) First Data Set (b) Second Data Set. NF, EF, UF and TALOS stand for north facing, east facing, up facing and Theoretical attenuated LOS respectively.

5.4.5 Velocity estimation

Since in many GNSS applications the Doppler observations are used to aid the position estimation and extract the velocity solution, the effect of Doppler estimation in harsh multipath environments on the velocity solution is considered. The A-GPS method was used whereby the Doppler measurements from an outdoor static antenna were exploited to wipe off the Doppler component caused by the satellite motion and clock drift from the indoor Doppler measurements. Then the measured Doppler values were used to estimate the velocity of the moving antenna. A least squares method was used to estimate the rover receiver velocity in each epoch. The least squares approach can be formulated as

$$\begin{bmatrix} v_{east} \\ v_{north} \\ v_{up} \end{bmatrix} = (\mathbf{H}^{\mathbf{T}}\mathbf{W}\mathbf{H})^{-1}\mathbf{H}^{T}\mathbf{W}\mathbf{f}_{d} \qquad \textbf{5-23}$$

where v_i is the velocity in the *i*-th direction (i.e. North, East and Up), $\mathbf{W}$ is the weighting matrix, which herein is assumed to be a unitary matrix, $\mathbf{f}_d$ is the Doppler measurements vector due to the receiver motion and $\mathbf{H}$ is the design matrix written as

$$\mathbf{H}_{K\times 3} = \begin{bmatrix} \cos(\varepsilon_1)\sin(\alpha_1) & \cos(\varepsilon_1)\cos(\alpha_1) & \sin(\varepsilon_1) \\ \vdots & \vdots & \vdots \\ \cos(\varepsilon_K)\sin(\alpha_K) & \cos(\varepsilon_K)\cos(\alpha_K) & \sin(\varepsilon_K) \end{bmatrix} \qquad \textbf{5-24}$$

where ε_i and α_i are the elevation and azimuth of *i*-th satellite respectively and *K* is the number of the satellites. Figure 5-12 and Figure 5-13 show the estimated velocity in the East, North and Up (ENU) coordinate for 400 ms coherent integration time of both data sets.

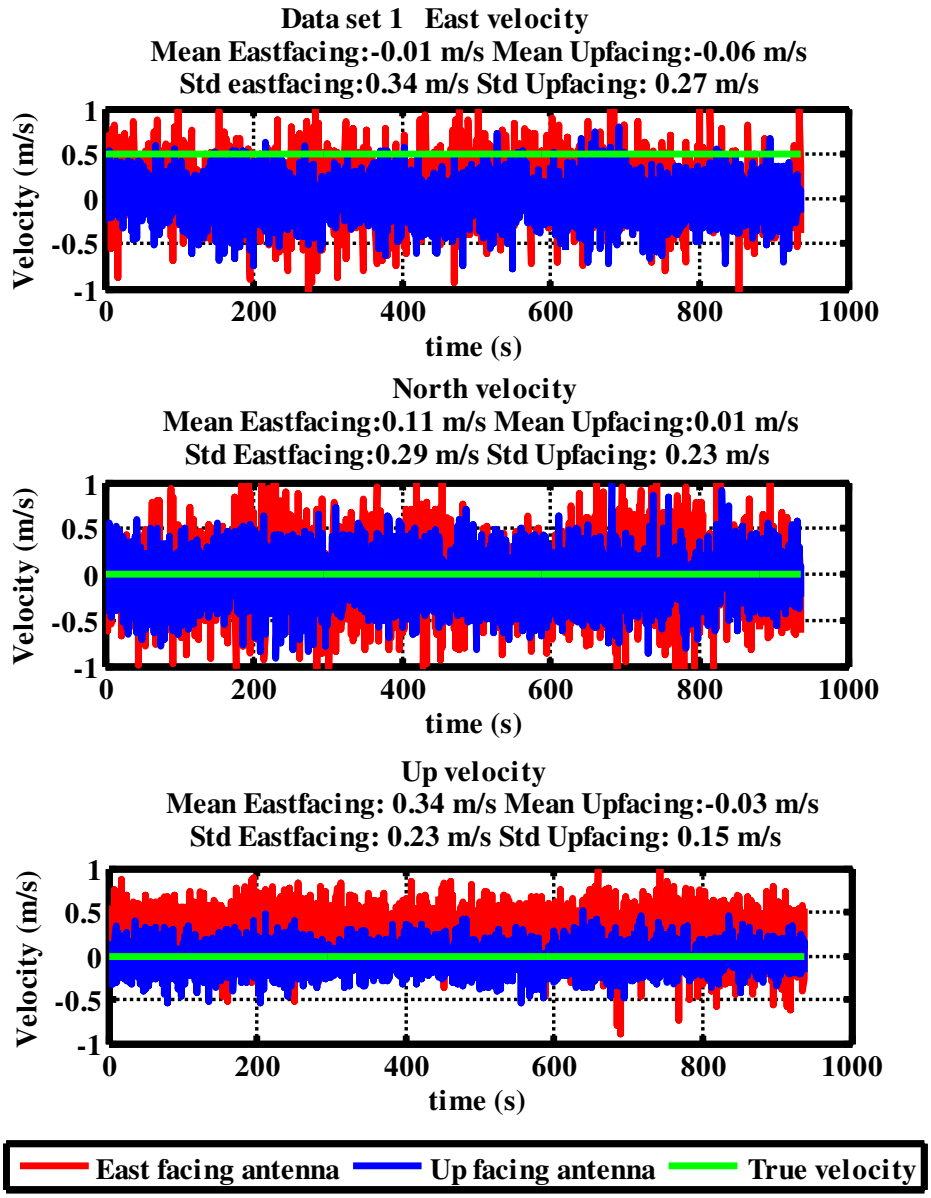

Figure 5-12:ENU velocity of first data set where the antenna performed east–west motion

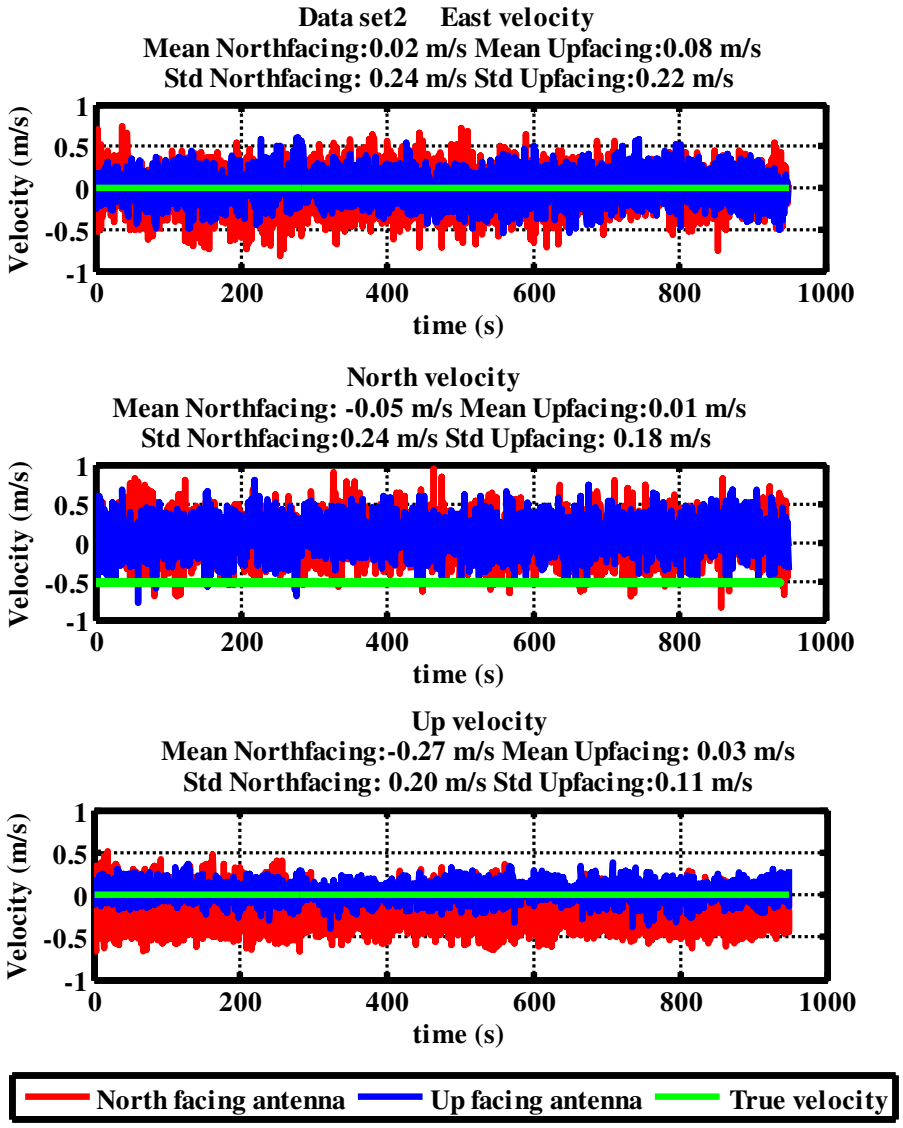

(a)

Figure 5-13: ENU velocity of second data set where antenna performed north–south motion

The observation from Figure 5-12 and Figure 5-13 can be summarized as follows:

1- The measured velocities in different directions in both data sets do not follow the true velocities.

2- The measured up velocities extracted from the East facing and the North facing antennas are biased. This is due to the fact that all Doppler measurements extracted from the antennas aligned with the motion direction are biased. This phenomenon was shown in Figure 5-9(a) and Figure 5-10(a). In the stand-alone velocity estimation method this bias is generally associated with the clock drift. However, in the reference-rover approach utilized here, since a common oscillator has been used the clock drift term has been removed from the estimation parameters of Eq. 5-23. As shown, the biased Doppler measurement is mostly associated with the up velocity. This is due to the fact that all available satellites are located on one side of the earth and hence this bias is reflected in the up velocity.

A more quantified analysis on the velocity solution can be made through the Root Mean Square Error (RMSE) analysis. The RMSE values for the individual cases are calculated by

$$\mathrm{RMSE}(\hat{v}_i) = \sqrt{\mathrm{E}\left[(\hat{v}_i - v_i)^2\right]} \qquad \textbf{5-25}$$

where $\hat{v}_i$ is the estimated velocity in i-th direction (i.e. North, East and Up) and v_i is the true velocity in the direction which extracted from the reference IMU. Table 1 and Table 2 tabulate the RMSE values of different scenarios using different coherent integration times for the first and the second data sets, respectively.

Table 1: RMSE velocity values for the first data set (m/s) (True velocity 0.5 m/s East)

	Up facing antenna			East facing antenna		
	200 ms	400 ms	800 ms	200 ms	400 ms	800 ms
North	0.35	0.28	0.25	0.42	0.33	0.32
East	**0.6**	**0.54**	**0.54**	**0.53**	**0.47**	**0.46**
Up	0.20	0.17	0.14	0.44	0.4	0.39

Table 2: RMSE velocity values for the second data set (m/s) (True velocity 0.5 m/s South)

	Up facing antenna			North facing antenna		
	200 ms	400 ms	800 ms	200 ms	400 ms	800 ms
North	**0.51**	**0.47**	**0.47**	**0.57**	**0.54**	**0.58**
East	0.22	0.17	0.17	0.26	0.25	0.26
Up	0.14	0.1	0.1	0.35	0.33	0.3

Considering the results of Table 1 and Table 2, the most important observation is the presence of significant errors on velocity solution especially in the antenna motion direction (shown by bold numbers). These velocity measurement errors are induced by neither accurate nor precise Doppler measurements. The RMSE values in the motion direction are around the actual velocity, which indicates very poor Doppler-derived velocity solution. Hence, it can be concluded that the velocity cannot be correctly estimated from the Doppler measurements in the test environment. Beside this main

observation, it was seen that increasing the coherent integration time can slightly enhance the velocity estimation performance for the up facing antenna cases. However, this is not the case for the east and north facing antennas. This slight enhancement is due to improvement in the Doppler measurements on satellites with dominant LOS components (e.g. PRNs 20 and 32 in the first data set).

5.5 Conclusions

Doppler measurement characterization in dense multipath environments for a mobile receiver has been considered. The Doppler measurements characteristics in terms of the Doppler spread and PSD metrics have been theoretically analyzed for different scatterer models. The effect of the antenna gain pattern on the Doppler PSD was also considered theoretically and practically utilizing antennas with different orientations. As shown the antenna gain pattern plays a critical role in the estimated Doppler values. A good agreement between the experimental and theoretical results was obtained. Of specific interest was to evaluate the velocity solution derived from the Doppler measurements in the dense multipath environments. The experimental results revealed poor velocity solution utilizing the Doppler measurements. Inaccurate Doppler measurements due to the multipath propagation cause inaccurate velocity estimation. It was also shown that the estimated velocity in the multipath environments does not follow the reference velocity making its usage limited to cases when a dominant LOS signal is present. Considerable biases, large variances and very poor Doppler-derived velocity solutions make Doppler measurements of limited value in harsh multipath environments for positioning purposes. The use of Doppler measurements in diversity systems is not recommended

Chapter Six: DIVERSITY SYSTEM PERFORMANCE AT THE MEASUREMENT AND POSITION LEVELS.

In Chapter 4, the detection performance of a diversity system composed of spatially separated antennas was assessed. It was shown that by utilizing spatially separated antennas and establishing diversity schemes, the detection performance is enhanced and the probability of outage is reduced. Measurement results in Chapter 5 showed that Doppler measurements are of limited value for indoor positioning in harsh multipath environments. In this chapter, the other GNSS observable (pseudorange) is studied. The pseudorange measurements extracted from the diversity branches are combined in order to improve the measurements and positioning accuracies. Performance of combining methods are practically assessed using real GPS data. The remainder of this chapter is organized as follows. First in Section 6.1, pseudorange measurements are introduced. In Section 6.2, the theoretical background of combining methods are described and practical methods for combining the pseudoranges are proposed. Section 6.3 presents some experimental results. In Section 6.4, performance of combining methods in the position domain is assessed. Section 6.5 summarizes the chapter.

6.1 Code pseudorange measurements

The apparent time shift between the receiver's replicated code and the code received at the antenna yields a function of the travel time between satellite transmission and antenna recipient (Kaplan & Hegarty 2006). The transmission is referenced to the satellites time and the reception is referenced to the receiver time, thus actually not measuring the time of travel between satellite and antenna, but the apparent time of travel. Multiplying this

time difference by the speed of light yields a biased range; hence, the observable is called a pseudorange. The pseudorange observation equation of the *j*-th satellite is given as

$$\rho^j = cd\tau = \rho_G^j + d\rho^j + c(dt^j + dT\ ) + d_{atm} + \varepsilon_{noise} + \varepsilon_{Multipath} \qquad \textbf{6-1}$$

where c is the speed of light, $d\tau$ represents the apparent time of travel, ρ_G^j represents the geometric range between *j*-th satellite and receiver. dt^j and dT represent the satellite clock error and the receiver clock error respectively, both clock errors are calculated with respect to GPS time. d_{ion} represents the ionospheric error and d_{trop} represent the tropospheric error. ε_{noise} is the error due to noise and $\varepsilon_{Multipath}$ represents the error due to multipath.

6.1.1 Differential pseudoranges

Eq. 6-1 shows that several sources of errors can influence the pseudorange measurement accuracy such as orbital errors, atmospheric effects, noise and multipath. The ionospheric error is known as the most severe error that can affect the accuracy of the pseudorange measurements. Therefore, it would be convenient to eliminate or severely reduce these errors.

A strategy called between-receivers differential GPS (DGPS) is often utilized to mitigate some of these error sources in order to improve the pseudoranges precision and accuracy (Lachapelle 2009). The between-receiver DGPS can be written as

$$\Delta\rho\ = \rho_{Rx1} - \rho_{Rx2} \qquad \textbf{6-2}$$

where $\Delta\rho$ represents the differential pseudorange measurements and ρ_{Rxi} represents the pseudorange measurements of the *i*-th receiver. Between-receivers DGPS eliminates the satellite clock error and reduce the orbital, ionospheric and tropospheric errors but amplifies the noise and multipath errors of receivers. If the spatial distance between the two receivers is short enough, the orbital, ionospheric and tropospheric can be assumed to be eliminated.

Using a short distance and assuming that errors due to noise and multipath are independent of each other and errors of two receivers are independent, the total variance of differential pseudoranges can be written as

$$\sigma^2_{\Delta\rho_{total}} = \sigma^2_{noiseRx1} + \sigma^2_{noiseRx2} + \sigma^2_{MultipathRx1} + \sigma^2_{MultipathRx2} . \quad \textbf{6-3}$$

In this work, differential pseudorange measurements are calculated between a reference outdoor antenna and indoor diversity branches. Considering the fact that the outdoor errors can be considered negligible with respect to the indoor ones, Eq. 6-3 can be approximated by (Sadrieh et al 2012)

$$\sigma^2_{\Delta\rho_{total}} = \sigma^2_{noiseIndoor} + \sigma^2_{MultipathIndoor} \quad \textbf{6-4}$$

6.1.2 Indoor pseudorange errors

Noise and multipath are two major error sources for indoor pseudorange estimation. Utilizing the between-receivers DGPS approach, noise and multipath will be the only error sources. These error sources are elaborated in the following part.

6.1.2.1 Noise

The pseudorange measurement performance due to noise, using the ML estimator in the block processing approach as described in Chapter 2, can be expressed by the Time of Arrivals (TOA) estimation variance. The TOA estimation variance can be formulated as (Stein 1981)

$$\sigma_{TOA}^2 = \left(\frac{1}{\beta}\right)^2 \frac{1}{\text{PSNR}} \quad (\text{s}^2) \qquad \textbf{6-5}$$

where PSNR represents the Post-SNR and β is the effective bandwidth, defined as

$$\beta = \frac{1}{2\pi}\left[\frac{\int_{-\infty}^{+\infty} f^2 \Omega_s(f)\, df}{\int_{-\infty}^{+\infty} \Omega_s(f)\, df}\right]^{\frac{1}{2}} \qquad \textbf{6-6}$$

where $\Omega_s(f)$ represents the signal power density spectrum as received by the receiver, defined to be zero centroid. Multiplying Eq. 6-5 by the speed of light it will yield the variance of pseudorange errors due to noise as

$$\sigma_{\rho,noise}^2 = \left(\frac{c}{\beta}\right)^2 \frac{1}{\text{PSNR}} \quad (\text{m}^2) \qquad \textbf{6-7}$$

$\sigma_{\rho,noise}^2$ represents the variance of pseudorange errors due to noise. Replacing the GPS L1 spectrum and the receiver's bandwidth in Eq. 6-6 and inserting the resultant effective bandwidth in Eq. 6-7, the noise effect on pseudorange can be quantified.

Figure 6-1: shows the pseudorange error standard deviation due to noise for different receiver bandwidths.

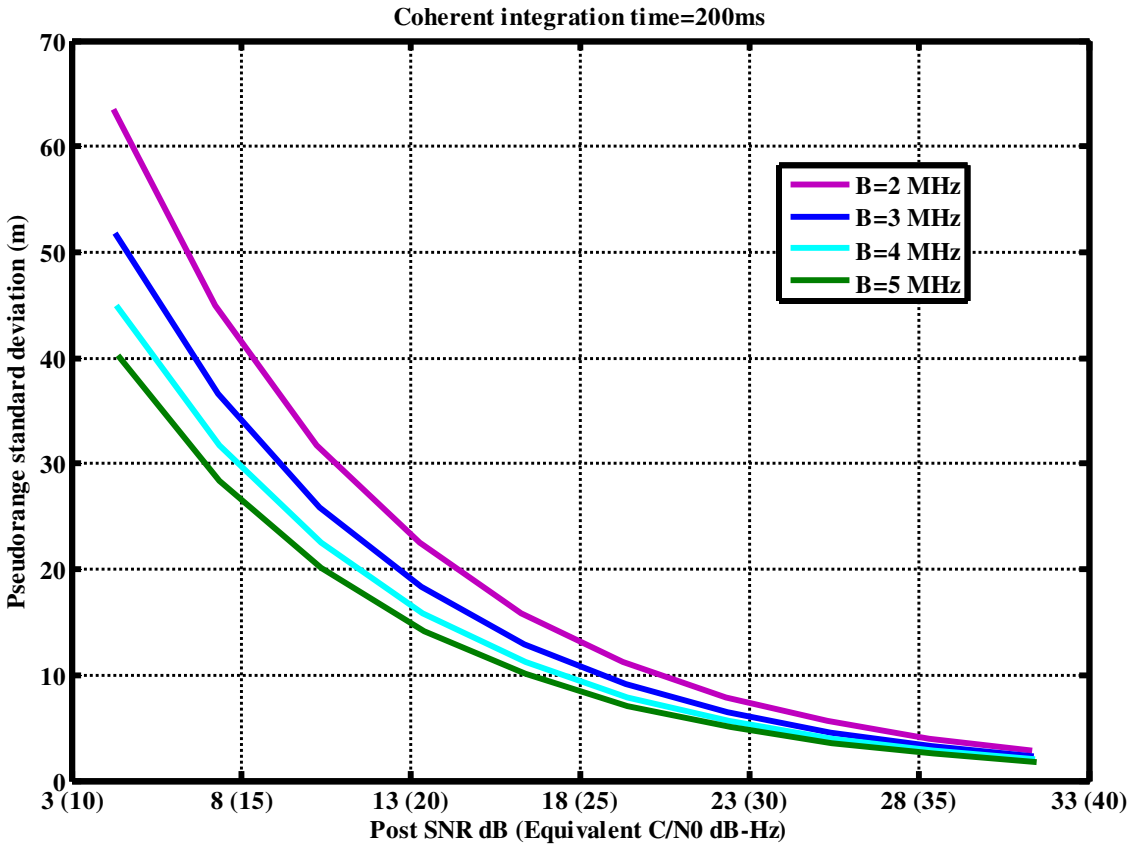

Figure 6-1: Pseudorange error standard deviation due to noise for different receiver bandwidths

6.1.2.2 Multipath

As discussed in Chapter 5, a reflected signal is a delayed and usually weaker version of the direct signal. Thus, in multipath circumstances, the C/A-code correlator output consists of a superposition of delayed, scaled replicas of the autocorrelation function. This summation does not necessarily provide a sharp undistorted peak, resulting in a pseudorange estimation error. When the LOS signal is not available, the pseudorange is derived only from the superposition of reflected signals. In indoor cases with no LOS, the pseudorange multipath error variance is related to reflectors geometry with respect to

satellite and receiver. Hence, it is complicated to characterize the pseudorange error. However, it relates in some cases to the size of the building room when operating indoors (Lachapelle 2009). As a closing remark, it can be concluded that despite the noise, it is very complicated to statistically model the errors due to multipath.

6.1.3 Pseudorange estimation using block processing method

Using the block processing method introduced in Chapter 2, the correlator output can be expressed as

$$\begin{aligned} x\left[\tau_i, \Delta f_j, n\right] &= \frac{1}{T}\int_{(n-1)T_c}^{nT_c} r(t)\,\hat{s}_o^{\tau_i,\Delta f_j}(t)^* dt \\ &= \frac{1}{T}\int_{(n-1)T_c}^{nT_c} A(\mathbf{p}(t))\, s_o(t)\hat{s}_o^{\tau_i,\Delta f_j}(t)^* dt + \frac{1}{T}\int_{(n-1)T_c}^{nT_c} w(t)\hat{s}_o^{\tau_i,\Delta f_j}(t)^* dt \end{aligned} \quad \textbf{6-8}$$

Here, the pseudorange estimation is of interest. Hence, using an outdoor nearby antenna and an Inertial Measurement Unit (IMU), the true Doppler associated with LOS is aided to the process and the bank of correlators are implemented only for a limited range of pseudoranges confined around the estimated code phase extracted from the outdoor antenna. This can significantly decrease the computational burden of realizing the bank of correlators. Hence, the correlators output can be written as

$$\begin{aligned} x\left[\tau_i, n\right]\Big|_{\Delta f_j=\Delta f} &= \frac{1}{T}\int_{(n-1)T}^{nT} r(t)\,\hat{s}_o^{\tau_i}(t)^* dt \\ &= \frac{1}{T}\int_{(n-1)T}^{nT} A(\mathbf{p}(t))\, s_o(t)\hat{s}_o^{\tau_i}(t)^* dt + \frac{1}{T}\int_{(n-1)T}^{nT} \eta(t)\hat{s}_o^{\tau_i}(t)^* dt \end{aligned} \quad \textbf{6-9}$$

Realizing a bank of correlator for each processing epoch, the Maximum Likelihood (ML) code phase can be obtained by selecting the correlator with maximum value (Borio et al 2011) as

$$\begin{aligned}\hat{\tau}(n) &= \arg \max_{\Delta f_j, \tau_i} \left| \frac{1}{T} \int_{(n-1)T}^{nT} r(t) \hat{s}_o^{\tau_i}(t)^* dt \right|^2 \\ &= \arg \max_{\Delta f_j, \tau} \left| x[\tau_i, n] \right|^2\end{aligned} \quad \textbf{6-10}$$

Since τ_i s are distributed around the code phase of the outdoor antenna, $\hat{\tau}(n)$ can be interpreted as the relative delay with respect to that antenna. Hence, the standalone pseudorange can be written as

$$\hat{\rho}(n) = \rho_{reference} + \hat{\tau}(n) c \quad \textbf{6-11}$$

where $\rho_{reference}$ is the pseudorange measured by the reference antenna and *c* is the speed of light. This procedure is shown in Figure 6-2.

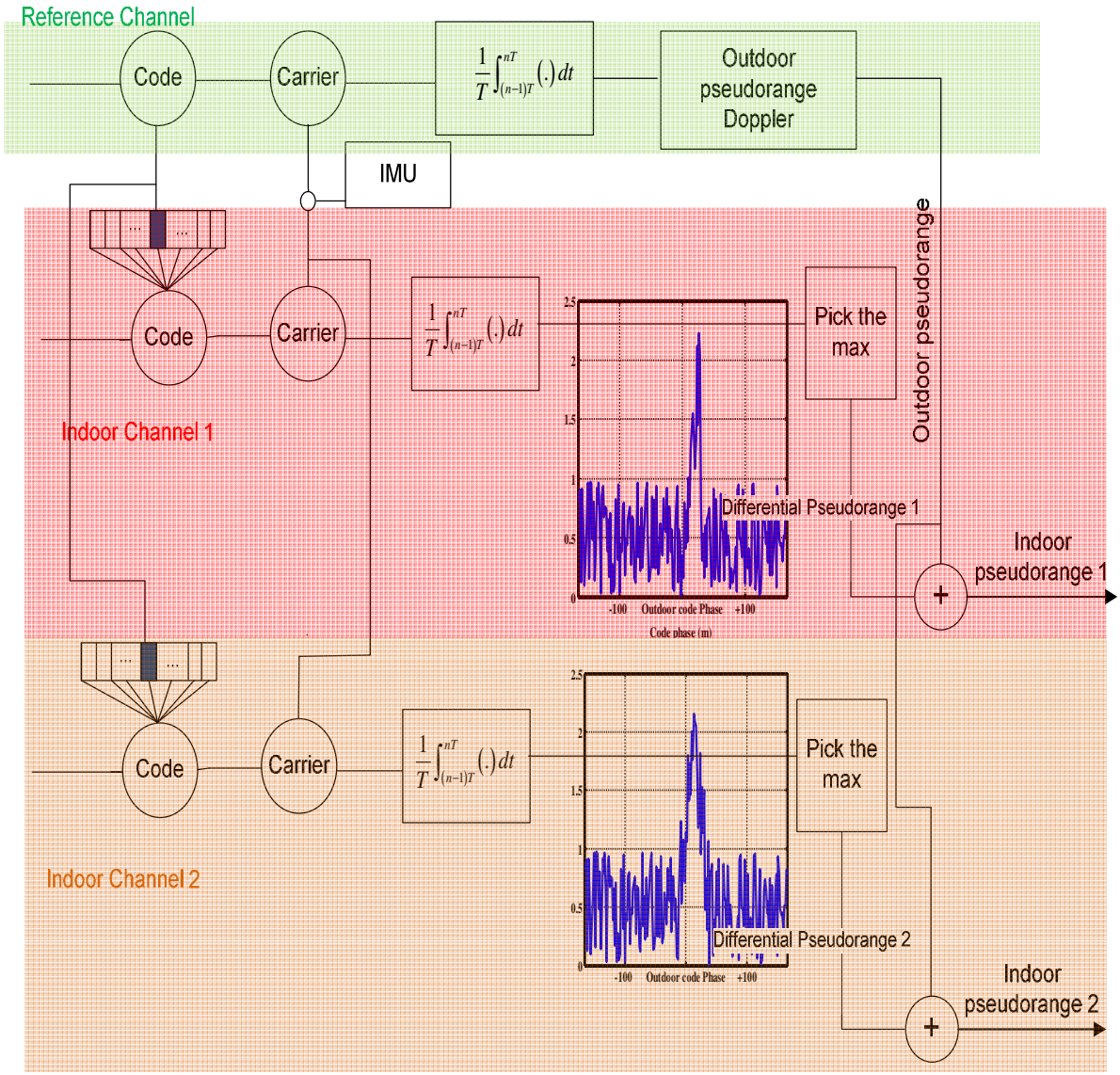

Figure 6-2: Code phase estimation procedure in the block processing method

6.2 Combining method theoretical Background

The problem of combining *M* pseudorange measurements in order to estimate a combined pseudorange can be formulated as the least squares estimation problem. The least squares method is introduced in the following part.

6.2.1 Least Squares Estimation

Least-Squares (LS) estimation relate to the estimation of a set of *m* unknown values, called state vector $\mathbf{x}$, using the set of *n* observations, called observation vector of $\mathbf{z}$. The most common model for observation for navigation-related applications is the parametric model where the observation vector can be expressed as an explicit function of the state vector. Using the parametric model and by further considering the measurements errors, the observation model can be written as (Petovello 2009)

$$\mathbf{z} = h(\mathbf{x}) + \mathbf{v} \qquad \textbf{6-12}$$

where $\mathbf{v}$ represents the effect of measurements errors and $h(\mathbf{x})$ is a function of the state vector. Although $h(\mathbf{x})$ dose not need to be a linear function, it is often convenient to consider the linear case. The linear case can be written as

$$\begin{bmatrix} z_1 \\ \bullet \\ \bullet \\ \bullet \\ z_n \end{bmatrix} = \begin{bmatrix} h_{11} & \bullet & \bullet & \bullet & h_{1m} \\ \bullet & \bullet & & & \\ \bullet & & \bullet & & \\ \bullet & & & \bullet & \\ h_{n1} & & & & h_{nm} \end{bmatrix} \begin{bmatrix} x_1 \\ \bullet \\ \bullet \\ \bullet \\ x_m \end{bmatrix} + \begin{bmatrix} v_1 \\ \bullet \\ \bullet \\ \bullet \\ v_n \end{bmatrix} \qquad \textbf{6-13}$$

For brevity, Eq. 6-13 can be expressed as

$$\mathbf{z} = \mathbf{H}\mathbf{x} + \mathbf{v} \qquad \textbf{6-14}$$

where $\mathbf{H}$ is $n \times m$ matrix, called the design matrix. If $\mathbf{H}$ dose not have full rank ($n < m$) the problem is under-determined which means that the number of observation is less than the number of unknowns. If $n = m$, the problem is uniquely determined and when $n > m$ the problem is overdetermined. Least Squares is a method to compute a unique solution for overdetermined cases. In (Petovello 2009) and indeed many other references it is proven that the LS unique estimate of the state vector can be given as

$$\hat{\mathbf{x}} = \left(\mathbf{H}^T R^{-1} \mathbf{H}\right)^{-1} \mathbf{H}^T R^{-1} \mathbf{z} \qquad \textbf{6-15}$$

where R is the covariance matrix of observation errors. The state covariance matrix can be written as

$$C_{\hat{x}} = \left(\mathbf{H}^T R^{-1} \mathbf{H}\right)^{-1} \qquad \textbf{6-16}$$

6.2.2 Least squares for combining pseudoranges

Having pseudorange measurements of a specific satellite extracted from *M* diversity branches and intended to estimate the pseudorange is an overdetermined problem with *M* observations and only one unknown.

As shown by Eq. 6-11, all of *M* pseudorange observations have a common part (the pseudorange at the outdoor antenna) plus the indoor differential measurements. In order to focus on indoor error sources, herein the differential pseudorange (code phase) combining is considered and formulated as

$$\begin{bmatrix} \Delta\rho_1^j \\ \bullet \\ \bullet \\ \bullet \\ \Delta\rho_M^j \end{bmatrix} = \begin{bmatrix} 1 \\ \bullet \\ \bullet \\ \bullet \\ 1 \end{bmatrix} \left[\Delta\rho^j\right] + \begin{bmatrix} v_1 \\ \bullet \\ \bullet \\ \bullet \\ v_M \end{bmatrix} \qquad \textbf{6-17}$$

where $\Delta\rho_i^j$ represents the differential pseudorange extracted from the *i*-th diversity branch for the *j*-th satellite. $\Delta\rho^j$ is the differential pseudorange to be estimated for the *j*-th satellite and v_i represents the differential pseudorange error extracted from the *i*-th diversity branch.

Note that although in the above equation, it is assumed that all antennas measure the same differential pseudorange, in fact they measure slightly different pseudoranges because of their different spatial distance. Herein, since the spacing (around 10 cm) is negligible with respect to the measurements errors (10 s of metres) it can be conveniently assumed that all differential pseudoranges are the same. Hence, the LS estimate of the differential pseudorange for the *j*-th satellite can be written as

$$\Delta\hat{\rho}^j = \left(\begin{bmatrix} 1 & 1 & \bullet & \bullet & \bullet & 1 \end{bmatrix} R^{-1} \begin{bmatrix} 1 \\ 1 \\ \bullet \\ \bullet \\ \bullet \\ 1 \end{bmatrix} \right)^{-1} \begin{bmatrix} 1 & 1 & \bullet & \bullet & \bullet & 1 \end{bmatrix} R^{-1} \begin{bmatrix} \Delta\rho_1^j \\ \bullet \\ \bullet \\ \bullet \\ \Delta\rho_M^j \end{bmatrix} \qquad \textbf{6-18}$$

By assuming that errors of differential measurements of different diversity branches are independent of each other, R will be a diagonal matrix and Eq.6-18 can be written as

$$\Delta\hat{\rho}^{j} = \left(\begin{bmatrix} 1 & 1 & \cdots & 1 \end{bmatrix} \begin{bmatrix} \sigma_1^{-2} & 0 & \cdot & \cdot & 0 \\ 0 & \sigma_2^{-2} & & & \cdot \\ \cdot & & \cdot & & \cdot \\ \cdot & & & \cdot & \cdot \\ 0 & & & & \sigma_M^{-2} \end{bmatrix} \begin{bmatrix} 1 \\ 1 \\ \cdot \\ \cdot \\ \cdot \\ 1 \end{bmatrix} \right)^{-1} \begin{bmatrix} 1 & 1 & \cdots & 1 \end{bmatrix} \begin{bmatrix} \sigma_1^{-2} & 0 & \cdot & \cdot & 0 \\ 0 & \sigma_2^{-2} & & & \cdot \\ \cdot & & \cdot & & \cdot \\ \cdot & & & \cdot & \cdot \\ 0 & & & & \sigma_M^{-2} \end{bmatrix} \begin{bmatrix} \Delta\rho_1^{j} \\ \cdot \\ \cdot \\ \cdot \\ \Delta\rho_M^{j} \end{bmatrix} \quad \textbf{6-19}$$

where σ_i represents the standard deviation of the differential pseudorange of the *i*-th diversity branch. After some manipulations, Eq.6-19 can be simplified to

$$\Delta\hat{\rho}^{j} = \frac{\sum_{i=1}^{M} \Delta\rho_i^{j} \sigma_i^{-2}}{\sum_{i=1}^{M} \sigma_i^{-2}} \quad \textbf{6-20}$$

The standard deviation of the estimate can be written as

$$\sigma_{\Delta\rho} = \left(\frac{1}{\sum_{i=1}^{M} \sigma_i^{-2}} \right)^{\frac{1}{2}} \quad \textbf{6-21}$$

Assuming the same error variances for all diversity branches, the variance of the combined pseudorange will be $\left(\frac{1}{M}\right)$ of the variance of individual branches.

6.2.3 Practical methods

As discussed in the preceding part, in order to establish an LS approach the covariance matrix of differential pseudoranges is required. Recalling the non-stationary nature of a channel, the covariance matrix is required to be updated epoch-by-epoch. Since it is not

feasible to calculate the covariance matrix statistically, two practical alternatives are considered herein:

1- Ignoring the covariance matrix. Although ignoring the covariance matrix degrades the LS performance, it does not disrupt its application conceptually. Eliminating the measurements error covariance matrix the estimated differential pseudorange will be the mean of differential pseudoranges extracted from diversity branches. This method is called the Non-Weighted LS (NWLS) hereafter and can be formulated as

$$\Delta\hat{\rho}^{j}(n)=\frac{\sum_{i=1}^{M}\Delta\rho_{i}^{j}(n)}{M} \qquad \textbf{6-22}$$

where n represents the epoch number.

2- Using the epoch-by-epoch estimated SNR to generate the measurements covariance matrix. As discussed earlier the major error sources for differential measurements are noise and multipath. Errors due to noise can be modeled by Eq. 6-7 whereas the multipath effect is very complicated to model. Ignoring it, the measurements covariance matrix can be generated based on SNR. Note that if any statistical information about the multipath effect is available, it can also be considered on the measurement error covariance matrix. However, due to the lack of such information herein, the covariance matrix is generated based on SNR. This method is called SNR based Weighted LS (SNRWLC) hereafter and can be expressed as

$$\Delta\hat{\rho}^{j}(n)=\frac{\sum_{i=1}^{M}\Delta\rho_{i}^{j}(n)w_{i}(n)}{\sum_{i=1}^{M}w_{i}(n)} \qquad \textbf{6-23}$$

where $w_i(n)$ are generated based on PSNR as

$$w_{i}(n)=\frac{1}{\sigma^{2}_{\mathrm{Pr}ange,i}(n)}\propto \mathrm{PSNR}_{i}(n) \qquad \textbf{6-24}$$

.

In addition to the above methods, two combining methods at the correlator outputs namely Equal Gain Combiner and Weighted Combiner, whose detection performance are assessed in Chapter 4, can also be tested at the measurement level. Hence, a total of four combining methods are to be assessed at the measurement level (see Figure 4-2).

6.3 Experimental results

In order to investigate the performance of the aforementioned combining methods, practical experiments are carried out. Herein, the same data sets utilized in Chapter 4 have been considered. As mentioned in Chapter 4 two data sets were collected in two harsh multipath environments. For brevity, the data collection setting and setups are not described again. The reader is referred to Chapter 4 for a comprehensive explanation of the data collections settings and setups. Table 6-1 summarizes some information about the data collection plans.

Table 6-1: Data collection specifications

Data set	1	2
Location	Laboratory	Workshop
Speed of moving (Rover) antennas	5 cm/s	25 cm/s
Number of diversity branches	4	2

6.3.1 Data processing

In order to enable the block processing method, the PLAN group software receiver GSNRx-rr was used. As discussed in Chapter 4, GSNRx-rr is a modified version of the standard GSNRx (O'Driscoll et al 2010) software receiver and allows the joint processing of several input channels. The first channel should be an outdoor reference channel, which provides the aiding information. For each of the other channels (diversity branches), GSNRx-rr provides correlator outputs for each processing epoch. There is an option file to manage the correlation process in terms of correlator ranges in code phase and Doppler, correlator spacing and coherent integration time. Table 6-2 tabulates the setting used in GSNRx-rr to process the data.

Table 6-2: GSNRx-rr settings for data processing

Data set	1	2
Location	Laboratory	Workshop
Code phase range	±150 m with the center of outdoor antenna's code phase	
Code phase step size	3 m (about 0.01 chip)	
Frequency range and step size	0 Hz (the true LOS Doppler is aided)	
Coherent integration time	200 ms	400 ms
Elevation mask	10^{o}	15^{o}

6.3.2 Differential pseudorange standard deviation

The performance of combining methods at the measurement level is assessed through the analysis of the differential pseudorange standard deviation. As discussed earlier the standard deviation of differential pseudoranges with very short baseline represents the combined effect of noise and multipath of indoor and outdoor antennas. Since the indoor error sources are considerably more severe than outdoor ones, it can be assumed that the standard deviation of differential pseudorange represents the noise and multipath of the indoor receiver. Figure 6-3 presents the differential pseudorange standard deviations of single branches, combining methods at correlator output and combining methods at the measurement level.

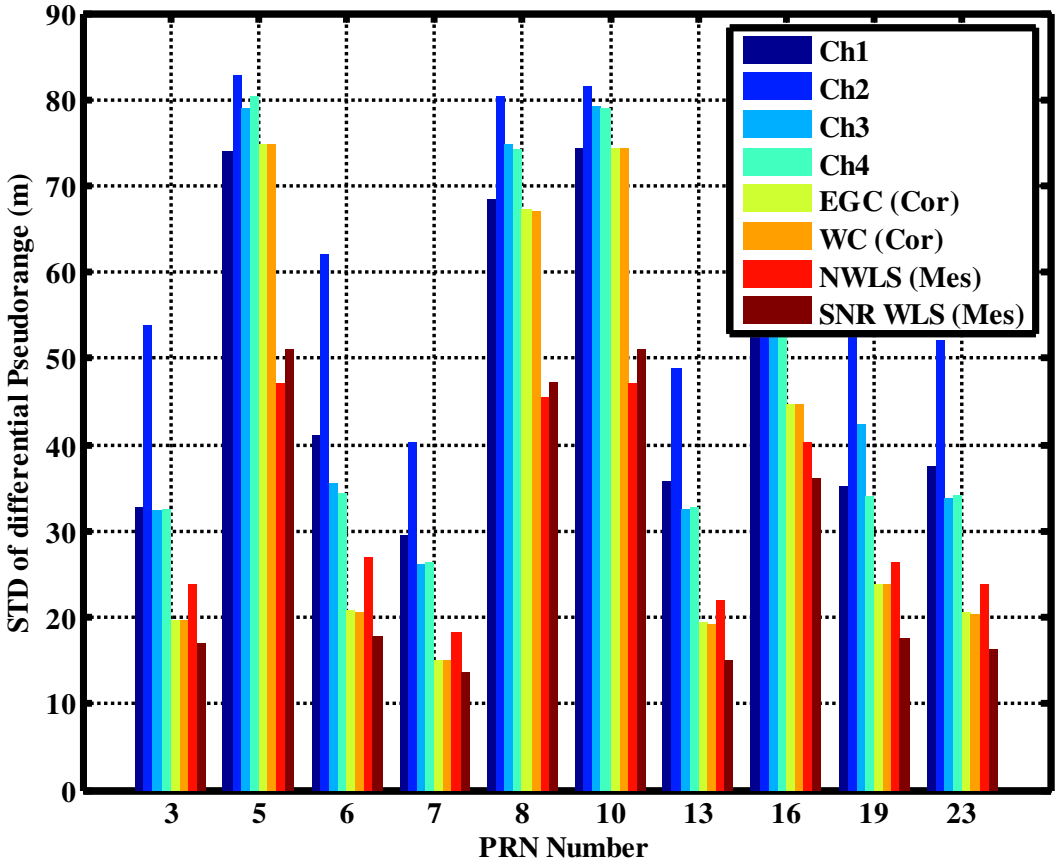

Figure 6-3: Standard deviations of differential pseudoranges of single branches and combining methods

Figure 6-4 shows the differential pseudorange standard deviations of single branches and all combining methods for the second data set.

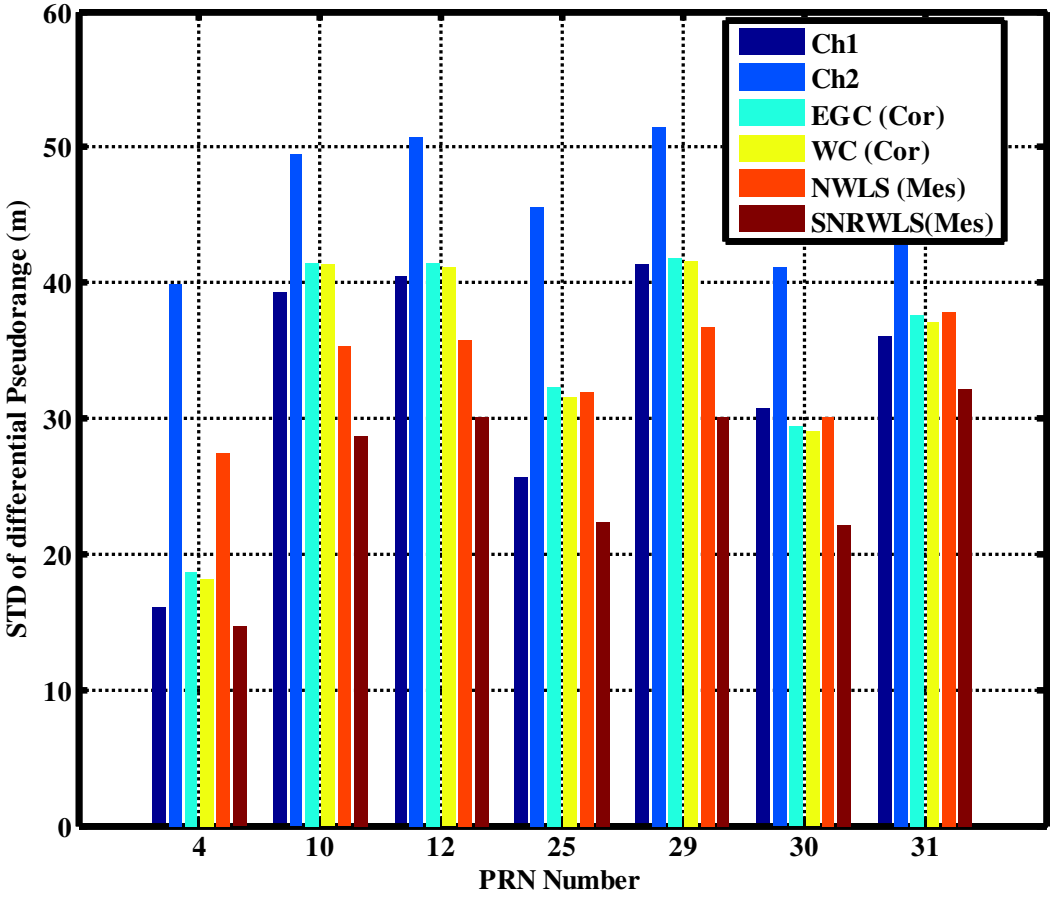

Figure 6-4: Standard deviation of differential pseudoranges of single branches and combining methods for the second data set

Analysing Figure 6-3 and Figure 6-4, the following observations can be made:

1- In both data sets, applying combining methods enhances the measurements precision.

2- NWLS is vulnerable to discrepancy of channel quality (e.g. PRN 6 first data set and PRN 4 second data set).

3- SNRWLS performs best among all combining methods and single branches. However, there are few exceptions in the first data set namely PRNs 5, 8 and 10

where NWLS performs better than SNRWLS. This is due to the fact that the qualities of these PRNs are too poor (see the standard deviation of single branches) for the SNR estimator to perform properly. Hence, weights, which are designed based on estimated SNRs, do not work properly either. For other PRNs in the first data set using SNRWLS set, the standard deviation of measurements is reduced to approximately half of the standard deviation of single branches.

4- Since the number of diversity branches in the first data set is higher than the second data set, enhancement achieved through combining methods in the first data set is more than in the second data set.

It is of interest to compare the performance of combining methods at the correlator outputs (e.g. ECG and WC) with combining methods at the measurement level (NWLS and SNRWLS).

As alluded in Chapter 4, the aim of combining methods at the correlator outputs is to enhance the detection performance. Hence, these methods are not designed to improve the measurements precision. However, as shown by Eq. 6-7 enhancing the PSNR enhances the pseudorange precision. Hence, the enhancement achieved by applying combining methods on measurement precision is associated to the PSNR enhancement achieved by non-coherent combining of diversity branches at correlator outputs.

The combining methods at the measurement level are designed to enhance the measurement precision. However, the drawback of combining at the measurement level is that they require the signal detection to be performed by single branches. Hence, the satellite availability will degrade.

To consider a satellite available with the SNRWLS method, at least one of the diversity branches should correctly detect that satellite, which is likely to be the branch with the best SNR. Hence, satellite availability in combining methods at the measurements level depends on the performance of the branch with the highest SNR, which is the same as satellite availability in the Selection Combiner (SC) method at the correlator outputs presented in Chapter 4. As a closing remark, combining methods at the measurement level performs significantly better than combining methods at the correlator outputs to enhance the measurement precision. However, in terms of satellite availability combining methods at the measurement level perform like selection combining at the correlator outputs, which is slightly below WC (see Figure 4-11and Figure 4-12).

6.3.3 Bias analysis

Although the precision of measurements is of significant value, their accuracy is more important. However, accuracy analysis for pseudorange is a complicated task because of the clock bias term in pseudoranges. Considering the difficulties associated to determine indoor channels clock bias, the accuracy analysis will be performed in the position domain.

6.4 Position domain

The process of estimating the Position, Velocity and Time (PVT) from the measurements is called the navigation solution. Since the ultimate goal of many GNSS applications is to estimate the users' position, the performance of the proposed combining methods are assessed at the position level below as the final step.

6.4.1 Least Squares positioning

There are different methods for position estimation such as Least Squares (LS) and Kalman Filtering (KF). Herein, the single point non-weighted LS approach is utilized. It should be noted that using a Differential GPS (DGPS) together with KF instead of LS or using the weighted LS could enhance the position solution performance in certain situations. However, since the aim of this research is to evaluate the performance of diversity systems at the position level and compare it with individual diversity branches, the epoch by epoch single point non-weighted LS is opted as the preferred method to avoid smoothing effects. The estimated pseudorange values provided by single branches and the combining methods are used to estimate the position and clock bias. The linear LS method was introduced in Section 6.2.1. Since the relation between pseudorange and position is not linear, the non-linear LS approach should be used. In non-linear LS, the observation equation is expanded around the current state using the Taylor series. Approximating the Taylor series by the first order term linearize the equation. Linearizing the observation equation around the local level reference (position and clock bias of the outdoor antenna), the linearized observation equation can be written as

$$\delta\boldsymbol{\rho} = \mathbf{H} \begin{bmatrix} \Delta E \\ \Delta N \\ \Delta U \\ \Delta T \end{bmatrix} + \mathbf{v} \qquad \textbf{6-25}$$

where ΔE is the easting correction, ΔN is the northing correction and ΔU is the up correction with respect to the local level reference. $\delta\boldsymbol{\rho}$ is the pseudorange misclosure vector with respect to the local level and clock bias references. Note that for combining

methods, each element of $\delta\boldsymbol{\rho}$ vector is the combined pseudorange (resultant of combining M pseudoranges extracted from diversity branches) and $\mathbf{H}$ is the $K \times 4$ design matrix written as

$$\mathbf{H}_{K\times 4} = \begin{bmatrix} \cos(\varepsilon_1)\sin(\alpha_1) & \cos(\varepsilon_1)\cos(\alpha_1) & \sin(\varepsilon_1) & 1 \\ \vdots & \vdots & \vdots & 1 \\ \cos(\varepsilon_K)\sin(\alpha_K) & \cos(\varepsilon_K)\cos(\alpha_K) & \sin(\varepsilon_K) & 1 \end{bmatrix} \quad \textbf{6-26}$$

where ε_i and α_i are the elevation and azimuth of the *i*-th satellite, respectively, and *K* is the number of satellites. Then the position corrections can be written as

$$\begin{bmatrix} \Delta E \\ \Delta N \\ \Delta U \\ \Delta T \end{bmatrix} = (\mathbf{H}^{\mathbf{T}}\mathbf{H})^{-1}\mathbf{H}^{T}\delta\boldsymbol{\rho}_{K\times 1} \quad \textbf{6-27}$$

6.4.2 Standard deviation of single point positioning

Epoch-by-epoch positions can be estimated for single branches and different combining methods using the LS approach. Figure 6-5 shows the estimated positions for single branches and the EGC method for the second data set.

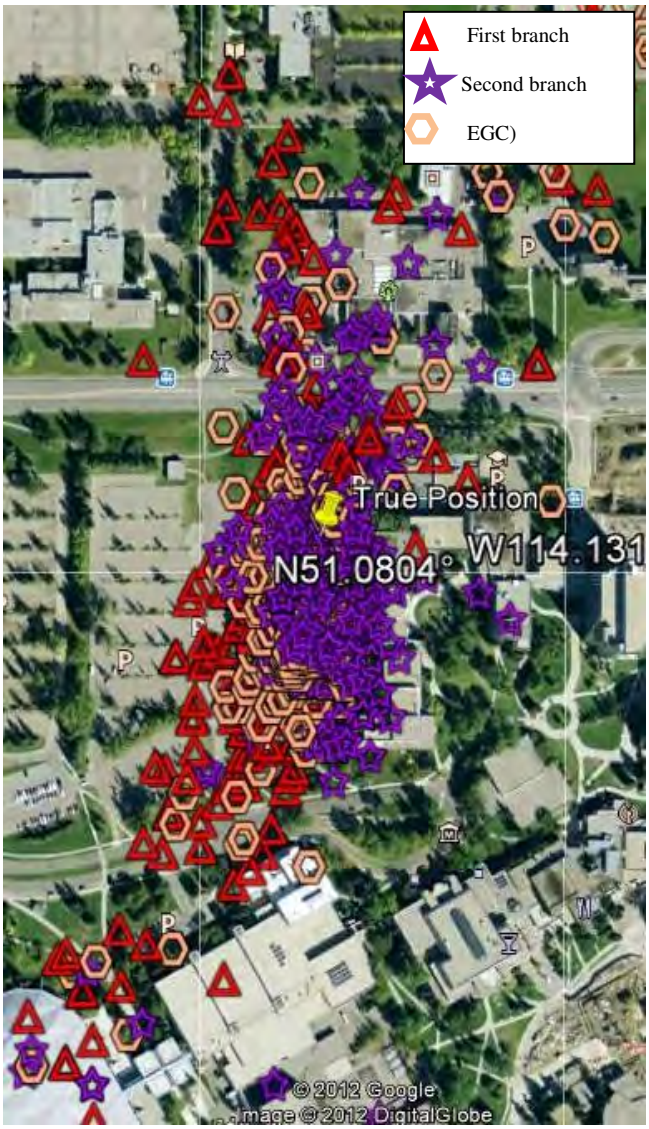

Figure 6-5: Estimated positions for single branches and EGC method for second data set

It can be observed from Figure 6-5 that the estimated positions are distributed on a broad area specifically in the north direction. Hence, it can be concluded that the northing error is higher than easting in this case, which is due to satellite geometry. Although it is an expected observation because of the relatively high latitude of Calgary, in this case unsuitable position of outdoor antenna (the south sight of outdoor antenna was partly

blocked by the CCIT building) amplifies this phenomenon. A Dilution of Precision (DOP) analysis backs up this observation, and the measured North DOP (NDOP) was around 1.35 whereas the East DOP (EDOP) was around 0.66.

In order to provide a better insight using the estimated positions, the 2D confidence ellipses were formed. The 2D confidence ellipses show a region that contains the true position at a probability level of 39%. Figure 6-6 shows the 2D ellipses associated to single branches and different combining methods for the second data set.

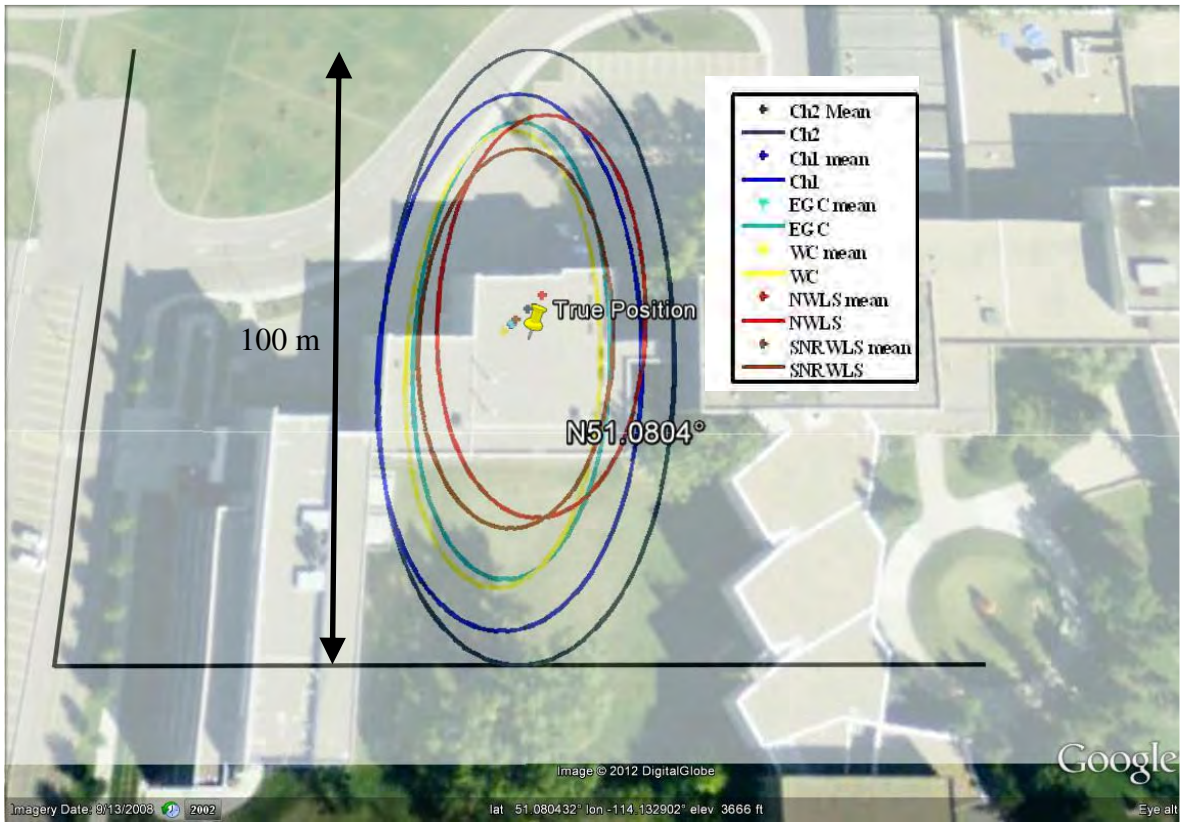

Figure 6-6: 2D ellipses for single branches and different combining methods of second data set

The estimated position means are also overlaid in Figure 6-6.

Observations from Figure 6-6 are as follows:

1- All single branches and combining methods are performing in an acceptable manner in terms of bias. Even the estimated position means using NWLS method, which performs the worst in terms of bias, are just 5 m off from the true position in horizontal plane.
2- Applying combining methods, the positioning accuracy improves significantly.
3- SNRWLS performs best since it has the smallest confidence ellipse (the brown ellipse) and very slight bias (less than 2 m in the horizontal plane)

Quantifying analysis for 3D positioning can be carried out through analysing the positioning standard deviations. Figure 6-7 compares the position standard deviations for single branches and different combining methods for the first data set.

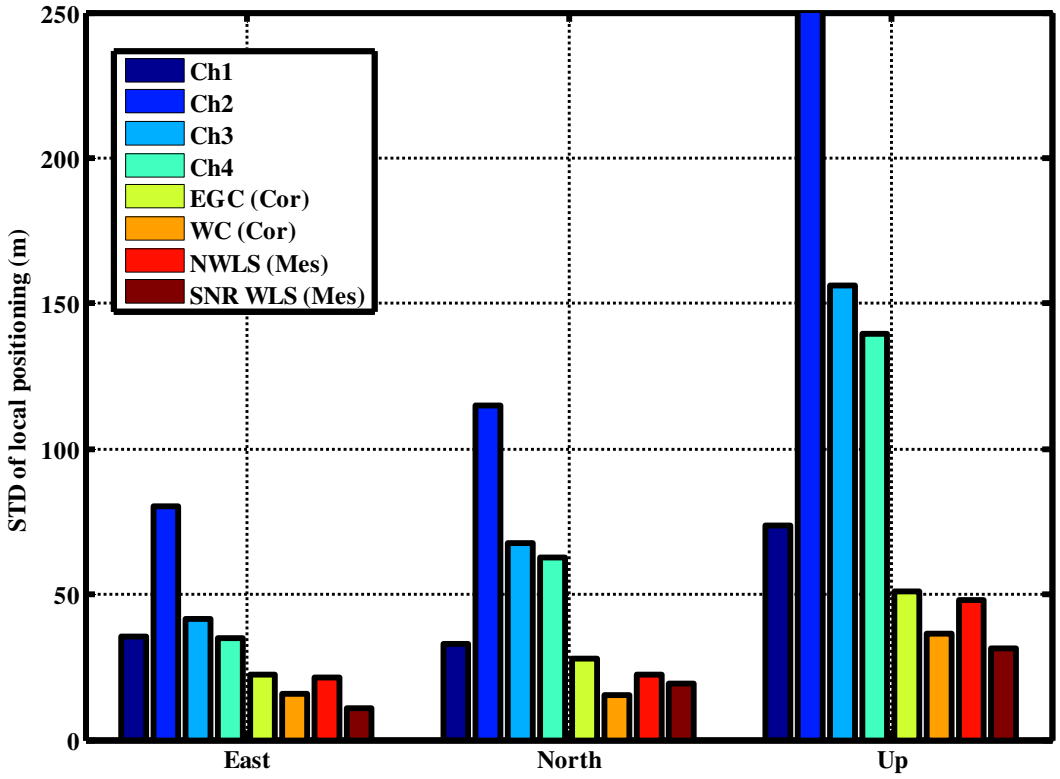

Figure 6-7: Standard deviations of local single point positions of single branches and different combining methods for first data set

The results for the second data set are presented in Figure 6-8.

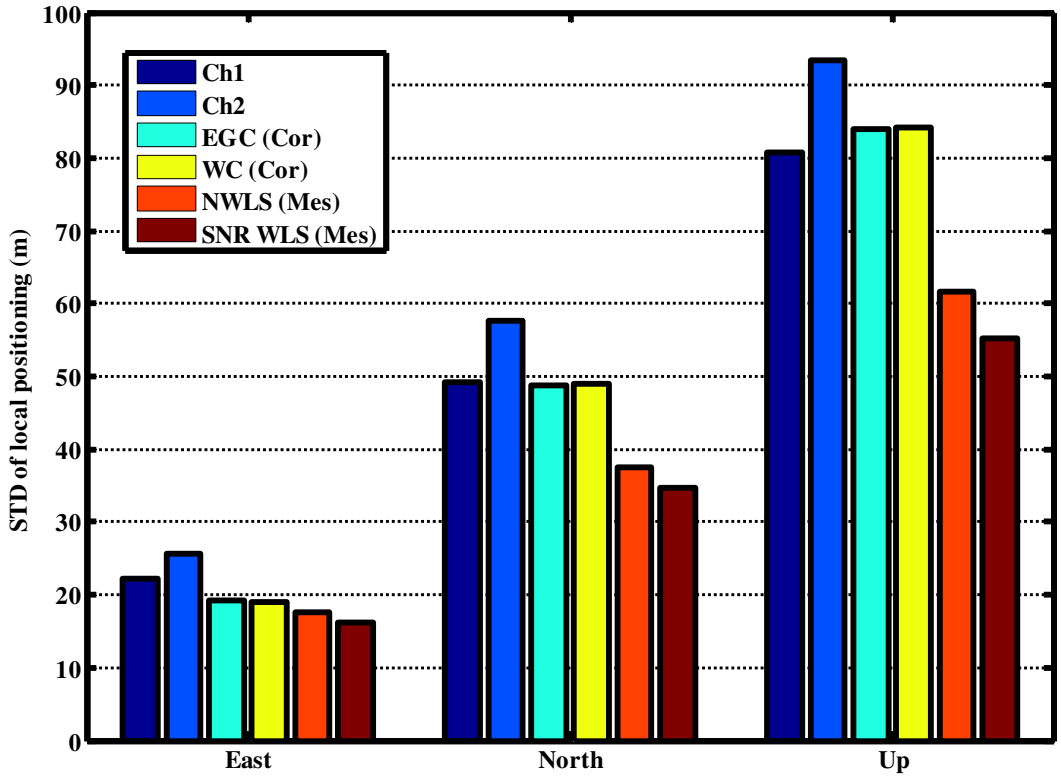

Figure 6-8: Standard deviations of single point positions of single branches and different combining methods for second data set

Since in the first data set, one of the diversity channels quality is considerably lower than others (Ch2), NWLS and EGC, which treat all the branches equally, experience degraded performance. In the second data set, where the discrepancy of channels quality is slighter than in the first data set, EGC and NWLS perform closer to their weighted versions, namely WC and SNRWLS.

In order to summarize the positioning accuracies in the horizontal plane, the Distance Root Mean Squared (DRMS) value for all single branches and combining methods for

both data sets are calculated. DRMS is a single number that expresses 2D accuracy and can be calculated as follow

$$DRMS = \sqrt{\sigma_N^2 + \sigma_E^2} \qquad \textbf{6-28}$$

where σ_N^2 represents the variance of northing and σ_E^2 represents the variance of easting. Table 6-3 tabulates the DRMS values for single branches and all combining methods of both data sets.

Table 6-3: DRMS of single branches and combining methods

	CH1	CH2	CH3	CH4	EGC	WC	NWLS	SNRWLS
First data set	48 m	140 m	78 m	71 m	34 m	22 m	30 m	**21 m**
Second data set	53 m	57 m	N/A	N/A	51 m	50 m	40 m	**38 m**

In the first data set where four single branches were available to combine, the enhancement achieved through combining methods is more significant than the second data set with only two single branches on hand. SNRWLS performs best for both data sets. Reaching an accuracy of 20 m in the first data set is remarkable, given the tremendous level of attenuation (C/N0 between 15-30 dB-Hz).

6.5 Summary

Combining methods at the measurement level were studied in this chapter. Reviewing the theoretical background, two suboptimal practical methods were proposed, namely NWLS and SNRWLS. The performance of the proposed methods and two combining methods at the correlator output level, namely EGC and WC were assessed using the real GPS L1 signals. At the measurement level, the precision of combined measurements was assessed through analysing the differential pseudoranges standard deviations. At the position level, the 2D confidence ellipses and 3D positioning standard deviations were analysed. The DRMS values were finally calculated in order to facilitate the horizontal accuracy analysis. Significant DRMS value enhancements were achieved by utilizing combining methods.

Chapter Seven: CONCLUSIONS AND RECOMMENDATIONS

This chapter outlines the conclusions and recommendations for future work from this thesis.

7.1 Conclusions

Based on the results and analysis presented throughout this thesis, this section summarizes conclusions drawn from GNSS indoor channel characterization and spatial diversity system.

7.1.1 GNSS indoor channel characterization

With regards to GNSS indoor channel characterization, the following conclusions are made:

1. The spatial and temporal analysis of multipath indoor GPS signals revealed that spacing of half a wavelength (about 10 cm for GPS L1) between receiving antennas results in the latter to capture uncorrelated signals in harsh multipath environments. However, in moderate multipath environments, more spacing is required for the same level of decorrelation.

2. An analytical model was developed in order to model and compensate the noise effect on the correlation coefficient measurements. A remarkable agreement between the analytical model and practical measurements was obtained. Utilizing the proposed model for complex correlation coefficient measurements with a C/N_0 of 10 dB-Hz and a coherent integration time of 100 ms, an improvement of up to 10% is acheived on measurements.

3- An analytical model based on the sphere of scatterers model and antenna gain pattern was developed and found useful to characterize the observed Power Spectral Density (PSD) by a moving antenna in harsh multipath GNSS channels. A notable agreement between analytical PSD curves and the empirically measured ones was obtained.

4- Analytically modeled and practically measured PSD curves of differently oriented antennas are analyzed. The analysis revealed that the antenna gain pattern plays a critical role in the observed PSD and estimated Doppler values.

5- Since in many GNSS applications the Doppler observations are used to aid the position estimation and extract the velocity solution, the effect of Doppler estimation in harsh multipath environments on the velocity solution is considered. The experimental results shown poor velocity solution utilizing the Doppler measurements in harsh multipath environments. Inaccurate Doppler measurements due to the multipath propagation cause inaccurate velocity estimation. Considerable biases, large variances and very poor Doppler-derived velocity solutions make Doppler measurements of limited value in harsh multipath environments for positioning purposes.

7.1.2 Spatial Diversity system

Based on the results and analyses provided, the following conclusions with respect to the spatial diversity system can be made:

1- Utilizing multiple antennas with a spacing of 10 cm and combining their corresponding signals at the correlator output level was found effective to mitigate the fading phenomenon.

2- A new method for combining the signals from multiple antennas at the correlator output level, called Weighted Combiner (WC), was developed for the case when a reliable epoch-by-epoch SNR estimation is available. The WC method was found to be more powerful for signal detection than the Equal Gain Combiner (EGC) and Selection Combiner (SC) methods.

3- An analysis of the number of available satellites revealed that utilizing the Weighted Combiner method for a four-branch diversity system can reduce the probability of outage from around 50% to less than 10%.

4- At the measurement level, a non-weighted least squares approach for combining the pseudoranges extracted from the diversity branches was found vulnerable to the discrepancy of the diversity channels quality.

5- An analytical weighting method based on the effect of noise on pseudorange accuracy was proposed for weighting the indoor pseduranges extracted from *M* diversity branches. Utilizing the weighting method, an alternative method for combining the pseudoranges of the diversity branches at the measurement level was developed and analyzed. The new method, called SNRWLS, was found to be useful in enhancing measurement precision. Using the SNRWLS method with a four-branch diversity system, the standard deviation of pseudoranges decreased (hence improved) to half the standard deviation of the pseudoranges extracted from the individual diversity branches.

6- In the position domain, through analyzing biases, 2D confidence ellipses, 3D standard deviations of positioning and the DRMS values, it was found that utilizing multiple antennas can be useful in enhancing positioning accuracy. Utilizing the SNRWLS method for a four-branch diversity system, an accuracy of 20 m was achieved, which is remarkable, given the tremendous level of attenuation (C/N_o between 15-30 dB-Hz).

7.2 Recommendations

Based on the results and the experience gained throughout this work, the following recommendations can be made for future work:

1- In this research work, the area over which the experiments could be performed was limited by the measurement setup as reference-rover strategy requires both reference and rover antennas to be physically connected to the front-end. In order to overcome this limitation, other data processing strategies that do not require a physical connection between reference and rover antennas should be considered. Utilizing such a data collection strategy, the analysis performed in this thesis can be extended to other locations of interest.

2- Increasing the number of diversity branches could enhance the detection, parameter estimation and positioning performance of the system. However, finding proper equipments capable of handling more diversity branches could be challenging and costly at this time.

3- Regarding application of this research to low cost handheld receivers, test equipment and assumptions should be kept as practical as possible. However, there are two major practical limitations in the way of utilizing this research in practice at this time:

    a. Oscillator instability: In this research, utilizing relatively stable oscillators, the coherent integration time was extended to hundreds of ms. However, for low cost oscillators typically used in handheld devices their temporal instability should be taken into account for such coherent integration times.
    b. Computational burden: Realizing the bank of correlators requires a massive computational power. Any consideration for reducing the

computational burden such as reducing the size of bank of correlators or performing the computations by another party such as a Mobile Station Assisted (MSA) standard, would be a significant step towards utilizing this research in practice.

4- As discussed in Chapter 5, Doppler measurements in harsh multipath environments are not reliable observables for positioning purposes. However, Doppler measurements extracted from satellites with a dominant LOS component were found to be useful. It is strongly recommended to verify the presence of a dominant LOS component on satellite signals before using their Doppler measurements. The Rician K factor can be considered as a proper metric for this verification.

5- In the SNRWLS method, by ignoring the effect of multipath, the measurement covariance matrix was generated based on SNR. If any statistical information about the multipath effect can be obtained, it can also be considered in forming the measurement error covariance matrix in order to enhance performance.

6- At the position level, the non-weighted least squares method is preferred to avoid the smoothing effect of Kalman filter. Utilizing the Kalman filter could enhance the positioning accuracy.

7- The use of more advanced positioning strategies than single point positioning such as DGPS or height constraint could be applied to enhance the positioning accuracy.

8- GNSS spatial diversity systems could be integrated with INS. GNSS diversity system could provide more accurate and reliable observations, which would enhance the performance of GNSS/INS integrated systems.

9- This research work focused on spatial diversity systems. Different diversity systems such as polarization, pattern and frequency diversity systems could also be developed and assessed as alternatives.

References

Abdi, A., W. C. Lau, M. S. Alouini, and M. Kaveh (2003) "A New Simple Model for Land Mobile Satellite Channels-First and Second order statistics," *IEEE Transaction on Wireless Communication*, vol 2, no 3, May 2003, pp. 519 – 528.

Allen, B. and M. Ghavami (2005) *Adaptive Array Systems: Fundamentals and Applications*, John Wiley & Sons, New York NY, pp. 154-156

Aminian, B. (2011) *Investigations of GPS Observations for Indoor GPS/INS Integration*, MSc Thesis, Department of Geomatics Engineering, The University of Calgary, Canada, (Available at http://plan.geomatics.ucalgary.ca)

Aminian, B., V. Renaudin, D. Borio and G. Lachapelle (2010) "Indoor Doppler Measurements and Velocity Characterization Using a Reference-Rover Software Receiver," in *Proceedings of ION GNSS10,* 21-24 September, Portland OR, 11 pages

Blaunstein, N. and J. B. Andersen (2002) *Multipath Phenomena in cellular networks*, Artech House, Boston-London.

Borio, D., C. Gernot, F. Macchi and G. Lachapelle, (2008) "The Output SNR and its Role in Quantifying GNSS Signal Acquisition Performance" Proceedings of European Navigation Conference (Toulouse, 23-25 April)

Borio D., N. Sokolova and G. Lachapelle (2011) "Doppler Measurement Accuracy in Standard and High-Sensitivity GNSS Receivers," *IET Radar, Sonar & Navigation*, vol 5, no 6, pp 657-665.

Broumandan, A. (2009) *Enhanced Narrowband Signal Detection and Estimation with a Synthetic Antenna Array for Location Applications,* PhD Thesis, Department of Geomatics Engineering published as Report No 20292, University of Calgary, Canada.

Broumandan, A., J. Nielsen, and G. Lachapelle (2010) "Indoor GNSS Signal Acquisition Performance Using a Synthetic Antenna Array," IEEE *Transactions on Aerospace and Electronic Systems*, in press.

Broumandan, A., J. Nielsen, and G. Lachapelle (2011) "Coherent Integration Time Limit of a Mobile Receiver for Indoor GNSS Applications," *GPS Solutions,* Published online March 2011, 11 pages

Broumandan, A., J. Nielsen, and G. Lachapelle (2010) "Signal detection performance in Rayleigh fading environments with a moving antenna," *IET signal processing*, vol 4, no 2, pp. 117-129.

Clarke, R. H (1968)"A statistical theory of mobile-radio reception," in *Bell System Technical Journal*, vol. 47, 1968, pp. 957–1000.

Colburn, J. S., Y. Rahmat-Samii, M. A. Jensen, and G. J. Pottie (1998) "Evaluation of Personal Communications Dual-Antenna Handset Diversity Performance," in *IEEE Transactions on Vehicular Technology*, vol 47, no 3, August 1998, pp. 737-746.

Dietrich, C.B., J. Dietze, K. Nealy, and J. R. Stutzman (2001) "Spatial, Polarization, and Pattern Diversity for Wireless Handheld Terminals," in *IEEE Transactions on Antennas and Propagation,* vol 49, Issue 9, Sept. 2001, pp. 1271 – 1281.

Dehghanian, V., J. Nielsen and G. Lachapelle (2010) "Combined Spatial-Polarization Correlation Function for Indoor Multipath Environments,". *IEEE Antennas and Wireless Propagation Letters*, vol 9, pp. 950-953

Gao, J. (2007) Development of a Precise GPS/INS/On-Board Vehicle Sensors Integrated Vehicular Positioning System, PhD Thesis, published as UCGE Report No. 20255, Department of Geomatics Engineering, University of Calgary, Canada

Groves, P. D.: "GPS Signal to Noise Measurement in Weak Signal and High Interference Environments," in Proceedings of the Proceedings of ION GNSS, 3-16 September 2005, Long Beach, CA, pp. 643-658

Haykin, S. (2000) *Communication Systems,* 4th Edition, 2000, John Wiley & Sons, Inc.

He, Z., M. Petovello and G. Lachapelle (2012) Modeling HSGPS Doppler Errors in Indoor Environments for Pedestrian Dead-Reckoning. International Technical Meeting, Institute of Navigation, 30Jan-1Feb, Newport Beach, CA, 13 pages

Hu, T., G. Lachapelle and R. Klukas (2007) "Controlled GPS Signal Simulation for the Indoors". Journal of Navigation, Cambridge University Press, 60, 2, 265-280.

Jost, T. and W. Wang (2009) "Satellite-to-indoor broadband channel measurements at 1.51 GHz," in Proceedings of the ION GNSS International Technical Meeting, 26-28 Jan, Anaheim, CA, pp. 777-783

Kaplan, E. D., D. H. Hegarty (Editor) (2006) *Understanding GPS Principles and Applications*. Artech House.

Kay, S. M. (1998) *Fundamentals of Statistical Signal Processing: Detection Theory*, Prentice-Hall.

Keshvadi, H., A. Broumandan and G. Lachapelle (2012) Spatial Characterization of GNSS Multipath Channels. International Journal of Antennas and Propagation, in press

Lachapelle, G. (2009) *GNSS Theory and Applications*, ENGO 625 Lecture Notes, Department of Geomatics Engineering, The University of Calgary.

Lakhzouri, A., E. S. Lohan, I. Saastamoinen and M. Renfors (2005) "Interference and indoor channel propagation modeling based on GPS satellite signal measurements," in *Proceedings of the ION/GNSS 18th International Technical Meeting of the Satellite Division*, Long Beach, CA, Sept. 2005, pp. 896–901.

Misra, P. and P. Enge (2006) Global Positioning System – Signals, Measurements, and Performance, Ganga - Jamuna Press, second edition

Moafipoor S., D. A. Grejner-Brzezinska, and C. K. Toth (2004). "Tightly coupled GPS/INS/CCD integration based on GPS carrier phase velocity update," In: *Proceedings of ION NTM*, San Diego CA, pp. 1094–1102

Narayanan, R. M., K. Atanassov, V. Stoiljkovic, and G. R. Kadambi (2004) "Polarization diversity measurements and analysis for antenna configurations at 1800 MHz". IEEE Trans. on Antennas Propagat., 52(7): 1795-1810.

Novatel Inc (2011a) *Pinwheel™ Antennas Enhance Flexibility and Reduce Costs,* http://webone.novatel.ca/assets/Documents/Papers/GPS701_702GG.pdf, last accessed October 20, 2011

Novatel Inc (2011b) *Tactical Grade, Low Noise IMU Delivers 3D Position, Velocity and Attitude Solution as Part of SPAN Technology,* www.novatel.com/assets/Documents/Papers/IMU-LCI.pdf , last accessed October 20, 2011

O'Driscoll, C., (2006) "Performance Analysis of the Parallel Acquisition of Weak GPS Signals" Ph.D Thesis, Department of Electrical and Electronic Engineering, National University of Ireland, Ireland

O'Driscoll, C., G. Lachapelle and M.E. Tamazin (2010) "Investigation of the Benefits of Combined GPS/GLONASS Receivers in Urban Environments," in *proceeding on RIN NAV10 Conference on Position, Location, Timing: Everyone, Everything, Everywhere*, London, 30Nov-2Dec, 10 pages.

O'Driscoll, C., and D. Borio. (2009) *GNSS receiver design*, ENGO 638 Lecture Notes. Department of Geomatics Engineering, The University of Calgary.

Peterson, B., D. Bruckner and S. Heye (1997) "Measuring GPS Signals Indoors" in *Proceedings of ION GPS97*, Kansas City MO, September 16 - 19, pp.615 – 624

Petovello, M.G. (2003) *Real-time Integration of a Tactical-Grade IMU and GPS for High-Accuracy Positioning and Navigation*, PhD Thesis, published as UCGE Report No. 20173, Department of Geomatics Engineering, University of Calgary, Canada.

Petovello, M.G., C. O'Driscoll, G. Lachapelle, D. Borio, and H. Murtaza (2009) "Architecture and Benefits of an Advanced GNSS Software Receiver," *in Positioning*, Vol. 1, pp. 66-78

Petovello, M. (2009) *Estimation for navigation*, ENGO 699 Lecture Notes, Department of Geomatics Engineering, The University of Calgary.

Proakis, J. G. (2001) *"Digital Communications,"* [Chapter 14] *Digital Communications through Fading Multipath Channels,* 4th Ed, McGraw-Hill, New York.

Rappaport, T. S. (2002) *Wireless Communications: Principles and Practice*, Prentice Hall PTR, 2nd Edition.

Satyanarayana, S., D. Borio and G. Lachapelle (2010) "Power Levels and Second Order Statistics for Indoor Fading Using a Calibrated A-GPS Software," in *Proceedings of GNSS10*, Portland OR, 21-24 Sep, The Institute of Navigation, 14 pp.

Satyanarayana, S. (2011) GNSS Channel Characterization and Enhanced Weak Signal Processing. PhD Thesis, Report No. 20336, Department of Geomatics Engineering, The University of Calgary, Canada.

Satyanarayana, S., D. Borio and G. Lachapelle (2012) C/N0 Estimation: Design Criteria and Reliability Analysis under GNSS Weak Signal Scenarios. IET Radar, Sonar & Navigation, 6, 2, 81-89

Sadrieh, N., A. Broumandan and G. Lachapelle (2012) A Weighted Combining Method for GNSS Antenna Diversity. Proceedings of IEEE/ION PLANS 2012, Session C5, Myrtle Beach, SC, 24-26 April, 8 pages

Sadrieh, N., A. Broumandan and G. Lachapelle (2012) Doppler Measurement Characterization in Multipath Fading Channels for GNSS Applications. Journal of Navigation, Cambridge University Press,

Sadrieh, N. (2011) Spatial Antenna Diversity Performance for Indoor GNSS Applications. Proceedings of GNSS11 (Portland, OR, 20-23 Sep), The Institute of Navigation, 9 pages.

Sadrieh, N., A. Broumandan and G. Lachapelle (2010) Spatial/Temporal Characterization of the GNSS Multipath Fading Channels, Proceedings of GNSS10, Portland OR, September 2010.

Shanmugam, S. (2008) *New Enhanced Sensitivity Detection Techniques for GPS L1 C/A and Modernized Signal Acquisition,* PhD Thesis, published as Report No. 20264, Department of Geomatics Engineering, The University of Calgary.

Serrano, L., D. Kim, R. B. Langley, K. Itani and M. Ueno (2004) "A GPS Velocity Sensor: How Accurate Can It Be? - A First Look," in Proceedings of ION NTM, San Diego CA, pp. 875-885

Stein, S. (1981) Algorithms for ambiguity function processing in *IEEE Trans. Acoust., Speech, Signal Processing*, vol. ASSP-29, pp. 588–599, June1981.

Steingass, A. and A. Lehner (2003) "Land Mobile Satellite Navigation -Characteristics of the Multipath Channel," in Proceedings of the ION GNSS, , Portland, OR, pp. 1016-1022

Soloviev, A., F. Van Grass and S. Gunamardena (2009) "Decoding Navigation Data Messages from Weak GPS Signals," *IEEE Transactions on Aerospace and Electronic Systems*, vol 45, no 2, April 2009, pp. 660-666.

Souden, M., S. Affes, J. Benesty, and R. Bahroun (2009) "Robust Doppler Spread Estimation in the Presence of a Residual Carrier Frequency Offset," *IEEE Transaction on signal processing,* vol 57, no 10, October, pp.4148-4153

Turkmani, A. M. D., A. A. Arowojolu, P. A. Jefford and C. J. Kellett (1995) "An experimental evaluation of the performance of two-branch space diversity schemes at 1800MHz," in *IEEE Trans Vehicular Tech*, vol 44, no 2, May 1995, pp 318–326.

Uijt de Haag, M. (1999) An investigation into the application of block processing techniques for the Global Positioning System, PhD Thesis, Ohio University, United States

Van Graas, F., A. Soloviev (2004) "Precise Velocity Estimation Using a Stand-Alone GPS Receiver," Navigation, Journal of the Institute of Navigation, vol. 51, no. 4, Alexandria VA,

Van Graas, F., A. Soloviev, M. Uijt de Haag, S. Gunawardena, M.S. Braasch (2005) "Comparison of Two Approaches for GNSS Receiver Algorithms: Batch Processing and Sequential Processing Considerations," Proceedings of the 18th International Technical Meeting of the Satellite Division of The Institute of Navigation (ION GNSS 2005), September 2005, pp. 200-211, Long Beach, CA

Van Diggelen, F. (2009) *A-GPS: Assisted GPS, GNSS, and SBAS,* Artech House.

Van Trees, H. L. (2002) "Optimum Array Processing," [part IV] in *Detection, Estimation, and Modulation Theory*, John Wiley & Sons, New York 2002.

Watson, R (2005) *High-Sensitivity GPS L1 Signal Analysis for Indoor Channel Modelling*, MSc Thesis, published as Report No. 20215, Department of Geomatics Engineering, The University of Calgary, Canada.

Watson, R., G. Lachapelle, and R. Klukas (2006a) "Testing Oscillator Stability as a Limiting Factor in Extreme High-Sensitivity GPS Applications," Proceedings of European Navigation Conference, Manchester, U.K., 8-10 May 2006.

Watson, R., G. Lachapelle, R. Klukas, S. Turunen, S. Pietil, and I. Halivaara (2006b) "Investigating GPS Signals Indoors with Extreme High-Sensitivity Detection Techniques," in *Navigation*, Journal of the Institute of Navigation, Alexandria, VA, 52, 4, pp.199-213.

Zaheri, M. (2011) *Enhanced GNSS Signal Detection Performance Utilizing Polarization Diversity*, MSc Thesis, published as Report No. 20322, Department of Geomatics Engineering, The University of Calgary, Canada.

Zaheri, M., A. Broumandan and G. Lachapelle (2010) "Comparing Detection Performance of Polarization and Spatial Diversity for Indoor GNSS Applications," in Proceedings of IEEE/ION PLANS 2010, Indian Wells/Palm Springs, California, 4-6 May 2010, 8 pages.